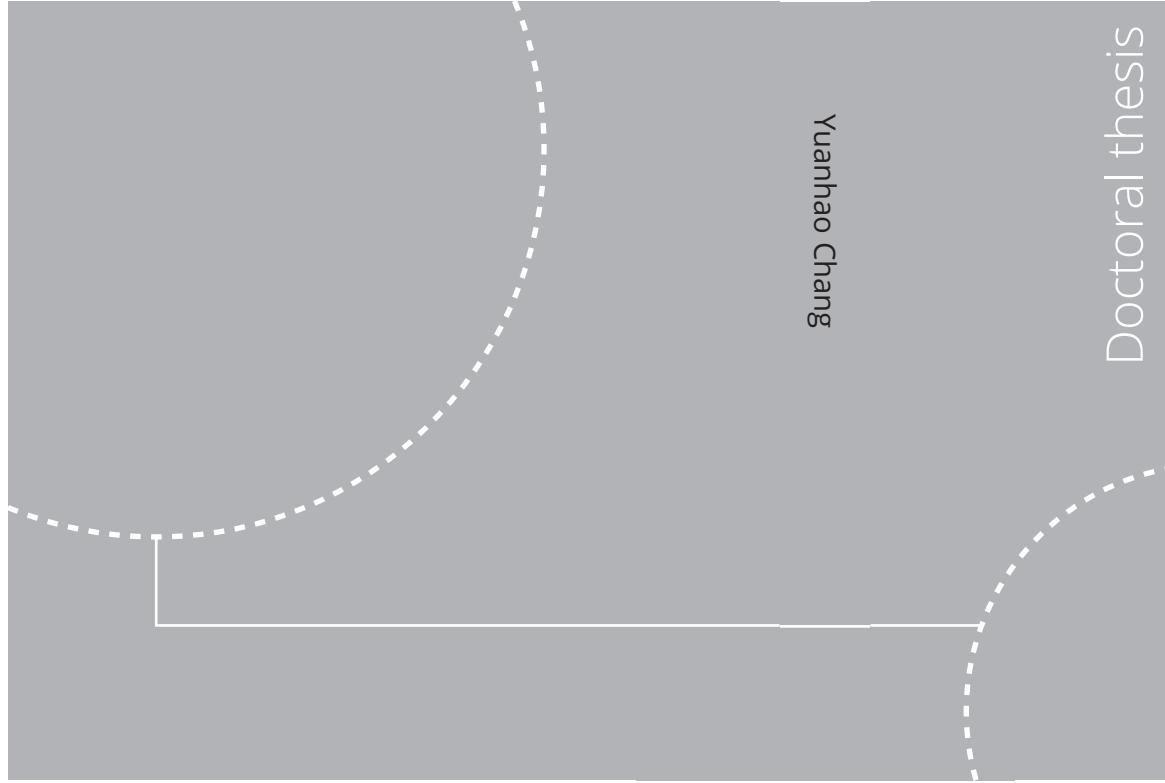


ISBN 978-82-326-5971-5 (printed ver.)  
ISBN 978-82-326-6817-5 (electronic ver.)  
ISSN 1503-8181 (printed ver.)  
ISSN 2703-8084 (electronic ver.)



Doctoral theses at NTNU, 2023:72

Yuanhao Chang

# Atomistic Insight into Nanofluid Enabled Enhanced Oil Recovery

Yuanhao Chang

# Atomistic Insight into Nanofluid Enabled Enhanced Oil Recovery

Thesis for the degree of Philosophiae Doctor

Trondheim, March 2023

Norwegian University of Science and Technology

Faculty of Engineering

Department of Structural Engineering



Norwegian University of  
Science and Technology

**NTNU**

Norwegian University of Science and Technology

Thesis for the degree of Philosophiae Doctor

Faculty of Engineering  
Department of Structural Engineering

© Yuanhao Chang

ISBN 978-82-326-5971-5 (printed ver.)  
ISBN 978-82-326-6817-5 (electronic ver.)  
ISSN 1503-8181 (printed ver.)  
ISSN 2703-8084 (electronic ver.)

Doctoral theses at NTNU, 2023:72



Printed by Skipnes Kommunikasjon AS

*The harder you work, the luckier you will be.*

-- Thomas Jefferson



## Preface

This thesis is submitted to the Norwegian University of Science and Technology (NTNU) for partial fulfillment of the requirements for the degree of Philosophiae doctor (Ph.D.).

The doctoral work has been conducted in the period between August 2019 and December 2022 under the supervision of Professor Jianying He, Professor Senbo Xiao, and Professor Zhiliang Zhang. All the simulation work was carried out at NTNU Nanomechanical Lab, Department of Structural Engineering (KT), Faculty of Engineering (IV), Norwegian University of Science and Technology (NTNU), Trondheim, Norway. The thesis comprises an introductory section, and four journal papers (three published and one submitted).

This work is supported by the Research Council of Norway and the China Scholarship Council. All the simulations were carried out on the computational resources provided by Norwegian Metacenter for Computational Science (NOTUR NN9110k and NN9391k).

*Yuanhao Chang*  
*Trondheim, October 2022*



## Abstract

Nanoparticles (NPs) possess great potential in applications to enhanced oil recovery (EOR) due to their outstanding features of ultra-small size, great surface and interface effect, high sustainability, etc. The underlying mechanisms of which however remain to be explored. Especially, revealing the displacement mechanisms of residual oil by NPs and the transport stability of NPs stabilized Pickering emulsion is of great significance. In this thesis, the trapped oil displacement in rough channels by nanofluids and the transport dynamics of NPs stabilized Pickering emulsion across the pore throat have been investigated by atomistic simulation.

The displacement dynamics of residual oil trapped in rough channels by different nanofluids are elucidated initially. The results indicate that both hydrophilic nanoparticles (NPs) and Janus NPs have a highly obvious oil displacement effect. Specifically, hydrophilic NPs increase the viscosity and enlarge the sweeping scope of injected fluid. Janus NPs alter the local surface wettability by sliding along the surface and remobilize the oil by sliding along the oil/water interface. Conversely, hydrophobic NPs further lock the trapped oil and impede the displacement by entering the oil phase. In addition, the oil displacement effect is found to be less significant with low pumping force. Yet, Janus NPs maintain a relatively great effect under low pumping force, thanks to sufficiently long contact time between Janus NPs and the oil phase. Further analysis of the capillary number not only verifies the simulation results but also highlights the applied prospect of Janus NPs in actual oil reservoirs.

Then, the local enlarged surface system is built for elucidation of the displacement dynamics and mechanisms of Janus NPs. It's found that Janus NPs with 25% and 50% hydrophobicity significantly recover more oil from the rough surface. The number, position, and orientation of adsorbed nanoparticles on the side wall of the groove determine the final amount of extracted oil. 'Adsorption invasion process' dominates the formation of Janus NPs adsorption structure, which is mainly contributed by the pinning effect and the collision between NPs. To modify such an 'adsorption invasion process', identification of the residual oil, displacement pressure, and the morphology of the inside oil-water interface are crucial factors. Furthermore, the effect of rough surface parameters on such displacement dynamics is studied. The applicable surface for JNPs to efficiently



displace residual oil is neutrally wetted or weakly hydrophobic. For the geometric parameters, the smaller entry angle and exit angle, the larger aspect ratio of the groove, and the big enough tip length of the bulge contribute to a considerable EOR effect. Separately, the tip length of the bulge affects the formation of the adsorption film; A smaller entry angle means a larger adsorption film area and better local wettability alteration effect, while a smaller exit angle limits the amount of trapped oil that cannot be covered at the outlet side; Given the certain JNPs adsorption film, a larger aspect ratio of the oil trapping grooves can guide the oil-water interface downward to bottom. Among the four parameters, aspect ratio controls the EOR effect provided the tip length of the bulge is over the threshold.

Lastly, the nanomechanical property of the Pickering emulsions and their transport through the nanopore throat are investigated. It's found that Pickering emulsions are mechanically robust by the JNP shell and recover from large deformations. Pickering emulsion is able to rupture on the hydrophobic surface due to the strong interactions between the oil core and surface. The larger  $\phi$  of the emulsion, the greater deformation and stress can be withstood at rupture. More importantly, the critical  $\phi$  of the emulsion determines that the JNP shell can form an ordered quasi-solid structure and act the effective shielding, while the size of the emulsion decides the weakening rate of such barrier effect in compression. In addition, Pickering emulsions with varied  $\phi$  share a similar force response in the transport across the hydrophilic pore throat. While for the case of hydrophobic pore throat, the Janus NP shell acts as a protection pad, screening the interaction of the oil core with the residual oil on the surface. Such an effect enables the transport stability of Pickering emulsion with large  $\phi$  across the pore throat. In addition, the smaller opening angle of the pore throat is proved to magnify the Jamin effect and increase the probability of the partial Janus NP shell being captured at the entrance.

Our research not only uncovers the displacement mechanism of trapped oil by nanofluids but also reveals the transport dynamics of NPs stabilized Pickering emulsion in the pores, which is significant for understanding and guiding the nanofluids-enabled EOR applications.

## Acknowledgements

Three years ago, when I came to Norway with apprehension and hesitation, I never imagined that I could complete my doctoral thesis so smoothly. 'I can do everything through him who gives me strength.' (Philippians 4:12-13) Thank you, my God. Again it was he who gave me wisdom and patience to do whatever I did for his glory. Of course, this thesis would not come into being if I had not received help from my supervisors, colleagues, friends, and family. I sincerely thank all those who have accompanied me on this amazing journey. You are the salt in my plain life in Norway, giving me energy and making my life tasteful. No matter the ups and downs, the joys and sorrows, I am grateful for this journey, and I love you.

First and foremost, I am very grateful to my supervisor, Prof. Jianying He. It was she who gave me the opportunity to study and work in the NML group. Over the years, she offers me all-around help. She provides a relaxed scientific research environment for me and fully mobilizes my subjective initiative through goal-oriented management. Also, both her innovative thinking on scientific research issues and her excellent control of the combination of fundamental science and industrial application have benefited me a lot. In daily life, she is more like a close friend, helping me wherever I need it, and continuing to convey an open-minded and optimistic attitude. More than that, I am really impressed by her high emotional intelligence and efficient communication skills.

I would also like to extend my sincere gratitude to my co-supervisor Prof. Zhiliang Zhang. He shows me what a real scientist is like. His ambitions for the 'big question' have always spurred me to look deeper and more meticulous. I am quite admire him and have always been in awe of him. I have to admit that such a sense of distance prevents me from communicating with him frequently. Although it is a pity, I think his scientific spirit and attitude will affect me everlastingly.

My heartfelt thanks are also presented to my co-supervisor Associate Prof. Senbo Xiao. He is my closest scientific research leader for the past three years. For me, he is my guide in my MD learning journey. I am grateful that he taught me a lot of skills and implanted much pursue me to statistics, theory, and science and I can deeply feel that he tries his best to guide me and is very ambitious for me. I am proud to be his first official student. I also hope he will be proud of me in the future.

Besides my supervisors, I would thank all my colleagues at NTNU Nanomechanical Lab and the Department of Structural Engineering. Here, special thanks to my colleagues: Prof. Kjell Magne Mathisen, Prof. Victorien Prot, Rui Ma, Haiyang Yu, Xiao Wang, Jianyang Wu, Verner Håkonsen, Sigrid Rønneberg, Merete Falck, Ingrid Snustad, Li Sun, Yizhi Zhuo, Feng Wang, Susanne Sandell, Sandra Sæther, Siqi Liu, Yuequn Fu, Thorstein Wang, Yu Ding, Meichao Lin, Xu Wang, Jing He, Paul Rübsamen-von Döhren, Håvard Mo Fagersand, Robin Plantey, Martha Seim Gunstad, Erling Velten Rothmund, Torstein Wiiger Opsahl, Yifan Zhang, Yuyu Liu, Xinshu Zou, Jinhuan Hu, Mengnan Yu, Mingjie Zhang, Haiyan Yu, Tengjiao Jiang, Sihai Luo, Ziyue Lu, Shengyi Xu, Qingbo Wang, Wei Guan, Xiaolan Ma, Qi Xu, Tao Lu, Prof. Zhen Gao, Zhenhui Liu, Jie Wu, Haoge Liu, Naiquan Ye, Fangfang Lu, Shanshan Jiang and Jirang Cui for the colorful & family-like life during the Ph.D. career.

Last but not least, many thanks to my family for their love and support. Because of the crazy epidemic, I haven't been home for quite a long time. This brings them endless misses and worries. I really hope to go back soon and give each of them a big hug. Especially, I want to thank my destiny girl, Sunny Huan. Although I suffered from anxiety because of my utter miss to you, it was all worth it. Thank you for your understanding, tolerance, persistence, and companionship for me. You are an infinitely deep potential trap that I spontaneously fell into. Being tightly captured by you will be the most stable state in infinite time. I love you.

## List of Papers

The thesis is organized based on the following five papers, which have been published or submitted:

### Journal Papers included in this thesis

- I. Chang Y, Xiao S, Ma R, Wang X, Zhang Z, He J. Displacement dynamics of trapped oil in rough channels driven by nanofluids[J]. Fuel, 2022, 314: 122760.
- II. Chang Y, Xiao S, Ma R, Zhang Z, He J. Atomistic insight into oil displacement on rough surface by Janus nanoparticles[J]. Energy, 2022, 245: 123264.
- III. Chang Y, Xiao S, Ma R, Zhang Z, He J. Unravelling the Influence of Surface Roughness on Oil Displacement by Janus Nanoparticles[J]. Petroleum Science, 2023.
- IV. Chang Y, Xiao S, Ma R, Fu Y, Zhang Z, He J. Deformation and rupture of Janus nanoparticle stabilized Pickering emulsion on the solid surface. To be submitted.
- V. Chang Y, Xiao S, Ma R, Fu Y, Zhang Z, He J. Transport of Pickering emulsion across nanopore throat. To be submitted.

### Journal Papers not included in this thesis

- I. Chang Y, Xiao S, Fu Y, Wang X, Zhang Z, He J. Nanomechanical characteristics of trapped oil droplets with nanoparticles: a molecular dynamics simulation[J]. Journal of Petroleum Science and Engineering, 2021, 203: 108649.
- II. Yan L, Chang Y\*, Hassanizadeh S M, Xiao S, Raoof A, Berg C F, He J. A quantitative study of salinity effect on water diffusion in n-alkane phases: From pore-scale experiments to molecular dynamic simulation[J]. Fuel, 2022, 324, 124716.
- III. Chang Y, Xiao S, Yu H, He J, Zhang Z. Atomistic insight into interface rupture of ice from solid surfaces. To be submitted.
- IV. Chang Y, Xiao S, Ma R, Fu Y, Zhang Z, He J. Comparison of Pickering emulsion and traditional emulsion in oil-filled nanopore throat. To be submitted.

- V. Ma R, Xiao S, Chang Y, Fu Y, He J, Zhang Z. An interfacial gas-enrichment strategy for mitigating hydrate adhesion and blockage. *Chemical Engineering Journal*, 2022, 139918.
- VI. Ma R, Wang F, Chang Y, Xiao S, English N, He J, Zhang Z. Unraveling Adhesion Strength between Gas Hydrate and Solid Surfaces[J]. *Langmuir*, 2021, 37(47): 13873-13881.
- VII. Fu Y, Xiao S, Liu S, Chang Y, Ma R, Zhang Z, He J. Atomistic Insights into the Droplet Size Evolution during Self-Microemulsification[J]. *Langmuir*, 2022, 38(10): 3129-3138.
- VIII. Fu R, Xu Y, Liu Y, Lin Y, Xu K, Chang Y, Fu Y, Zhang Z, Wu J. Thermally induced hex-graphene transitions in 2D carbon crystals[J]. *Nanotechnology Reviews*, 2022, 11(1): 1101-1114.

#### **Conference Papers and oral presentations**

- I. Chang Y, Xiao S, Zhang Z, He J. Atomistic Insight into Oil Displacement on Rough Surface by Janus Nanoparticles. The Norwegian NanoSymposium 2021. Online, Oct. 05-06, 2021.
- II. Chang Y, Xiao S, Zhang Z, He J. Atomistic Insight into the Nanomechanical Characteristics of Trapped Oil Droplet/Nanofluid System in Confined Nanochannels. 3rd European Symposium on Nanofluids; Online, Sept. 09-11, 2021.
- III. Chang Y, Xiao S, Zhang Z, He J. Displacement of Trapped Oil on Rough Surfaces by Nanoparticles. The 8th European Congress on Computational Methods in Applied Sciences and Engineering; Norway, Oslo, Jun. 06-09, 2022.

## Contents

<b>Preface</b> .....	<b>i</b>
<b>Abstract</b> .....	<b>ii</b>
<b>Acknowledgements</b> .....	<b>iv</b>
<b>List of Papers</b> .....	<b>vi</b>
<b>Contents</b> .....	<b>viii</b>
<b>Chapter 1. Introduction</b> .....	<b>1</b>
1.1 Background and motivation.....	1
1.2 Research objects .....	3
1.3 Main contributions.....	3
1.4 Thesis outline.....	4
<b>Chapter 2. EOR mechanisms of NPs</b> .....	<b>5</b>
2.1 Potential of NPs for EOR application.....	5
2.2 Interfacial tension reduction by NPs.....	7
2.3 Wettability alteration by NPs.....	10
2.4 Structural disjoining pressure of NPs .....	13
2.5 NP-stabilized Pickering emulsion.....	16
2.6 Modification in viscosity and preventing asphaltene precipitation .....	20
<b>Chapter 3. NPs-enabled EOR by MD Simulation</b> .....	<b>23</b>
3.1 Overview of MD simulation .....	23
3.2 Application potential of MD simulations in EOR .....	29
3.3 NPs in liquid/liquid system.....	30
3.4 NPs in oil/water/surface system.....	33
<b>Chapter 4. Main Results</b> .....	<b>37</b>
4.1 Displacement of trapped oil in rough channels.....	37
4.2 Oil displacement on the rough surface by Janus nanoparticles .....	38
4.3 Deformation and rupture of Pickering emulsion in transport .....	41
<b>Chapter 5. Recommendations for further studies</b> .....	<b>43</b>
<b>Bibliography</b> .....	<b>45</b>
<b>Appendix A Appended papers</b> .....	<b>53</b>
A.1 Paper I .....	53
A.2 Paper II.....	89

A.3 Paper III .....	119
A.4 Paper IV .....	147
A.5 Paper V.....	173
<b>Appendix B .....</b>	<b>201</b>

# Chapter 1. Introduction

---

## 1.1 Background and motivation

Nowadays, the world's demand for energy is sharply increasing. In a context where the application of renewable energy is still immature, petroleum is indispensable as the most widely used fossil fuel in the world [1, 2]. The aggressive exploration of petroleum has exhausted most of the worldwide oil fields via primary and secondary oil recovery and currently calls for new technologies of tertiary oil recovery, also named enhanced oil recovery (EOR), for extracting the residual and more than 60% of the original oil in place (OOIP) [1-3]. However, the development effect of three traditional EOR methods including the thermal method, gas injection method, and chemical flooding is declining under varied challenges [4, 5]. Due to harsh reservoir adaptation conditions and low economic benefits, the application of gas injection development and thermal method is greatly restricted. The effect of conventional chemical flooding (surfactant or polymer flooding) is also close to the limit due to its high cost and unstable performance [6, 7]. Therefore, there is an urgent need to find more efficient EOR agents or methods.

As the research of nanomaterials in the field of materials engineering is getting mature, the latest research trend in chemical EOR is gradually turning towards exploring suitable nanomaterials that can enhance micro- and macro-displacement efficiency [8, 9]. Among them, nanoparticles (NPs) are considered potential substitutes and/or boosters for traditional chemical EOR materials [10]. NPs have been implemented in EOR in the form of foams, hydrosols, or organosols to take advantage of the attractive features of NPs,



including their high surface area and mobility as well as the relative ease of preparation [11, 12]. So far, NPs have shown a bright EOR future in laboratory experiments [13-15]. While the mechanisms that contribute to the promising results are still under debate despite the previous great efforts [16]. Wettability alteration is the most accepted mechanism for NPs in EOR. It's reported that rock surfaces can be changed from oil-wet to water-wet with the insertion of NPs, which leads to the detachment of the residual oil [17-20]. Nevertheless, the mechanism of wettability alteration remains controversial [20-22]. The reduction of interfacial tension is another important mechanism, which has been witnessed in many studies. Yet, some researchers believe that it hardly contributes to the effect of EOR [23-25] and some do not even observe the changes in interfacial tension in their experiments [26, 27]. In 2003, Wasan and Nikolov postulated the structural disjoining pressure as another mechanism of EOR [28]. They proposed that the NPs can form a wedge-like structure in the three-phase contact area and exert structural disjoining pressure to move forward and detach the oil droplets. Although this theory is supported by static analytical calculation and was used to explain related nanoparticle aggregation phenomena in experiments, the direct quantification of the pressure distribution resulting from structured NPs in the small three-phase contact area has not been reported. Therefore, there is still ambiguity concerning the intrinsic mechanisms of nanofluids for EOR. More fine-scale work is in desire for elucidating the mechanism of various NPs under different reservoir conditions.

Atomistic modeling and molecular dynamics (MD) simulations are proven to be highly suitable for inspecting the basis of EOR in nanoparticle/fluid/rock systems [29, 30]. As a complementary toolset to experiments, MD simulation is very powerful thanks to its accurate controls on the properties of the nanochannels, oil droplets, and NPs, with an atomic resolution. As such, MD simulations were able to uncover the characteristics of the self-assembly of the specific NPs at interfaces and on the droplet [31-34] and were also utilized in investigating oil droplet displacement by nanofluids [35], offering insights into the microscopic transportation mechanism for nanofluids in confined capillaries. Among them, simulation systems with rocks or nanochannels are still sparse due to computational cost constraints. Numerous questions remain to be addressed regarding the NP-involved transportation or displacement in the confined channel.

Thus, with the accurate representation of channels and residual oil in the EOR stage, mastering the displacement or transport dynamics of NPs and their special phenomena or mechanisms at the interface or surface will provide a nano-level understanding of the basic theory of the application of NPs in EOR.

## **1.2 Research objects**

The present thesis is funded by the NTNU - CSC scholarship program. The aim is to provide atomic insights into a fundamental understanding of the specific mechanisms in the EOR process with the involvement of NPs. The main objectives in this thesis are described as follows:

- To clarify the effect and control mechanism of the specific NPs on the displacement of residual oil from rough surfaces.
- To uncover the dynamics and dominant factors of wettability alteration by Janus NPs.
- To discover the role of Janus NPs in the transport of the Pickering emulsion across the pore throat.
- To provide guidance to screen and application of NPs for EOR.

## **1.3 Main contributions**

With molecular dynamics (MD) simulations, the thesis presents a systematic study on the displacement mechanism of NPs for remaining oil in rough channels, the dynamics of the Janus NP-guided wettability alteration, and the transport characteristics of Janus NP stabilized Pickering emulsion across narrow pore throats. The main contributions of this thesis are summarized briefly in the following:

- The specific effects and corresponding dominant mechanisms of NPs with different wettability on the displacement of residual oil on rough surfaces are clarified.
- The special wettability alteration dynamic, the crucial ways of its optimization, and the influence of rough surface topography are proposed for JNPs in displacing residual oil from the surface.

- The effect of JNP surface coverage ratio on the mechanical stability of a single JNP-stabilized Pickering emulsion is demonstrated by nanomechanical testing, which further contributes to the explanation of the transport of the Pickering emulsion through narrow pore throats.

## 1.4 Thesis outline

The thesis consists of an introductory section and a collection of four peer-reviewed papers. The introductory section is decomposed into five chapters. In **Chapter 1**, the background and motivation, research objectives, and main contributions are stated. In the following, **Chapter 2** will review the literature on the EOR Mechanisms of NPs. **Chapter 3** introduces the overview of MD simulation and the existing studies on NP-enabled EOR by Molecular Simulations. The main findings are summarized in **Chapter 4**. Finally, recommendations for further work are given in **Chapter 5**.

## Chapter 2. EOR mechanisms of NPs

---

The application of NPs in EOR process has drawn increasing attention globally. In this chapter, a short research review is employed on EOR mechanisms of NPs.

### 2.1 Potential of NPs for EOR application

NPs are small particles that range between 1 to 100 nanometers in size. It may be in the form of latex, polymer, ceramic particles, metal particles, and carbon particles. Due to their ultra-small size, NPs have a small size effect, large specific surface area, and macroscopic quantum tunneling effect. As plotted in Figure 2.1, they have special physical and chemical properties that conventional materials do not have in magnetic, thermal, electrical, optical, catalytic, biological, mechanical, and other aspects. Therefore, they lead to broad application prospects in many fields such as medical treatment, electronics, material science, and so on [36-38]. With the development of existing oil and gas development technologies entering a bottleneck period, the application of NPs in the oil and gas industry has also attracted great attention. Research on nanoparticles in the oil and gas industry has grown steadily over the past decade.

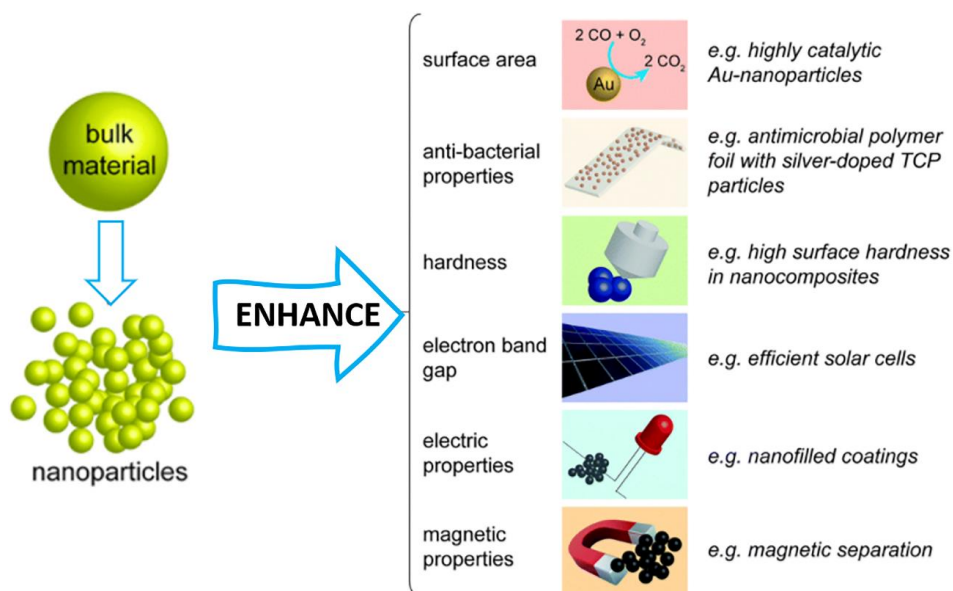


**Figure 2.1** Properties that are improved as bulk material are produced as nanoparticles, and the respective applications are derived from them.

The nanoparticles form the nanofluid by suspending in the base fluid. Compared with traditional sols and surfactant colloidal systems, nanofluids show more attractive features. Suspensions of NPs display high stability against sedimentation owing to the relatively high extent of surface forces which preserves the particles against aggregation, allowing entropic forces to easily against gravity [12, 39]. One major advantage of NPs in EOR application is their sustainability in harsh reservoir conditions with high temperature, high pressure, and high salinity. While the commonly used surfactants and polymers are not as sustainable as NPs because of their early-stage degradation under such conditions [40]. Furthermore, the main characteristics of nanofluids: including optical, stress-strain, thermal, rheological, magnetic, and electrical properties can be engineered by modifying the morphology and/or the size of the NPs during the synthesis process for possible targeted release in the porous media [41, 42]. The major features that enable NPs to be potential chemicals for EOR are summarized in the following:

- Ultra-small size: which allows effective transport or propagation into the micron-size pores of the reservoir.

- High surface effect: which allows it to adsorb strongly on an oil-water interface hence forming stable interfacial films or networks such as foam and emulsion.
- Surface and interfacial properties: which allows numerous interactions among different phases such as reduction in oil-water interfacial tension (IFT), altering the rock wettability and in-situ emulsion generation, or displaying special interfacial behaviors.
- Dispersion ability: which allows nanoparticles to be dispersed in the injected fluid throughout the flood.
- High sustainability: which enables them to be stable even in harsh reservoir conditions where other conventional EOR chemicals start degrading.
- Detectable: which allows detecting the path of the NPs inside the porous media or reservoir.
- Tunable: which allows modifying the specific properties of NPs by different treatments according to the requirement such as hydrophobicity and hydrophilicity, core-shell arrangement of NPs, Janus NPs, and other tailor-made NPs, etc. or to deliver the desired chemicals to the target location or zone in the porous medium.
- Viscosity modifier: which allows increasing the viscosity of the injected fluids.
- Agglomerative nature: which allows forming agglomerate that further increases the pore-blocking efficiency and contributes to the conformance control which ultimately helps in improving the subsequent displacement effect.
- Recycling: which allows for the collection and recycling of the injected NPs after production which can be environmentally friendly and also save the development cost.

## **2.2 Interfacial tension reduction by NPs**

Interfacial tension is the force of attraction between the molecules at the interface of two fluids. It could also define the energy creating a boundary between two immiscible liquids per unit area due to unbalanced forces [10]. As described in the oil/water system in Figure 2.2, the oil molecules at the top are attracted to each other resulting in a net attractive force of zero as the oil molecules are pulled in all directions. While the oil

molecules at the interface between oil/water have a force acting upon them from the water molecules below resulting in an unbalanced force. It is known that the reduction of oil-water IFT increases the capillary number (ratio of viscous to capillary forces) which is one of the essential requirements of EOR [43]. Due to the surface-active properties of the NPs, they are able to adsorb strongly at liquid-liquid and /or liquid-air interfaces. This phenomenon has the potential to reduce interfacial tension, owing to the minimized total system energy.

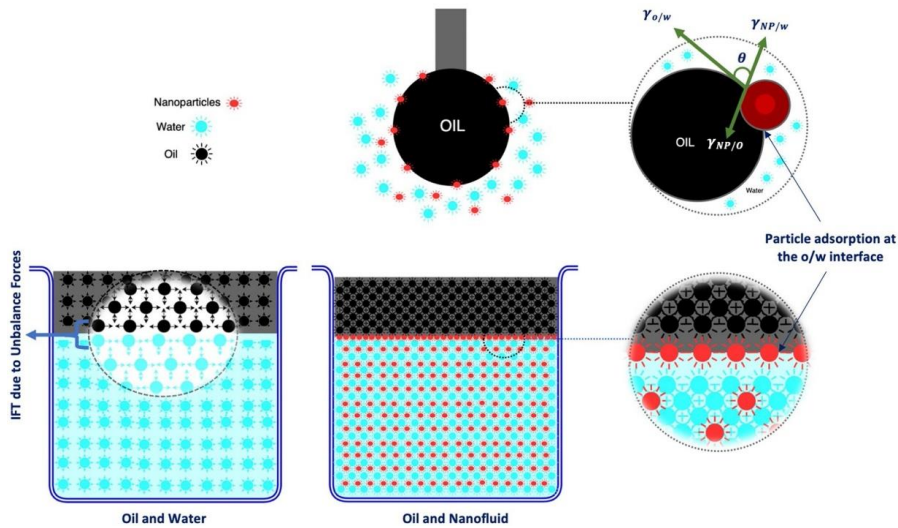


**Figure 2.2** Mechanism of IFT reduction using NPs showing particle adsorption (contact angle) at the oil-water interface and formation of a monolayer which replaces the existing oil-water interface, reprinted from Ref. [10].

In fact, it is a long ongoing debate on the reduction of IFT in the presence of NPs [40]. Hendraningrat et al. have reported a decline in the IFT in the presence of hydrophilic poly-silicone nanoparticles in which solid surfaces get more water-wet [44]. Roustaei et al. detected that the presence of polysiloxane nanoparticles caused a decrease in the oil-water interfacial tension from 26 to 2 mN/m [45]. Moghadam and Azizian have confirmed a significant decline in the interface tension of the surfactant and oil in the presence of zinc oxide nanoparticles [46]. In addition, a lot of experimental studies have declared the obvious decrease in IFT with charge-stabilized titania, ethyl cellulose particles, partially hydrophobic fumed silica particles, carboxyl-terminated carbon black (CB) particles, cellulosic particles, and gold particles [47-50]. However, some scholars have put forward

a completely different conclusion. Vignati et al. investigated the effect of different concentrations and hydrophobicity of silica nanoparticles and showed that no parameters could alter the IFT [51]. Saleh et al. have reported that highly charged poly(styrene sulfonate)-grafted silica nanoparticles are very effective in reducing IFT while bare silica alone cannot reduce IFT [52]. Also, no obvious change in IFT was proposed in the experiments with functionalized silica particles, ZnO, and hydrophilic silica particles [46, 53]. Considering that such inconsistency might be attributed to chemical contamination like additions of stabilizers in the experiments, the measurement criteria and indicator division are urgently needed.

On the other hand, there is a relatively uniform understanding of the mechanism by which nanoparticles may reduce IFT. Murshade et al. observed that hydrophilic titanium NPs dispersed in distilled water could reduce the IFT of oil-based solutions by about 20 mN/m. They concluded that the decrease in IFT was due to the adsorption of NPs at the interface [54]. Similarly, Giraldo reported that SiO<sub>2</sub> NPs reduced IFT by adsorption at the O/W interface depending on their hydrophobicity and the binding energy of NPs to the interface [55]. Li et al. reported that IFT reduction and adsorption with NPs may be due to the presence of the hydrophobic and hydrophilic parts of NPs which also exist in the O/W phase respectively, replacing the existing interface and reducing the friction force between the two phases [56]. Therefore, the IFT reduction mechanism of NPs starts with the adsorption of the particles at the O/W interface forming a monolayer that replaces the existing O/W interface acting as a mechanical barrier or interfacial particle film. There on, the formed monolayer reduces the interfacial energy between the two phases depending on the particle's distribution at the interface and surface energy of the NPs [56, 57].

Overall, most studies support the reduction of interfacial tension as the main mechanism for nanofluids in EOR, while a few studies did not find the modification of oil-water interfacial tension by nanoparticles. In more detail, almost all studies using NPs combined with surfactants or surface-modified NPs claim that reducing interfacial tension is one of the main mechanisms in NP-enabled EOR. Questions mainly come from the research with bare NPs. For the case with the same chemical agent, it is speculated that the conflict of views mainly lies in the chemical contamination caused by the additions like stabilizers or whether the degree of reduction of the interfacial tension in the



experiment can be regarded as significant. For this, rigorous detection workflows and criteria for IFT applied to EOR should be established. In addition, simulation techniques that can precisely control the specific experimental conditions are the better option.

### 2.3 Wettability alteration by NPs

Wettability is defined as the spreading or adhering propensity of fluid onto a solid surface in presence of other immiscible fluids [58]. In EOR context, when water prefers to stick to the reservoir rock in presence of oil, water, and oil are considered as wetting phases and non-wetting phases respectively. The rock in reservoirs may be the water-wet, mixed-wet, or oil-wet depending upon the initial hydrocarbon deposition history, interaction between different fluid phases, rock mineralogy, pore structure, roughness, etc. (Figure 2.3). It is one of the important properties of the reservoir rock which further affects the efficiency of EOR [59].

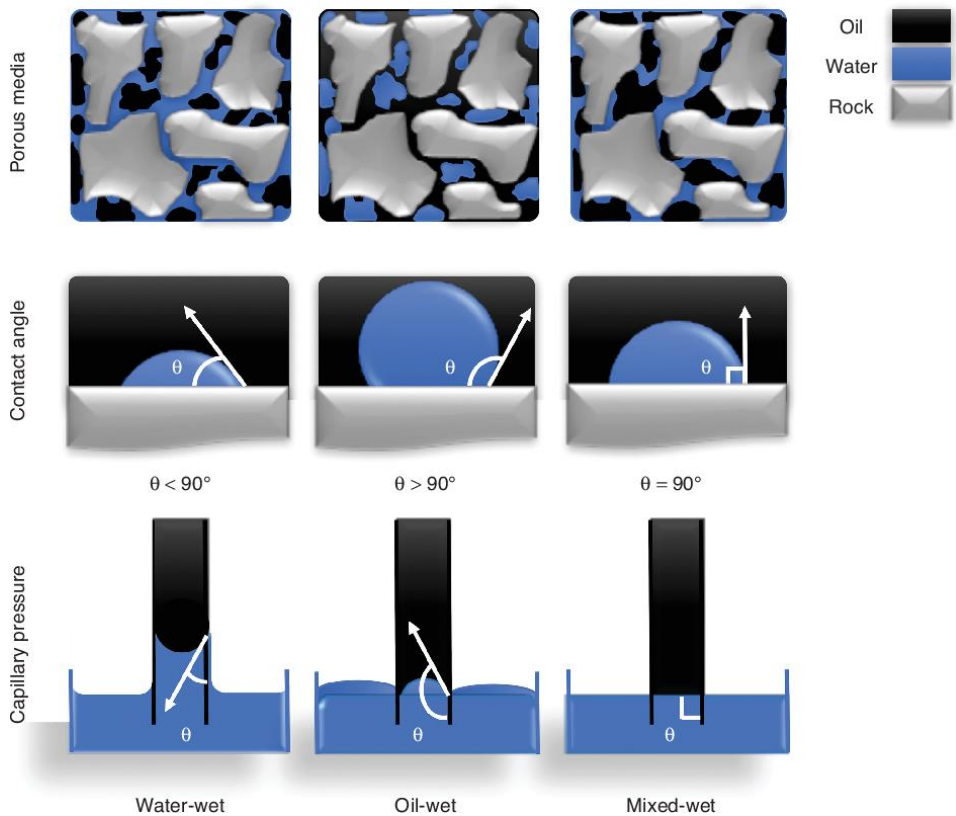


**Figure 2.3** Schematic of wettability definition in porous media with oil/water/rock system illustrating water-wet, oil-wet, and mixed-wet conditions in terms of contact angle and capillary pressure, reprinted from Ref. [59].

In recent years, wettability alteration has been regarded as a dominating mechanism for NPs in EOR [60-62]. Many studies reported improvement in EOR using NPs via wettability alteration [14, 27, 63]. Relying on the surface properties of NPs, they can adsorb on the rock surface and stabilize a water layer to subsequently alter the wettability of the rock towards water-wetness. Injection of NPs based fluids into the reservoir leads to a change of rock wettability from oil-wet to more water-wet which helps remobilize the adsorbed oil and hence enhances the recovery of residual oil. Moreover, it's reported that the wettability alteration of substrates by NPs is sensitive to many factors including NP size and concentration, initial contact angle, NP charge, the surface wettability of NPs, charge, and roughness of the substrate surface, stabilizer concentration, type and concentrations of ions in the nanoparticle-fluids, bulk pressure and temperature, etc [64-66]. However, some inherent limitations in the contact angle measurements may prevent studies from concluding the effect and mechanism of wettability alteration by NPs in real reservoirs. In the current method, the aged substrates are submerged in the NP-fluid for 2-3 hours or 2 days before employing the contact angle measurements. Other unaged or as-is substrates are exposed to NP-fluid in the cell of the pendant drop apparatus before the droplet is attached to the surface for measuring the contact angle. That is to say, in all these cases, the NPs would already exist at the surface before the measurement (Figure 2.4) while the injected NPs would not touch the surface earlier than residual oil under the reservoir conditions. Focusing on this point, Sofla et al. adopted H<sup>+</sup> protected method to disperse NPs in seawater for measurement. They claimed that the results based on the apparent contact angle measurement may be skewed and overestimated on the change of contact angle. Also, silica NPs can significantly reduce the contact angle only when the initial conditions of the substrates are water-wet.

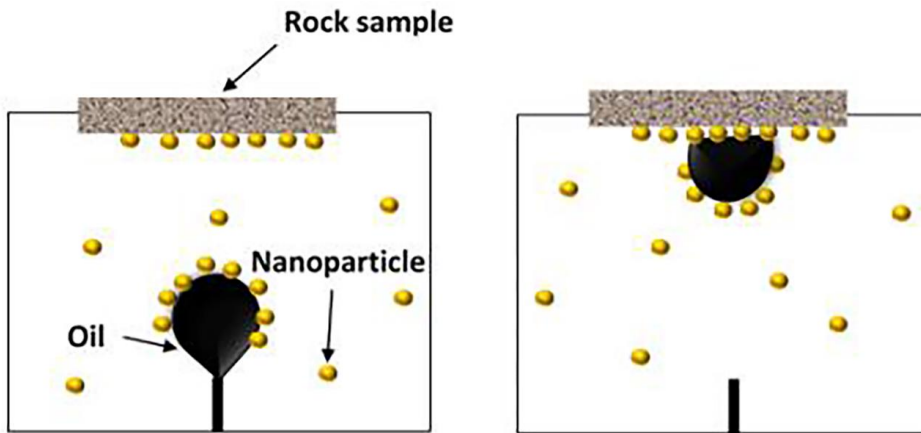


**Figure 2.4** Nanoparticles at the oil-rock interface during conventional contact angle measurements, reprinted from Ref. [66].

In addition, the micro mechanism of wettability alteration by NPs remains controversial. Li et al. observed the adsorption of NPs and adopted it directly as the explanation for wettability alteration by NPs [21]. A few years later, in their recent study, Atomic Force Microscopy (AFM) was used to characterize the structure of NPs covering a glass surface and did research on the impact of roughness on changes in wettability (Figure 2.5). They found that the adsorption of NPs causes uneven roughness and water may stay inside these nanostructures and form a thin water film, preventing oil, which finally induces wettability alteration [67, 68]. Another important point of view was reported by the group of Wason, their studies indicated that structural disjoining pressure is the main reason for wettability alteration by NPs [31, 32], which details would be stated in the following section. Also, the synergic effect of structural disjoining pressure and capillary pressure reduction is also proposed as the mechanism of wettability alteration [66]. In a word, the micro mechanism of wettability alteration by NPs needs more researches to be concluded. Also, like that for IFT, the standard evaluation workflows for wettability alteration by NPs should be established.

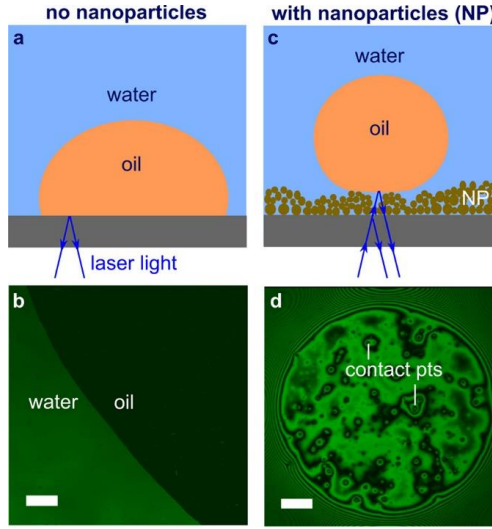


**Figure 2.5** (a, b) Schematic and micrograph showing the oil droplet in contact with the glass substrate with no nanoparticles. The scale bar is  $100\mu\text{m}$ . (c, d) The nanoparticles are able to stabilize a thin water film beneath the oil droplet and the droplet is in contact only with the topmost tips of the nanoparticle aggregates, reprinted from Ref. [67].

## 2.4 Structural disjoining pressure of NPs

In 2003, Wason's research group first presented structural disjoining pressure as the main mechanism for NPs in EOR [28]. They observed an ordered structure for NPs near three-phase contact lines in experiments. They proposed that the NPs tend to form a wedge-like structure in this region and exert extra pressure to push the NPs to move forward and separate the two surfaces. The extra pressure is named structural disjoining pressure. Figure 2.6 shows the schematic diagram of structural disjoining pressure. Structural disjoining pressure was calculated based on statistical mechanics using an analytical expression by the model of hard sphere particles in a vacuum confined between two walls [69].

$$\Pi_{st}(h) = \Pi_1 \cos(\omega h + \Psi_2) e^{-\kappa h} + \Pi_2 e^{-\delta(h-d)} \quad \text{For } h \geq d \quad (2.1)$$

$$\Pi_{st}(h) = -P \quad \text{For } 0 \leq h < d \quad (2.2)$$

In eq. (2.1),  $d$  is the diameter of the nanoparticle and all other parameters ( $\Pi_1$ ,  $\Psi_2$ ,  $\omega$ ,  $\kappa$ ) are fitted as cubic polynomials. In eq. (2.2),  $P$  is the bulk osmotic pressure of the nanofluid. As shown in Figure 2.7, the structural disjoining pressure has an oscillatory decay with the increasing film thickness and the number of nanoparticles inside the film.

In addition, such inner lines or extra pressure were not observed in the case without NPs. Thus, alteration of the structural disjoining pressure by NPs contributes to mobilizing the adsorbed oil on the surface.

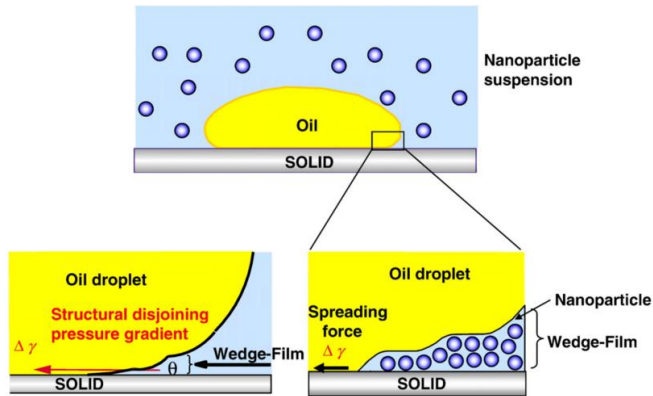


**Figure 2.6** Nanoparticle structuring in the wedge-film resulting in structural disjoining pressure at the wedge vertex, reprinted from Ref. [69].

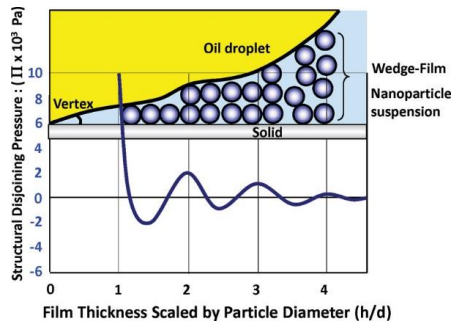


**Figure 2.7** Pressure on the walls of the wedge for  $0.5^\circ$  contact angle at the vertex as a function of radial distance. Particle volume fraction  $\phi = 0.36$  and particle diameter  $d = 10$  nm, reprinted from Ref. [64].

Furthermore, the influence of different parameters such as curvature of oil drop, NPs diameter, effective volume, and nanofluid void fraction on disjoining pressure has also been explored [31,32,91,169]. It has been shown that NPs with higher volume fractions and smaller sizes were much easier to deform the fluid interface. A schematic representation of the effect of increasing the concentration of NPs on disjoining pressure which further leads to wettability alteration has been shown in Figure 2.8. It can be described how the adsorbed oil on the carbon rock surface separated or start desorbing

from the rock surface with increasing concentrations of NPs. It may also be seen that as the NPs concentration increases, the structural disjoining pressure increases. This results in the desorption of the oil layer from the rock surface, and the rock surface becomes water-wet from the oil-wet state.

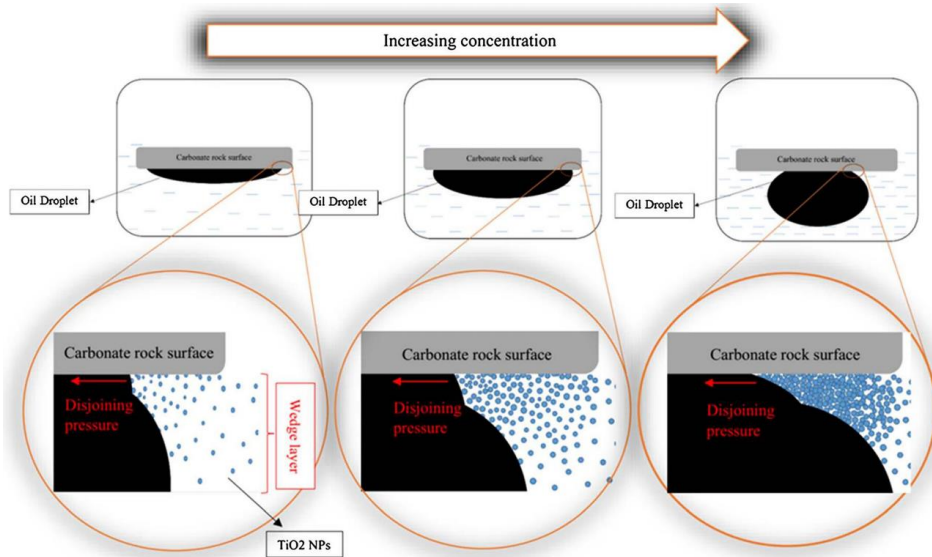


**Figure 2.8** Schematic representation of the effect of increasing concentration of NPs on contact angle and disjoining pressure, reprinted from Ref. [70].

Since it is unrealistic to directly testify whether structure disjoining pressure exists by current experiment conditions, some researchers proved it by theoretical calculation or other auxiliary proof of experimental phenomena. Most scholars just quote this view as the dominating mechanism for NPs-enabled EOR without verifying it. However, there is still certainly a possible weakness in the statement. For example, two contact lines could also occur in other cases of interfacial wetting. What's more, even if the ordered structure was observed, the structure may be like a new wetting phase compared to an oil droplet, so the detachment process is more like the process of the wetting phase replacing the non-wetting phase. That's decided by capillary force rather than structural disjoining pressure. To perfect such a theory, more direct experiments or nanoscale simulations should be further conducted in future studies.

## 2.5 NP-stabilized Pickering emulsion

A Pickering emulsion is an emulsion that is stabilized by solid particles (such as clays as well as synthesized particles) which adsorb onto the interface between the two phases [12]. Compared with the classical emulsions stabilized by surfactant, the Pickering emulsion may display high stability under harsh reservoir conditions owing to the irreversible adsorption of the particles at the interface (Figure 2.9) [71]. The proliferating application of NPs in EOR also brings NP-stabilized Pickering emulsion into the field of view [72]. One is the in-situ formation of Pickering emulsion in NPs EOR process, which results from the snap-off of oil droplets into nanofluids [73, 74]. The viscosity of the emulsions is highly dependent on temperature and the water fraction in the emulsion. Once forming within reservoirs, emulsions confine the flow in highly permeable zones, which forces the injected fluid into lower permeability zones leading to more effective recovery of trapped oil [12]. On the other hand, a Pickering emulsion can be directly adopted as a displacing chemical agent in EOR. Not only because it has better stability despite harsh conditions, but also because it can effectively control the fluidity ratio during the displacement [75, 76]. Kumar and Mandal compared the performance of emulsions stabilized with and without NPs [77]. The NPs stabilized emulsions showed improved wetting behavior, kinetic stability, and incremental oil recovery of 8.54% compared to the case without NPs. Jalilian et al. explored the application of emulsions for EOR using nine different mixtures of solvent, surfactant, and ZrO<sub>2</sub> NPs synthesized using high energy [78]. The results reported an outstanding EOR effect compared to waterflooding due to viscous pressure-drive and other possible EOR mechanisms such as IFT reduction, oil viscosity reduction, and wettability. Hence, the systematic understanding of the movement behavior and physical properties of Pickering emulsions is urgently evoked.

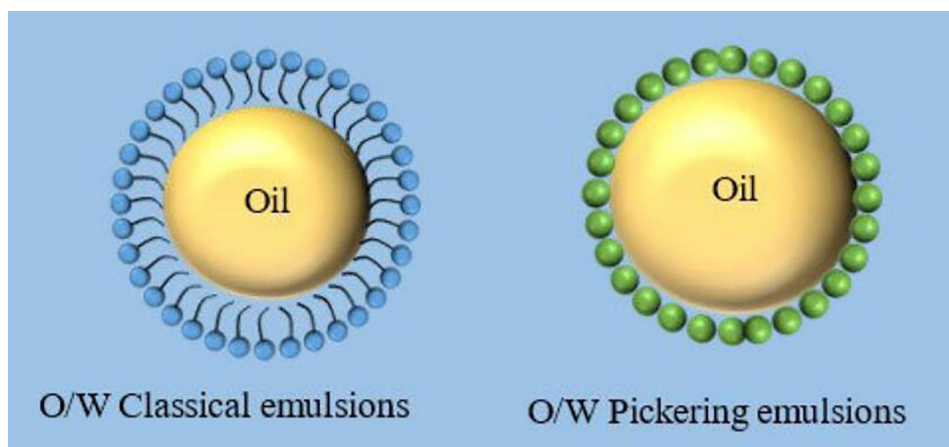


**Figure 2.9** Comparison of Pickering emulsion and traditional emulsion, reprinted from Ref. [71].

In fact, much fundamental work has been done on the stability mechanism of NPs stabilized Pickering emulsion. In general, NPs irreversibly adsorb at the oil/water interface in form of a densely packed layer which protects the droplets against flocculation and coalescence via a steric mechanism to generate stable emulsions [79]. Three main steps of conventional adsorption of NPs have been identified as (1) Particle collision with free newly created interfacial areas during droplet formation. (2) Adhesion of particles to the interface and (3) Oil displacement of water from the particle surface [80]. The adsorption position on the interface is decided by particle hydrophobicity while the duration of adsorbance at the interface is controlled by the surface energy [81, 82]. Although homogenous/bare NPs are surface-active, they are not amphiphilic like surfactants and are considered too hydrophobic or hydrophilic to stably adsorb at the interface. Thus, the partial coating is needed to attain the heterogeneous or ‘Janus’ NPs which are both surface-active and amphiphilic for adsorption kinetics. Apart from the stability mechanism, as shown in Figure 2.10, the properties of Pickering emulsions (such as emulsion type, droplet size, bulk viscosity, and interfacial characteristics) and the influencing factors (covering the NP type, particle concentration, salt concentration, pH of the aqueous phase, and the type of oil) on the emulsion properties have been elucidated in the areas of chemical engineering and materials science [83, 84].



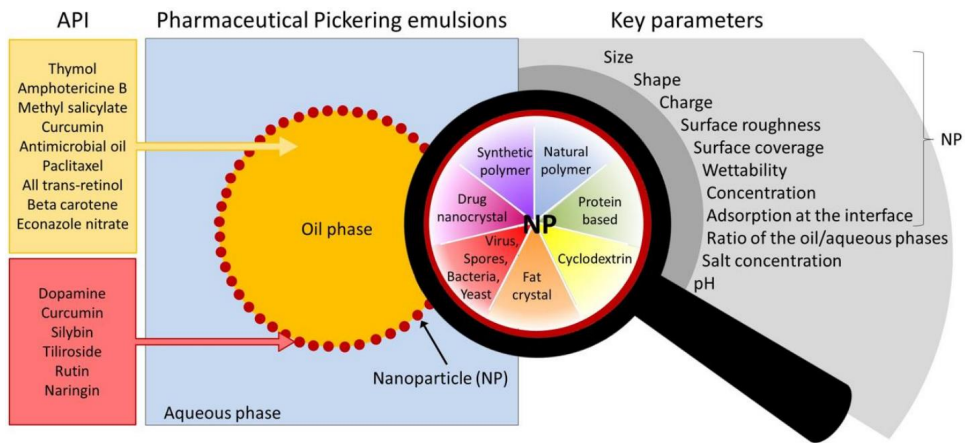


**Figure 2.10** The research topic around Pickering emulsion, reprinted from Ref. [85].

In terms of the EOR application background, the transport of Pickering emulsion in the porous medium should also be focused on. However, such detailed research has not been carried out widely. The related researches on the traditional emulsion are mainly around the plugging performance and fluidity of the emulsion [86, 87]. As depicted in Figure 2.11, three mechanisms are proposed for the plugging phenomena: a single large droplet trapped at the pore throat, multiple small droplets trapped at the pore throat, and narrowing caused by droplet adsorption [86, 88]. The recent work in visualized pore-scale models also verified the above three transport mechanisms [89] and was carried out with some influencing factors like emulsion quality, droplet size, and oil viscosity [90, 91]. In addition, some researchers developed mathematical models to describe the flow behaviors of Pickering emulsions in the porous medium [87, 92].

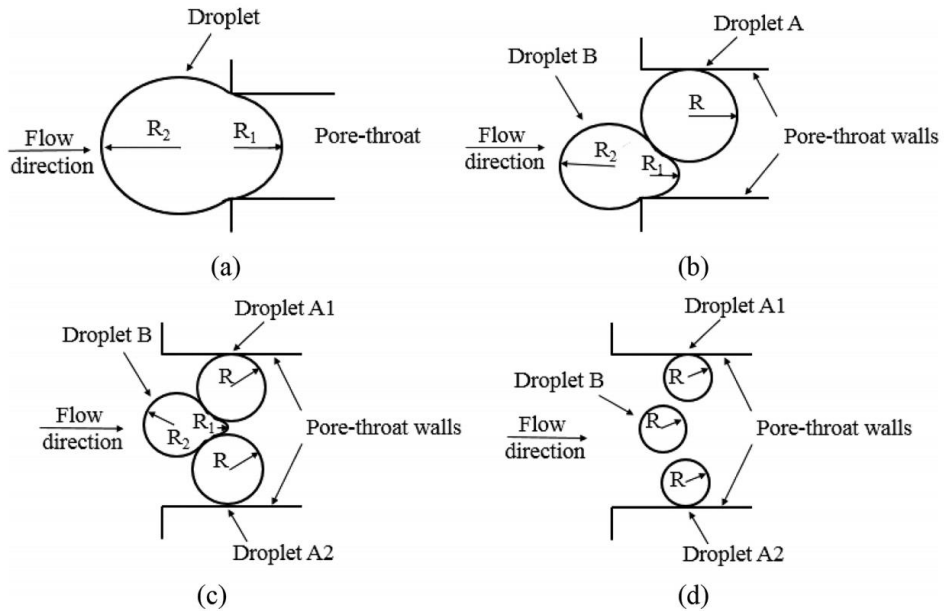


**Figure 2.11** Capture mechanisms of emulsion droplets with different sizes in pore throats: (a)  $d_e > d_t$ , (b)  $d_t/2 < d_e < d_t$ , (c)  $d_e < d_t/2$ , (d)  $d_e < d_t/3$ , reprinted from Ref. [86].  $R$  is the radius of an emulsion droplet,  $R_1$  and  $R_2$  are the curvature radii of the front and the end of an emulsion droplet when it is pushed to move through a pore throat, respectively, and  $d_e$  and  $d_t$  (not shown) are the diameters of an emulsion droplet and a pore throat, respectively.

Nevertheless, the obtained theories for the transport behaviors of the emulsion cannot be perfectly applied to that of the Pickering emulsion considering the special role of the NPs in the process. Because of the size limitation, the current experiments can only provide the overall characterization parameters of the Pickering emulsion flooding system, such as permeability change, pressure response, and oil recovery, which are usually the product of the combined influence of multiple factors or processes. While the specific flow properties and effects of Pickering emulsions are missed. Also, the existing theoretical model faces the challenges of difficulty in collecting certain parameters and model applicability. Thus, detailed information on the interaction of Pickering emulsions with fluids and pore throats is highlighted and warrants further study. Specifically, the nanoscale behaviors of NPs shells of the Pickering emulsion in the transport process are quite eye-catching.

## 2.6 Modification in viscosity and preventing asphaltene precipitation

Different NPs are found to increase the viscosity of injected fluids or decrease the viscosity of heavy oil. A key indicator in the displacement process, the mobility ratio is defined as follows:

$$\lambda_i = \frac{K_i}{\mu_i} \quad (2.3)$$

$$M = \frac{\lambda_D}{\lambda_d} \quad (2.4)$$

Where  $K_i$  is the absolute permeability of porous media,  $\mu_i$  is the displacing fluid viscosity,  $M$  is the mobility ratio,  $\lambda_D$  is displacing fluid and  $\lambda_d$  is displaced fluid. In any displacement process, the mobility ratio affects both the area sweep efficiency and the volume sweep efficiency. For a given injected fluid volume, the sweep efficiency decreases as  $M$  increases. At the same time, the mobility ratio also greatly affects the stability during the displacement process. If the viscosity of the injected fluid is higher than that of the oil in the reservoir, a more piston-like displacement process and a more uniform displacement front can be obtained. Conversely, poor mobility control due to the lower viscosity of the injected fluid can result in a low recovery due to viscous fingering.

Researchers have reported a tremendous increase in fluid viscosity using NPs. For example, Nguyen et al. reported that the viscosity of  $\text{Al}_2\text{O}_3$  and water increased by 5.3 times [93]. Abdullah et al. even claimed an increase of up to 329 times by using NPs [96]. They explained that NPs dispersion increases the injection fluid viscosity by reducing the mobility of the adjoining fluid molecules within the dispersion. NPs create a resistance in the dispersion fluid thereby reducing the original flow properties of the surrounding molecules due to particle collision. On the other hand, NPs have been proved to be a great viscosity reducer for heavy oil (Figure 2.12) [97]. The possible oil viscosity reduction mechanisms including asphaltene adsorption, disruption of asphaltene aggregates and heavy oil viscoelastic network, and recombination of hydrogen bonds for different nanoparticles. However, some of these mechanisms have not been confirmed by experimental characterization.

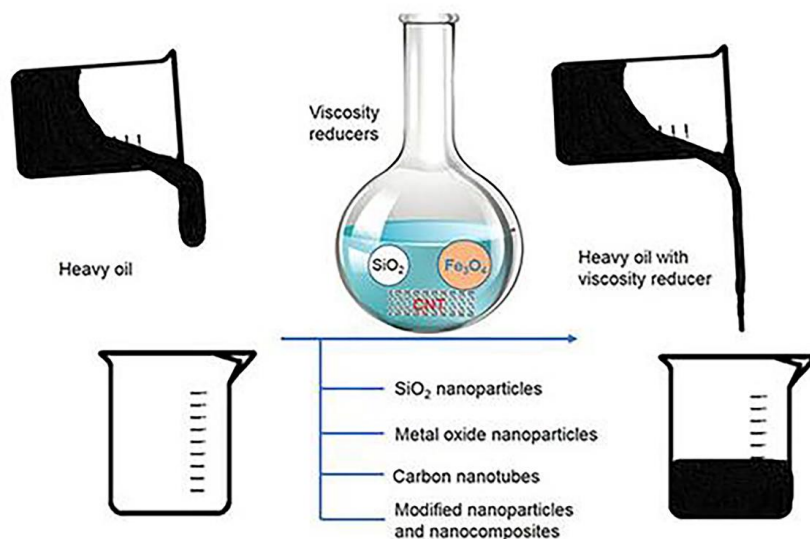


**Figure 2.12** Schematic diagram of nanoparticles as a great viscosity reducer for heavy oil, reprinted from Ref. [97].

Therefore, further research should be done to study the oil microstructure alteration in the presence and absence of NPs by advanced instruments such as X-ray photoelectron spectroscopy and scanning electron microscope. On the other hand, with the rapid development of computational chemistry, it is crucial to explore the interaction between NPs and components of the oil at the molecular level and targeted design NPs for adjustment of viscosity.

In addition, asphaltene precipitation is a process whereby asphaltene molecules leave the crude oil as a detached solid particle [98]. It is one of the major problems in oil recovery mainly caused by changes in the crude oil pressure, temperature, composition, and variations in the mixture of the injected fluid and crude oil. Deposition of the precipitated asphaltene can occur at various locations in the reservoir or production systems which leads to permeability reduction, pore blocking, pipeline transport problems, jamming, and damaging subsurface equipment [40]. It has been found that, with the injection of NPs, the asphaltene can adsorb onto the surface of NPs and prevents it to adsorb onto the pore surface [10]. As shown in Figure 2.13, NPs surround and break down the asphaltene molecules, thus reducing the viscosity and preventing aggregation, precipitation, and deposition onto the rock surface. It is worth noting that the most

efficient NPs in preventing asphaltene precipitation reported in the literature are  $\text{Fe}_2\text{O}_3$ ,  $\text{Al}_2\text{O}_3$ , nickel oxide, and cobalt oxide [99-101]. However, the effect of asphaltene adsorption on other oil displacement mechanisms of NPs remains to be studied. It is expected that in specific cases, the adsorption of asphaltenes may hinder the NPs from exerting their excellent surface-interface effects.

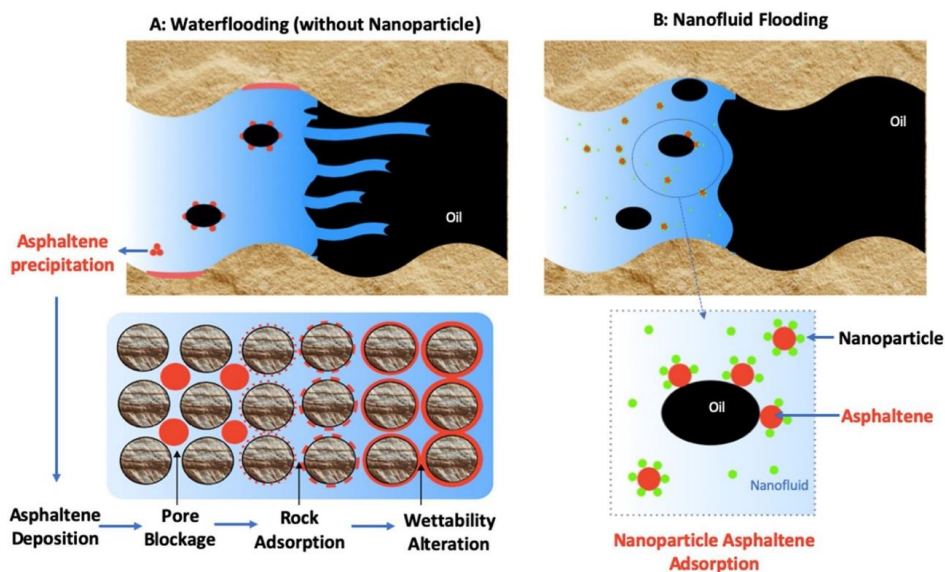


**Figure 2.13** Mechanism of oil viscosity reduction and asphaltene precipitation prevention (a) in the absence of NP, asphaltenes precipitation occurs which may lead to deposition, pore blockage, and wettability through rock adsorption (b) in the presence of Nanofluids, NPs prevent asphaltene precipitation by adsorbing onto the asphaltene molecules, reprinted from Ref. [10].

In summary, six main mechanisms of EOR by NPs have been summarized, namely, the interfacial tension reduction, the wettability alteration of the rock surface, structural disjoining pressure, NP-stabilized Pickering emulsion, modification of viscosity, and preventing asphaltene precipitation. Apart from that, there are some other proposed EOR mechanisms for using NPs, such as core plugging, and alteration of the heat transfer coefficient. However, there is still ambiguity concerning the intrinsic mechanisms of NPs for EOR. The nanoscale behaviors and atomistic mechanism of NPs in oil displacement need to be elucidated to get a comprehensive understanding of the EOR mechanism for NPs

## Chapter 3. NPs-enabled EOR by MD Simulation

---

Due to the limitation of scale, the current experiments cannot fully elucidate the complex mechanisms in the EOR process of nanoparticles. We need nanoscale information to explain the fundamental mechanisms. Molecular dynamics (MD) simulations are proven to be highly suitable for inspecting the basis of EOR in nanofluid/oil/rock systems. As a complementary toolset to experiments, MD simulation is very powerful thanks to its accurate controls on the properties of the nanochannels, oil droplets, and NPs, with an atomic resolution. Specifically, the MD simulation could not only provide the fundamental molecular interactions or the motion pattern but also could contribute to the fine-tuning of the parameters for microscale experiments or simulations. In the chapter, the basic theories about MD simulations, the application potential of molecular modeling in EOR, and simulations related NPs in EOR application will be presented respectively.

### 3.1 Overview of MD simulation

With the development of computer applications in scientific research, the molecular simulation technique is a combination of computer science and basic science. It relies on the software simulation platform and adopts the theory method to simulate the motion behavior of molecules [102]. The main methods of molecular simulations are Quantum Mechanics (QM), Molecular Mechanics (MM), Monte Carlo (MC), and Molecular Dynamics (MD). The research scales for these specific methods are plotted in Figure 3.1. Our focus in the study is the MD simulation. In the following parts, the basic principle

and workflow of MD simulation, and the most important ingredient to MD simulations (namely, the force field) are introduced.

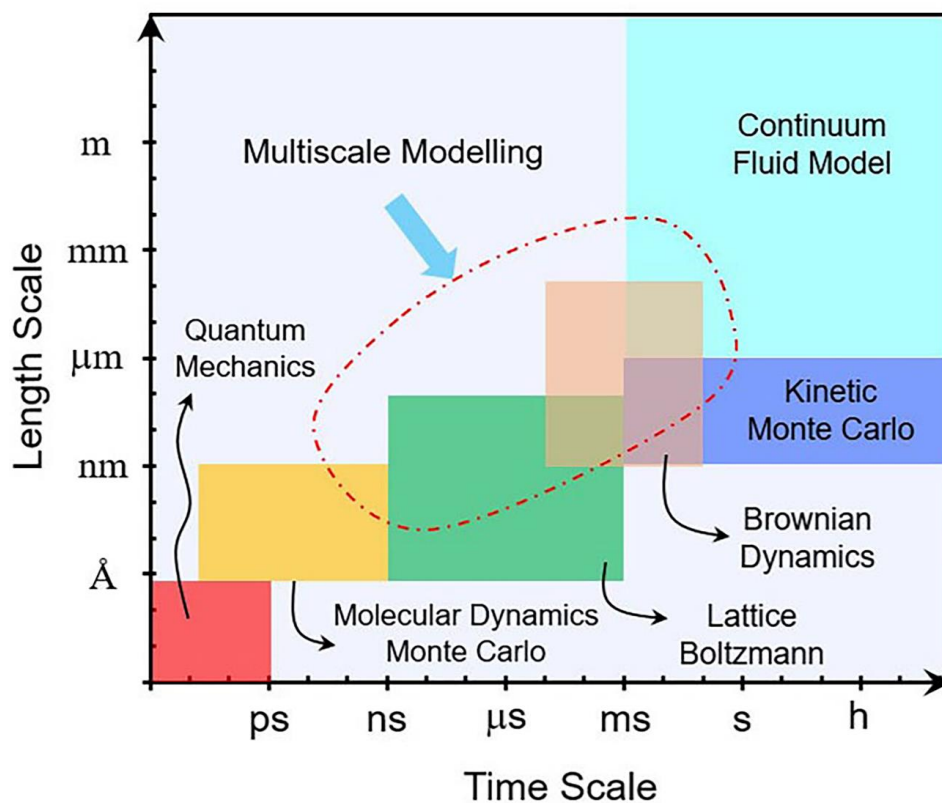


**Figure 3.1** Time and length scales in which atomistic MD simulations, lattice Boltzmann, kinetic Monte Carlo, macroscopic continuum fluid model, and multiple modeling approaches are used. The approach identified as “multiscale” seeks to reconcile the results from the different methods toward describing fluid transport both precisely (e.g., taking into consideration molecular phenomena) and effectively (e.g., achieving length scales relevant for the applications), reprinted from Ref. [103].

Molecular dynamics is a technique that dates back to the 1950s and has been widely used ever since. The principle behind MD is to investigate what happens in a system of atoms and molecules on the basis of Newton’s laws of motion. The individual atoms are considered as point masses with a given potential which describes how they will interact with other atoms in the system. The purpose is to as accurately as possible determine how a system behaves by asking the atoms in the system to find a low-energy state.

For the implementation, MD simulation starts with the integration of Newton's second law. Applying appropriate integral methods, such as the Gear finite-difference algorithm or the Verlet method, the basic dynamics parameters such as position, velocity, and interaction force can be decided. The macroscopic physical properties such as pressure, mean velocity, temperature, particle number density, etc. can subsequently be determined via statistical mechanics.

Here, take the fluid system in the channel as an example, through the MD method, the Newtonian equation for each fluid molecule is expressed as:

$$m_i \frac{d\vec{r}^2}{dt^2} = \sum_{j \neq i, j=1}^N \vec{F}_{ij} + \sum_{j_w \neq i, j=1}^{N_w} \vec{F}_{ij_w} + \vec{F}_{sou} \vec{l} \quad (3.1)$$

where the subscript  $i$  represents particle  $i$ , and  $\vec{l}$  is the unit vector in the  $x$ -coordinate. The first term of the right-hand side of eq. 3.1 is the molecular force due to Lennard–Jones (LJ) potential between particle  $i$  and other fluid molecules  $j$ . The second term is the molecular force between particle  $i$  and all the solid wall particles  $j_w$ . The last term in the equation represents the external force, which makes the fluid deviate from the equilibrium, such as electric force or pressure. When a two-body potential model is applied, the interaction force between a pair of molecules comes from the following relation:

$$F_{ij} = -\frac{\partial \varphi_{ij}}{\partial r_{ij}} \quad (3.2)$$

The LJ potential  $\varphi(r)$  is given by:

$$\varphi(r) = 4\varepsilon \left[ \left( \frac{\sigma}{r} \right)^{12} - \left( \frac{\sigma}{r} \right)^6 \right] \quad (3.3)$$

where  $r$  is the distance between two atoms or molecules,  $\sigma$  is the molecular length scale, and  $\varepsilon$  is the interaction strength parameter. The choice of cutoff distance has to be very careful. Beyond such distance, it is assumed that the molecules do not interact. If the value is too short, the atoms will not be able to see their neighbors. And even if set slightly higher than this, physical properties like pressure may not be accurate. The values of the parameters  $\sigma$  and  $\varepsilon$  are determined by the type of wall and fluid molecules. They are named as  $\sigma_{wf}$  and  $\varepsilon_{wf}$  when eq. 3.3 is applied for the potential interaction between fluid particles and solid wall particles.

Finally, combining eq. 3.3 and eq. 3.2 with eq. 3.1 and applying the shifted potential and shifted force, we obtain the basic equation for each fluid particle. The shifted force



technique ensures that the molecular force between fluid particle  $i$  and other fluid particles or other solid wall particles is reduced to zero once the distance between such fluid particle and other particles reaches or is beyond the cut-off distance. The main advantage of doing so is to save a lot of computational time for force integration.

$$24 \frac{\varepsilon}{\sigma} \sum_{j \neq i, j=1}^N \left[ 2 \left( \frac{\sigma}{r} \right)^{13} - \left( \frac{\sigma}{r} \right)^7 - 2 \left( \frac{\sigma}{r_c} \right)^{13} + \left( \frac{\sigma}{r_c} \right)^7 \right] \frac{\vec{r}_{ij}}{|r_{ij}|} + 24 \frac{\varepsilon_{wf}}{\sigma_{wf}} \sum_{j_w=1}^{N_w} \left[ 2 \left( \frac{\sigma_{wf}}{r} \right)^{13} - \left( \frac{\sigma_{wf}}{r} \right)^7 - 2 \left( \frac{\sigma_{wf}}{r_{cw}} \right)^{13} + \left( \frac{\sigma_{wf}}{r_{cw}} \right)^7 \right] \frac{\vec{r}_{ijw}}{|r_{ijw}|} + \vec{F}_{sou} \vec{l} = m_i \vec{a}_i \quad (3.4)$$

Thus, the movement of the fluid particles will be predicted by these basic physics laws and the dynamics of the systems will be finally obtained.

The main steps to set up and run an MD simulation are provided in Figure. 3.2. First, the built simulation box contains all molecules that can be described by the selected force field parameters and that are compatible with each other. The preliminary simulation box may contain conflicts between atoms that must be removed before running the MD simulation. These collisions are energetically unfavorable due to the steep gradient of the repulsive part of the LJ potential. The most recommended method is to run an energy minimization, i.e., an algorithm that, through a series of steps, optimizes the positions of each atom based on the potential terms. Among the existing different minimization methods, a gradient descent optimization algorithm is the most widely used. After the energy of the system has been minimized, MD simulations can be run.

To further apply control on the physiological conditions of the simulation, the MD integrator must be run with additional tools that restrain the system. a so-called thermostat and/or a barostat must be applied. Another boundary condition that must be applied concerns how to treat the edges of the simulation box, which has a finite size. For example, surface effects can be minimized by replicating the simulated box in all the dimensions, and applying the so-called periodic boundary conditions. Then, an additional period is mandatory to equilibrate the whole system. When the key thermal dynamics properties of the system have reached a plateau, the system can be considered at equilibrium and all the analyzes should be done on the equilibrated part of the trajectory, which is often referred to as the production part of the MD simulation.

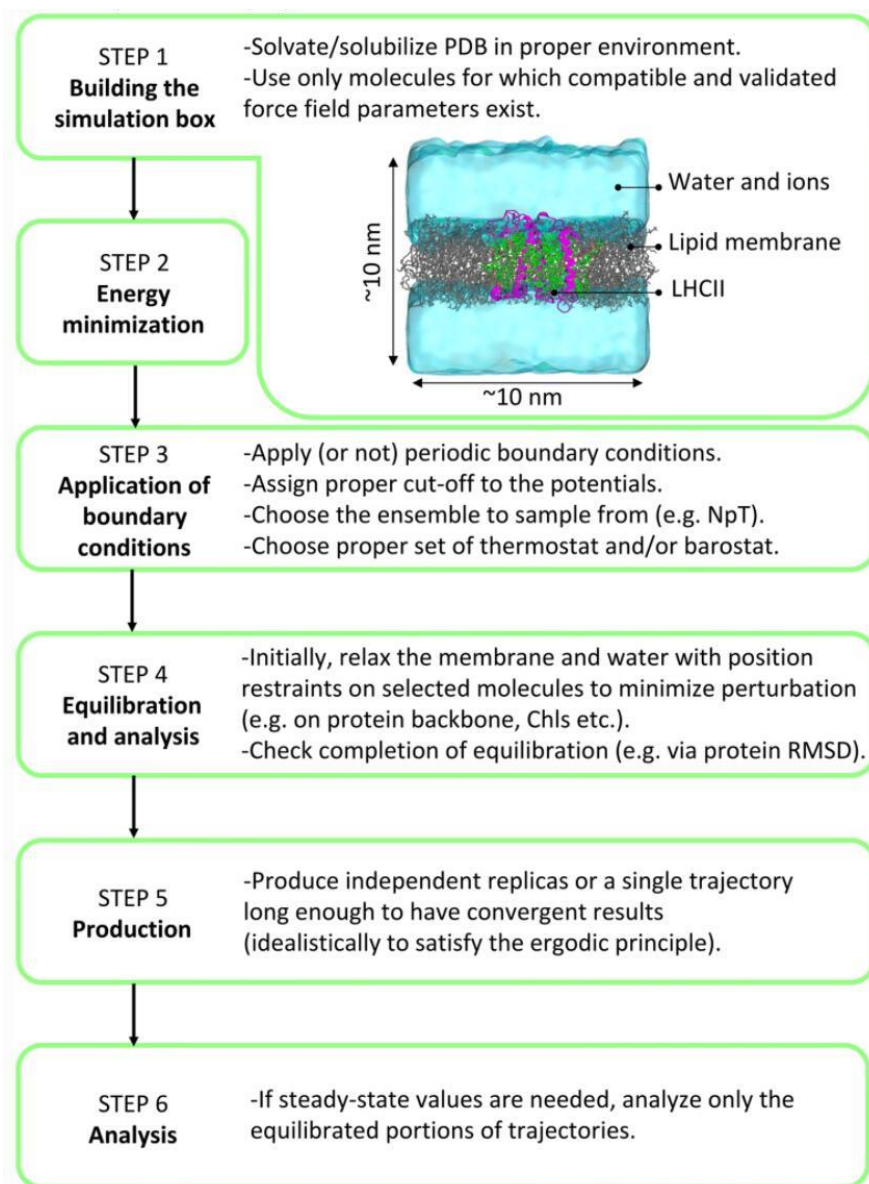


**Figure 3.2** Workflow of an MD simulation, as described in Sect. 2.3. The sequential steps are reported together with the associated main points that need specific attention. In the inset, an example of a simulation box for LHCII embedded in a model membrane is reported with water in cyan, lipid membrane in gray, protein in magenta, Chls in green, and Cars in orange, reprinted from Ref. [104].

For the whole MD simulation process, the most important ingredient is the force field. As mentioned, each molecule is approximated as a system of classical point particles,

or interaction sites. Depending on the chosen resolution, such particles may represent atoms or groups of atoms. The motions of the particles are obtained by solving the classical Newton equations for the system. The forces acting on the particles are computed over time and depend on the particle positions and the total potential energy of the system ( $V_{tot}$ ). Electrons are treated adiabatically which means that electronic degrees of freedom are not explicitly taken into account. The particles represent the properties of nuclei evolving on a Born–Oppenheimer potential energy surface. This also implies that molecules are studied in their electronic ground state.  $V_{tot}$  of the simulated system contains the bonded and non-bonded potential energies:

$$V_{tot} = V_{bonded} + V_{non-bonded} \quad (3.5)$$

$V_{bonded}$  is the sum of the potential energy associated with chemical bonds, bond angles, and torsional angles (dihedrals) between groups of, respectively 2, 3, and 4 particles. The mathematical description of the bonded potentials can be slightly different for the different models which are available, but typically, the bonded potentials are modeled either via harmonic potentials ( $V_{bond}$  and  $V_{angle}$ ) or via cosine-based functions ( $V_{dihedral}$ ), as described by the following equations:

$$V_{bonded} = V_{bond} + V_{angle} + V_{dihedral} + V_{improper} \quad (3.6)$$

$V_{non-bonded}$  describes the interaction between any pair  $i,j$  of particles. It is the sum of van der Waals, often modeled as a Lennard Jones (LJ) potential ( $V_{LJ}$ ), and Coulomb ( $V_{coulomb}$ ) interactions:

$$V_{LJ}(r) = 4\varepsilon_{ij} \left[ \left( \frac{\sigma_{ij}}{r} \right)^{12} - \left( \frac{\sigma_{ij}}{r} \right)^6 \right] \quad (3.7)$$

$$V_{coulomb} = \frac{q_i q_j}{4\pi \varepsilon_0 \varepsilon_r r} \quad (3.8)$$

Where  $\varepsilon_{ij}$  is the depth of the potential well of  $V_{LJ}$ , and  $\sigma_{ij}$  is the distance between the pair of particles at which the potential is zero. In  $V_{coulomb}$ ,  $q_i$  and  $q_j$  are the charges of two different particles, while  $\varepsilon_0$  and  $\varepsilon_r$  are vacuum permittivity and the relative dielectric constants, respectively. In both potential terms,  $r$  is the distance between the two atoms or molecules.

Thus, the set of all the information needed to build up the potential energy terms of a system of particles is the force field. It consists of the list of functional forms and parameters for all bonded potentials as well as for the non-bonded terms. Having a correct or suitable force field for the system is always the most crucial thing to MD simulations.

### 3.2 Application potential of MD simulations in EOR

As mentioned in section 3.1, with a reliable force field choice, MD simulations can accurately determine the physic and chemical properties of fluids, solids, and their interfaces under realistic and operational conditions. However, MD simulations require a significant computational effort to model the oil & gas industry systems. Usually, these phenomena involve longer dynamic processes, slow aggregation regimes, and fluids composed of large molecules with tens or hundreds of atoms. In this context, the research within the molecular modeling framework applied to EOR has benefited from the significant advances in computational hardware technology. In particular, with the recent development of molecular modeling on graphics processing units (GPU) which can accelerate the calculations tens of times. Recent advances in parallel computing allow tackling problems involving the understanding of molecular-level interaction effects under realistic conditions of reservoirs [105].

The application advantages of molecular simulation in EOR are mainly reflected in unraveling the interaction details of different bulk phases and their interfaces. This information is critical to the upstream oil and gas industry, as improved oil recovery efficiency in oil wells depends on brine-rock-oil interface properties, including wettability, viscosity, and specific interactions between rock and fluid. Molecular dynamics can characterize the physicochemical properties of these geologically relevant interfaces at the molecular scale. Not only that, MD simulations can help us visualize the laws of molecular motion and even the distribution of ions or hydrogen bonds. This contributes to fundamentally understanding the scientific mechanism of a specific oil displacement process. For example, the oil recovery by fluid injection into the dome above the oil zone can be favored by modifying the interfacial tension between the immiscible fluids. In this context, de Lara et al. investigated the interface wettability, diffusivity, and molecular orientations between crude oil and different fluids by molecular dynamics [106]. These findings indicate an increase in the salt concentration and pressure lead to an increase in the interfacial tension, which may enhance the mechanical contact between the fluids.

At present, molecular simulations have many successful cases in the research of EOR. The main content is the molecular simulation study of the interfacial properties of

oil/water systems involving surfactants, polymers, foams, and nanoparticles [107]. In these topics, MD simulation can analyze the aggregation behavior at the interface from a microscopic point of view, predict and supplement the experiment, and also provide a theoretical basis for many phenomena that cannot be explained by the experiment. It has great potential to bridge the gap between pure theoretical research and practical experiment.

Although molecular modeling technology has attracted a lot of attention in the petroleum field, it is still in the development stage in reservoir analysis. There are several aspects that need to be improved, and that require further study to make this technology a commonly used tool in EOR. That includes the use of MD simulation to design generally acceptable models and procedures to represent complex reservoir fluids and heterogeneous porous media, develop fluid and rock property prediction toolboxes, and further improve the fundamental understanding of the mechanism and the efficiency prediction of EOR technology, especially for less mature EOR methods such as the NP-enabled EOR studied in this work.

In fact, for the topic of NP-enabled EOR, many scholars have applied MD study. According to atomic modeling, it is usually divided into two categories: NPs in the system with or without the involvement of a solid surface. In the following sections, the literature review will be conducted separately.

### **3.3 NPs in liquid/liquid system**

The study of the interactions between the chemical agent and oil and water is key to the understanding of the EOR mechanism. Due to the limited system composition, the nanofluid/oil system is the most efficient one for exploring the behaviors and properties of NPs at the liquid interface in EOR. So far, a lot of molecular dynamics (MD) simulation and dissipative particle dynamic (DPD) simulation works have been reported on the oil/water system in the presence of NPs. A series of thermodynamic and structural properties such as three-phase contact angle, IFT, diffusion coefficient, and interfacial structure, have been explicitly studied [108-112].

Frost et al. employed MD simulation to observe the NPs' microscopic process of diffusion and migration to the interface [113]. It was found that when the interface is in an equilibrium state, hydrocarbon NPs are more likely to aggregate in hydrophobic media.

Cheung et al. studied the influence of NP size on transport properties using MD simulation [114]. It was reported that the larger the radius of the nanocluster, the greater the difference in diffusion coefficient between the interface and the bulk phase. Moreover, the influence of the charged ability of NPs on the interface properties was considered. Dai et al. studied the movement process of hydrocarbon nanoparticles from the water to the water/trichloroethylene interface, and the effect of charged nanoparticles on its migration and assembly process by MD simulation. It was concluded that pure hydrocarbon nanoparticles could migrate to the interface but could not exist stably at the interface. To some extent, they gathered into clusters in the trichloroethylene phase. When the electric charge is applied to the nanoparticles, the nanoparticles become more and more stable at the water/trichloroethylene interface with the increase of the charged amount [115]. Song et al. studied the oil/water interface and investigated the effect of the charge ability of hydrocarbon nanoparticles on the stability of the interface and get similar results to Luo et al [116]. They also presented that because of the electrical properties of water molecules, as the charge is increased to a certain value, all hydrocarbon nanoparticles will be immersed in water as plotted in Figure 3.3.

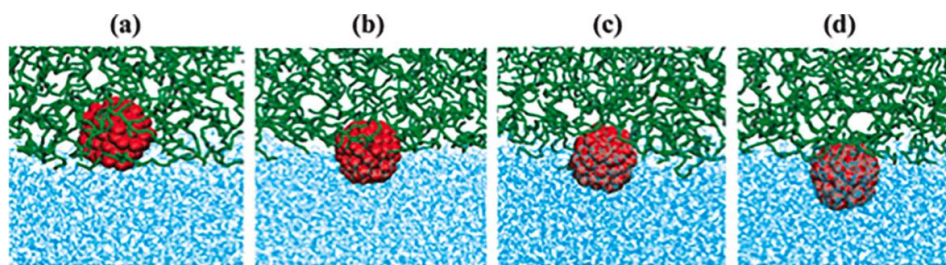


**Figure 3.3** The state of nanoparticles with the different charges at the interface. (a) No charge (b) 4 negative charges (c) 6 negative charges (d) 8 negative charges, reprinted from Ref. [116]. The nanoparticle is in the red sphere, the water phase is in blue, and the PDMS phase is in green.

With this type of system, another important research topic is the effect of NPs on IFT. Interestingly, the conclusions drawn by scholars with different systems are not consistent. Gao et al. explored the effect of the shape of Janus NPs on their interfacial activity at fluid/fluid interfaces via MD simulations [117]. It's found that changes in the shape of Janus particles strongly influence the IFT at the fluid-fluid interface. Lara et al. adopted all-atom MD to study the behavior of functionalized silica NPs at crude oil/brine interfaces with the influence of salt, brine concentration, temperature, and NP surface

functionalization [110]. For the first time, a multicomponent model for light crude oil has been employed to study this brine/NP/oil interface. The results show that the IFT is obviously reduced by adding NPs and the highest contact angles occur at higher salt concentrations. Fan et al. studied the effects of modification methods and modification concentration on the adsorption morphology of single silicon nanoparticles at the decane/water interface by all-atom MD simulations [118]. It was found that the ability of half-edge modified nanoparticles to reduce IFT was higher than that of uniformly modified nanoparticles, and the ability to reduce interfacial tension is the best when the modified concentration reached 50%. This is due to the different contact angles and desorption energies of nanoparticles at the oil/water interface by different modification methods. With the larger simulation scale, Alberto Striolo et al. used the dissipative particle dynamics (DPD) simulation method to study the interfacial behaviors and properties of NPs [32, 119]. It is also proved that the modification of nanoparticles and the three-phase contact angle of nanoparticles at the interface affect the self-assembly morphology of the interface. Based on this, they further uncovered the influence of the aspect ratio of ellipsoidal nanoparticles and the hydrophilic/lipophilic ratio of nanoparticles on their self-assembly behavior at the interface. They concluded that NPs can effectively reduce the IFT at a sufficiently high surface coverage. However, other researchers using MD simulation claimed that the oil-water IFT is independent of the presence of NPs and their concentration [110, 111]. Especially, Li et al used MD simulations to investigate the effects of NPs (hydrophilic, hydrophobic, and Janus NPs, respectively) and salt concentration (NaCl and CaCl<sub>2</sub>) up to ~11 wt% on the oil-brine IFT and other interfacial properties under typical oil reservoir conditions (Figure 3.4) [120]. Although oil-brine IFT increases as the salinity increases in their simulations, the three-phase contact angle is independent of the salinity and cation types. And also, the presence of NPs leads to a negligible influence on the oil-water IFT.

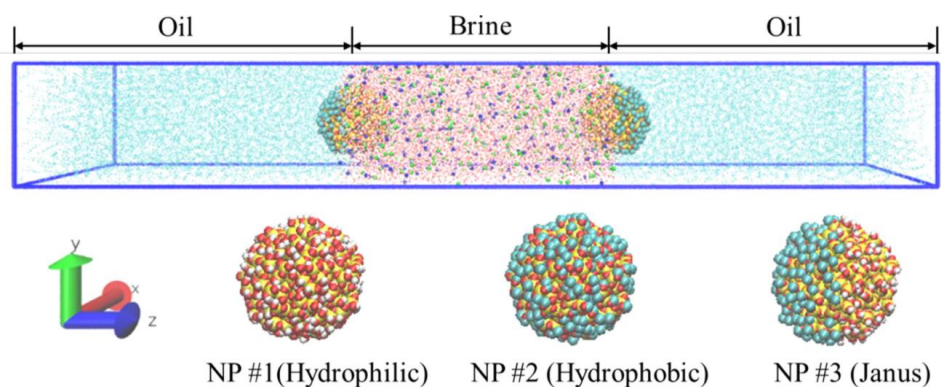


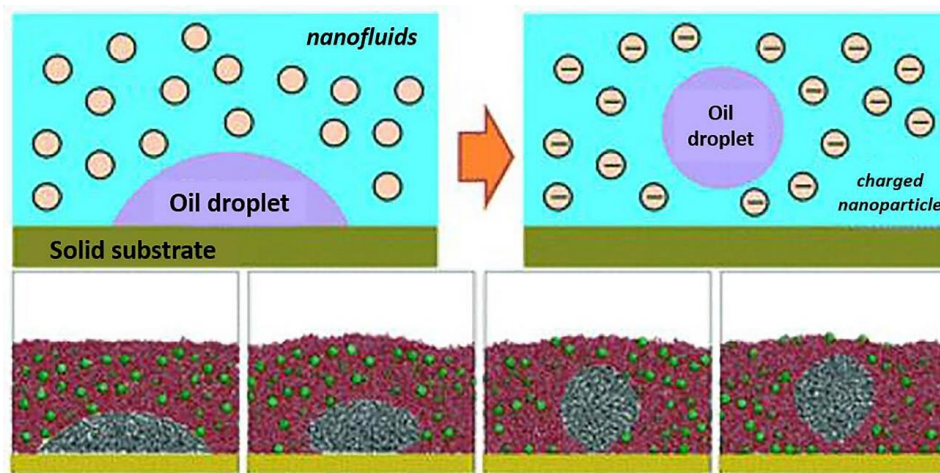
**Figure 3.4** Initial configuration of the system and various NPs. The blue and green spheres in the brine are  $\text{Na}^+$  and  $\text{Cl}^-$ . NPs are at both sides of the brine, reprinted from Ref. [120].

### 3.4 NPs in oil/water/surface system

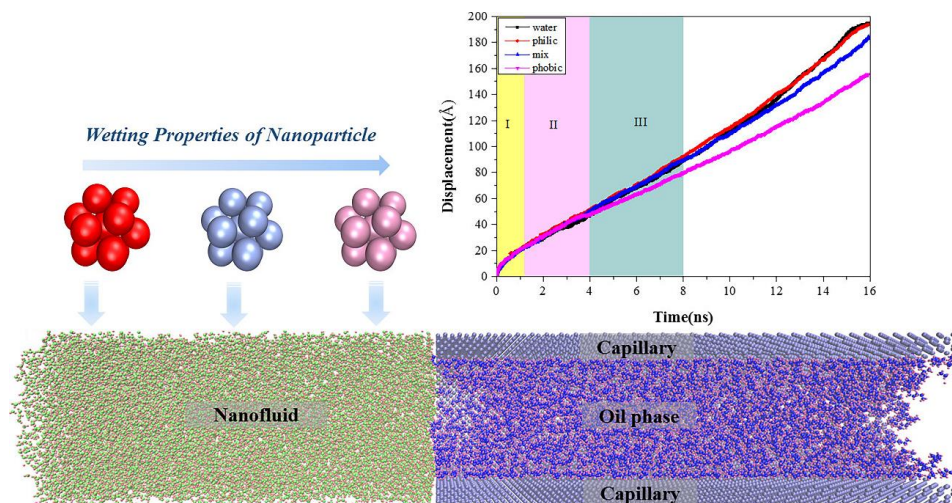
More than in the fluid/fluid system, the nanoscale dynamics of NPs in oil trapping channels directly reveal the mechanisms of nanofluids in EOR, which is challenging to capture with the current experimental conditions. Due to the high computational expense, only a small number of studies have been carried out on the NPs involved in displacement/transport in the channel. Wang and Wu established a simulation model of two immiscible fluids confined in a slit between two solid walls to analyze the effect of the bulk concentration of NPs on the motion of the three-phase contact line [121]. It's found that larger volume concentrations resulted in more pronounced NP adsorption on the solid surface. This further leads to a propulsive displacement of the contact line compared to the case without the NPs. Further, they investigated the detachment of oil droplets by charged NPs from solid surfaces (Figure 3.5) [122]. The results show that the charged nanofluids can significantly improve the oil removal efficiency. Only if the charge of the NPs exceeds a threshold, the oil droplets can spontaneously detach. Also, the surface wettability of NPs plays a crucial role in the oil removal process. Wu et al. simulated the flow behavior of nanofluids in confined channels filled with oil and focused on the displacement pressure change in the process [123]. It's reported that the displacement pressure increases with the propelled displacement without NPs while the pressure decreases with the displacement with the appearance of NPs in the system. Wang et al. systematically uncover the transport of nanofluid in the ultra-confined oil-filled channel with such nanofluid/oil/surface system. A representative system can be seen in



Figure 3.6. The series of works first uncovered the influence of NPs on spontaneous water imbibition into ultra-confined channels and proposed a competitive mechanism of NP effect on spontaneous imbibition [124]. Then spontaneous and pressure-induced water-oil displacement processes controlled by surface wettability of NPs were investigated respectively [125-127]. The dominating mechanism and the optimal types of NPs were provided.



**Figure 3.5** The detachment of the oil droplet from the solid surface by charged NPs, reprinted from Ref. [122].



**Figure 3.6** The system for studying the displacement of nanofluid in the oil-filled channel, reprinted from Ref. [125]. The bottom one is the side view of the simulation system containing a water-based nanofluid

(green and pink) laden with well-distributed spherical NPs, an oil phase (blue and purple), and a capillary (purple). The right top is the displacement of nanofluids into the capillary as a function of time.

Even though notable atomistic investigations considering the effects of rock surface properties have been done, it's still far from fully revealing the mechanism of NPs in the EOR process. The reported simulations were all based on a smooth solid surface, which cannot fully reflect the flow characteristics of nanofluids on rough rock surfaces in a realistic [128-130]. Apparently, the motion pattern and the roles of NPs in EOR in the rough channel are different from the ideally smooth surface adopted in the previous studies. Also, the fluid inside the confined channel in these systems was only oil, which cannot represent the residual oil characteristics in most pores in the EOR stage. Thus, more MD systems can be designed and simulated to provide a better understanding to perfect the theory of NPs in EOR applications.



## Chapter 4. Main Results

---

The main results obtained from MD simulations about nanofluids displacement and mechanisms in the channel are briefly summarized in this chapter.

### 4.1 Displacement of trapped oil in rough channels by nanofluids

Firstly, the displacement mechanisms of trapped oil in the rough channel by injection of nanofluids using MD simulations are uncovered (as described in Figure 4.1). The study indicates that hydrophilic and Janus NPs are able to drive significantly more trapped oil out of rough channels, while hydrophobic NPs have the lowest potential in trapped oil displacement with endangering probability of channel blockage. Specifically, hydrophilic NPs dispersed in water increased the viscosity of the injected fluid and disturbed the original stream field. This enhances the friction to the oil phase at the oil-water interface and enlarges the sweeping scope of the displacing phase. Janus NPs can adsorb not only at the oil-water interface to reduce the interfacial tension but also onto the rough surface. Driven by the injected flow, surface wettability, and possible structural disjoining pressure, Janus NPs can migrate along the solid surface and into the trapped oil phase, and further can exclude oil out of the trapping pockets and alter the local surface wettability. Meanwhile, the slippage of Janus NPs at the interface also contributes to the EOR effect. In contrast, hydrophobic NPs disperse into the oil phase and further form clusters, which shows a negligible displacement effect.

Moreover, the effect of pumping force on oil displacement is clarified. Higher pumping force leads to better oil displacement in all the systems. Particularly, Janus

NPs show outstanding EOR potential with low pumping force. The low force allows for more contact between Janus NPs and trapped oil, which is beneficial for the EOR effect. Such phenomena are supported by the analysis of the capillary number, which suggests the EOR application potential of Janus NPs in actual reservoir conditions.

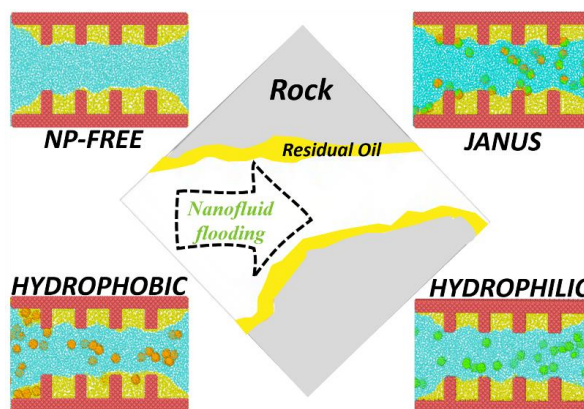


**Figure 4.1** Displacement of trapped oil in rough channels by NPs.

Highlights:

- Hydrophilic and Janus NPs are able to drive more trapped oil out of rough channels, while hydrophobic NPs hold the lowest displacement potential and can even block the channel.
- The main mechanism for the hydrophilic NPs to displace the residual oil is to increase the viscosity of the injected fluid. Janus NPs are able to remobilize residual oil by altering the local surface wettability. While the hydrophobic NPs further lock the trapped oil.
- With the displacement pressure reduce and close to the reservoir conditions, Janus NPs lead the best displacement effect on the residual oil.

## 4.2 Oil displacement on the rough surface by Janus nanoparticles

In order to elucidate the displacement dynamics and mechanisms of Janus NPs, the oil extraction from the rough surface by Janus NPs (JNP) is investigated using the local enlarged surface systems (Figure 4.2). It's found that Janus NPs with larger polar faces (25JNPs and 50JNPs) achieve the notable oil extraction effect, compared to 75 JNP and free-NP. The structure of adsorbed NPs on the side wall of the groove closely affects the oil extraction. Altering the solid wall to be more hydrophilic by adsorbed Janus NPs can lead to deeper migration of the NPs into the nano-pocket and more oil extraction.

Moreover, the ‘adsorption invasion process’ is observed in the formation of the adsorption structure of Janus NPs and also in the dynamics of wettability alteration by Janus NPs. Specifically, by identifying the oil-water interface, NPs adsorb on the surface. Constrained by the pinning effect, the adsorbed NPs slide at the oil-water interface and stay on the edge of the surface. Under the impetus of local water flow, the NPs embed into the groove along the surface. With the collision and pushing by other NPs, the embedded NPs continue to deepen inside the pocket until the lack of driving force. Besides, identification of the residual oil, displacement pressure, and the geometry of the inside oil-water interface are proposed as the controlling factors of the ‘adsorption invasion process’. Ultimately, the optimization case with huff-n-puff as the work mode gains outstanding effect and verifies our viewpoints.

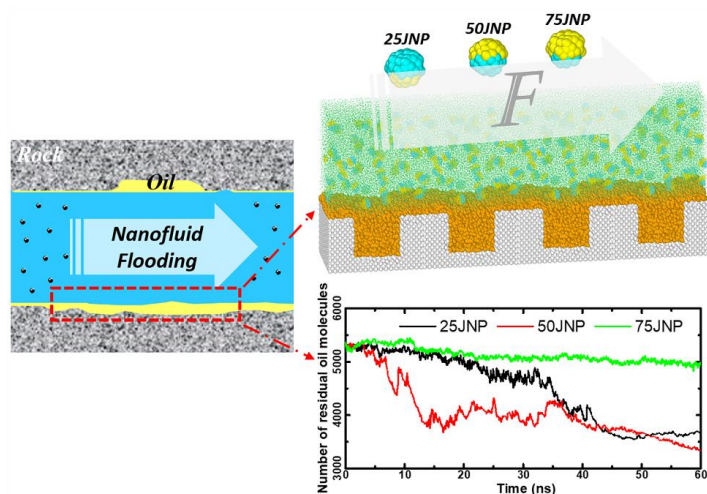


**Figure 4.2** Oil displacement on the rough surface by Janus NPs.

Furthermore, as shown in Figure 4.3, the effects of the surface geometric parameters in oil displacement by JNPs are analyzed. It's reported that only when the surface is neutrally wetted or weakly hydrophobic, JNPs can form an effective adsorption film through the ‘adsorption invasion process’ and obtain the great oil displacement effect. For the rough surface with a given wettability, the four geometric factors have specific effects on the displacement process and EOR results. The tip length of the bulge determines the amount of JNPs that can accumulate on the surface. The more JNPs on the plane can accelerate the formation of the adsorption film. As the tip length of the bulge reaches a threshold, the final properties of the adsorption film and the EOR effects maintain stable while the required displacement time decreases with the enlargement

of length in a certain range. Although the selectivity on EOR of entry angle and exit angle is similar (the smaller value is the preference). The different entry angles correspond to various areas of adsorption film and the contribution of adsorption film in wettability alteration while the exit angles master the amount of uncovered trapped oil at the exit side. Lastly, the aspect ratio has a huge impact on the morphology of the oil-water interface. The oil-water interface can reach the bottom of the surface under the case with a large aspect ratio, which brings an excellent displacement effect. Based on it, the shallow grooves are highly welcomed for JNPs' displacement. Among the four parameters, the aspect ratio will play a leading role in the final EOR effect as long as the tip length of the bulge reaches the threshold.

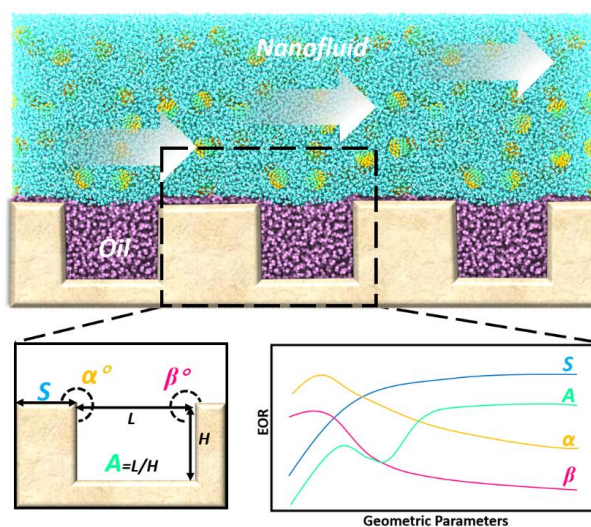


**Figure 4.3** The effect of the geometric parameters in oil displacement on the rough surface by Janus NPs.

#### Highlights:

- The local wettability alteration dynamics of Janus NPs are proposed, that is, the 'adsorption invasion process'.
- To enhance the 'adsorption invasion process', identification of the residual oil, displacement pressure, and the morphology of the inside oil-water interface are crucial factors.
- The applicable surface for JNPs to efficiently displace residual oil is neutrally wetted or weakly hydrophobic.

- For the process of Janus NPs displacing the residual oil, the aspect ratio of the oil-trapping grooves dominates the EOR effect among the key surface geometry parameters.

### 4.3 Deformation and rupture of Pickering emulsion in transport

Lastly, the nanomechanical property and the transport mechanism of Janus NPs stabilized Pickering emulsions with different JNP coverage ratios ( $\phi$ ) across the pore throat are studied. Through the compression test on the solid surface, Pickering emulsions are found to be mechanically robust by the JNP shell and recover from large deformations. Also,  $\phi$  has little effect on the deformation of the Pickering emulsion on the hydrophilic surface. While on the hydrophobic surface, emulsions rupture after deformation because of the strong attraction between the oil core and surface. The larger  $\phi$  of the emulsion, the greater deformation and stress can be withstood at rupture. More importantly, as long as the  $\phi$  of the emulsion reaches the critical value, the JNP shell can form an ordered quasi-solid structure and act as an effective protection pad. The increased droplet size of the emulsion retards the weakening of such barrier effect in compression, allowing greater deformation on hydrophobic surfaces.

In transport, different emulsions have similar force response patterns through the hydrophilic pore throat. Although the one with larger  $\phi$  experiences relatively less resistance at the entrance. The varied interaction of the specific emulsion with water, to some extent, narrows the gap in resistance. In addition, the smaller opening angle of the pore throat ( $\beta$ ) induces a larger Jamin effect and promotes the interaction between the emulsion and the pore throat, which increases the retention of JNPs at the pore throats on the emulsion. On the other hand, for the transport across the hydrophobic pore throat, the difference in resistance at the entrance between groups is more pronounced. This originates from the different shielding effects of JNP shells on the interaction between the oil core and the residual oil. More importantly, the effective enough shielding role of the JNP shell in the transport ensures the smooth entering of emulsion inside the pore throat.



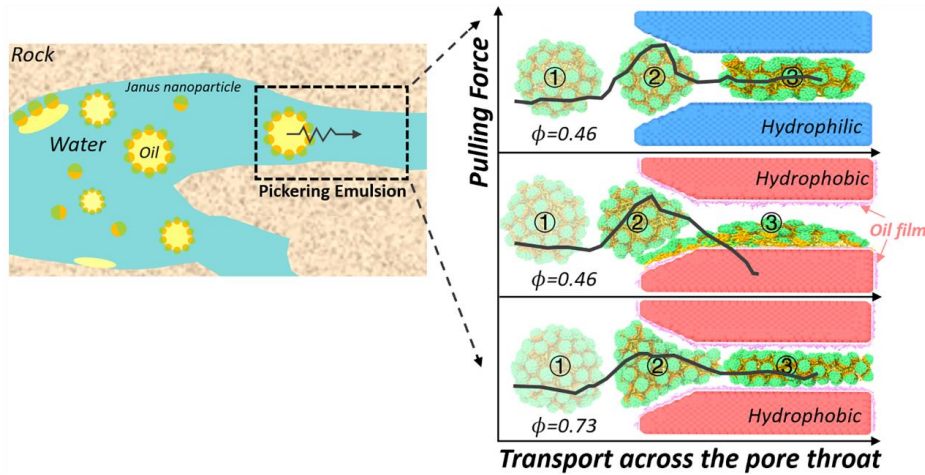


**Figure 4.4** The transport dynamics and force response of Pickering emulsion across the nanopore throat.

#### Highlights:

- Using tensile and compression simulations, the nanomechanical properties of a single Pickering emulsion are explored for the first time at the nanoscale.
- JNP surface coverage ( $\phi$ ) has little effect on the deformation of the Pickering emulsion on the hydrophilic surface, while the larger  $\phi$  of the emulsion, the greater deformation and stress can be withstood at rupture.
- There is a critical  $\phi$  that controls the formation of the ordered quasi-solid structure of JNP shell, which can act the effective shielding.
- Pickering emulsions with different  $\phi$  exhibit similar mechanical properties through hydrophilic pore throats.
- During the transport of Pickering emulsion through the hydrophobic pore throat, the JNP shell acts as a protective cushion, shielding the oil core from the interaction of residual oil at the surface.

Our researches shed light on the displacement dynamics and mechanisms of trapped oil displacement in rough channels by types of nanofluids and provide fundamental insight into the mechanical stability and transport dynamics of Pickering emulsion, which is significant for the understanding and application of the nanofluids in EOR process.

## Chapter 5. Recommendations for further studies

---

Some interesting and important findings about the displacement of nanofluids and transport of Pickering emulsion have been achieved in this study. However, the work in this thesis has also given rise to some extensional key topics needed to solve in future work. There are still several crucial issues that should be explored to get a comprehensive and deep understanding of nanofluids-enabled EOR applications from a nanoscale point of view.

- **More effect of factors/parameters to the displacement.** In our simulations, only the effect of surface wettability of NPs, surface roughness, and displacement pressure is studied. A large number of parameters remain to be investigated to perfect the systematic theory of trapped oil displacement by NPs. Such as properties related to NPs (diameter, shape, charge on NP, etc.), properties related to fluids (crude oil components, water salinity, etc.), properties related to the rock surface, and other environmental factors.
- **Design of intelligent NPs.** NPs have the potential to be modified the specific properties by different treatments according to the requirement. Thus, an intelligent NP would be the future focus, which could deliver the desired chemical agents to the target locations or zones in the porous medium. Similarly, the nano-robot has been a hot topic in the drug delivery field.

- **Extension of the single channel to the porous medium.** First, the displacement dynamics and mechanisms of nanofluids for several other types of residual oil systems should be complemented. So that a systematic understanding of residual oil displacement by NPs under a single pore channel can be formed. Subsequently, the results for the single channel with different residual oil distributions should be extended to the multi-channels even to the porous medium. Given the sheer volume of data, increasingly sophisticated machine learning would be an effective tool. Lastly, the bridge between the simulation results and that of experiments can be established.
- **The theoretical model for NPs involved in EOR.** With the appearance of the NPs, the model adopted in the continuum scale may break down. The theoretical analysis or equations to elucidate the multi-phase behavior or interactions should be introduced. Such models are beneficial for guiding the application of NPs in EOR.
- **Combination of machine learning and molecular modeling.** This may result in an essential toolbox to correlate physical and chemical properties exhibited by the complex and heterogeneous systems observed on the porous media (Figure 5.1). This approach may be particularly important to model the physical and chemical processes influencing interfacial properties, and that can involve several variables. Also, it would also be a promising tool to extend the laws of fluid in a single pore to that in the porous media.

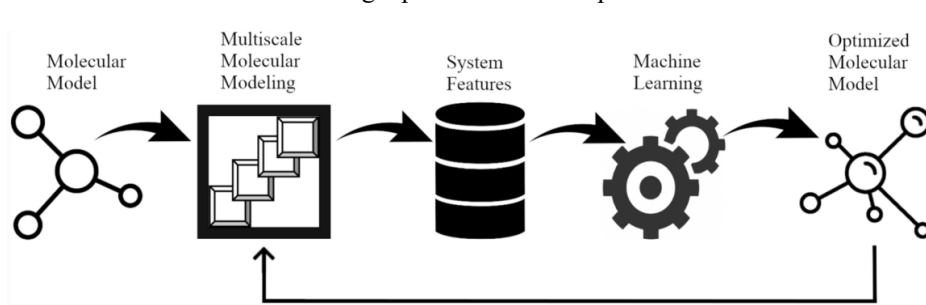


**Figure 5.1** Schematic representation of the computational protocol combining multiscale molecular modeling with data science tools. Such an approach can lead to optimized systems with fine-tuned properties, reprinted from Ref. [105].

## Bibliography

1. Asif, M. and T. Muneer, *Energy supply, its demand and security issues for developed and emerging economies*. Renewable and sustainable energy reviews, 2007. **11**(7): p. 1388-1413.
2. Bradley, H.B., *Petroleum engineering handbook*. 1987.
3. Bai, B., *Overview: eOR/IOR (January 2008)*. Journal of Petroleum Technology, 2008. **60**(01): p. 42-42.
4. Zhang, N., et al., *Development of a hybrid scoring system for EOR screening by combining conventional screening guidelines and random forest algorithm*. Fuel, 2019. **256**: p. 115915.
5. Thomas, S., *Enhanced oil recovery-an overview*. Oil & Gas Science and Technology-Revue de l'IFP, 2008. **63**(1): p. 9-19.
6. Gurgel, A., et al., *A review on chemical flooding methods applied in enhanced oil recovery*. 2008.
7. Sun, X., et al., *Enhanced heavy oil recovery in thin reservoirs using foamy oil-assisted methane huff-n-puff method*. Fuel, 2015. **159**: p. 962-973.
8. Peng, B., et al., *A review of nanomaterials for nanofluid enhanced oil recovery*. RSC advances, 2017. **7**(51): p. 32246-32254.
9. Sun, Y., et al., *Properties of nanofluids and their applications in enhanced oil recovery: a comprehensive review*. Energy & Fuels, 2020. **34**(2): p. 1202-1218.
10. Yakasai, F., et al., *Current developments and future outlook in nanofluid flooding: A comprehensive review of various parameters influencing oil recovery mechanisms*. Journal of Industrial and Engineering Chemistry, 2021. **93**: p. 138-162.
11. Alnarabiji, M.S., et al., *Nanofluid enhanced oil recovery using induced ZnO nanocrystals by electromagnetic energy: Viscosity increment*. Fuel, 2018. **233**: p. 632-643.
12. Alnarabiji, M.S. and M.M. Husein, *Application of bare nanoparticle-based nanofluids in enhanced oil recovery*. Fuel, 2020. **267**: p. 117262.
13. Hu, Z., et al., *Nanoparticle-assisted water-flooding in Berea sandstones*. Energy & fuels, 2016. **30**(4): p. 2791-2804.
14. Hendraningrat, L. and O. Torsæter, *A study of water chemistry extends the benefits of using silica-based nanoparticles on enhanced oil recovery*. Applied Nanoscience, 2016. **6**(1): p. 83-95.
15. Youssif, M.I., et al., *Silica nanofluid flooding for enhanced oil recovery in sandstone rocks*. Egyptian Journal of Petroleum, 2018. **27**(1): p. 105-110.
16. Ravera, F., et al., *Effect of nanoparticles on the interfacial properties of liquid/liquid and liquid/air surface layers*. The Journal of Physical Chemistry B, 2006. **110**(39): p. 19543-19551.
17. Al-Anssari, S., et al., *Wettability alteration of oil-wet carbonate by silica nanofluid*. Journal of colloid and interface science, 2016. **461**: p. 435-442.
18. Giraldo, J., et al., *Wettability alteration of sandstone cores by alumina-based nanofluids*. Energy & Fuels, 2013. **27**(7): p. 3659-3665.
19. Nazari Moghaddam, R., et al., *Comparative study of using nanoparticles for enhanced oil recovery: wettability alteration of carbonate rocks*. Energy & Fuels, 2015. **29**(4): p. 2111-2119.

20. Ni, X., et al., *Synthesis of an amphiphobic nanofluid with a novel structure and its wettability alteration on low-permeability sandstone reservoirs*. Energy & Fuels, 2018. **32**(4): p. 4747-4753.
21. Li, S. and O. Torsæter. *Experimental investigation of the influence of nanoparticles adsorption and transport on wettability alteration for oil wet berea sandstone*. in *SPE Middle East Oil & Gas Show and Conference*. 2015. Society of Petroleum Engineers.
22. Dehghan Monfared, A., et al., *Potential application of silica nanoparticles for wettability alteration of oil-wet calcite: A mechanistic study*. Energy & Fuels, 2016. **30**(5): p. 3947-3961.
23. Keykhosravi, A. and M. Simjoo, *Insights into stability of silica nanofluids in brine solution coupled with rock wettability alteration: An enhanced oil recovery study in oil-wet carbonates*. Colloids and Surfaces A: Physicochemical and Engineering Aspects, 2019. **583**: p. 124008.
24. Rostami, P., et al., *Enhanced oil recovery using silica nanoparticles in the presence of salts for wettability alteration*. Journal of Dispersion Science and Technology, 2019.
25. Jha, N.K., et al., *Pore scale investigation of low salinity surfactant nanofluid injection into oil saturated sandstone via X-ray micro-tomography*. Journal of Colloid and Interface Science, 2020. **562**: p. 370-380.
26. Kuang, W., S. Saraji, and M. Piri, *A systematic experimental investigation on the synergistic effects of aqueous nanofluids on interfacial properties and their implications for enhanced oil recovery*. Fuel, 2018. **220**: p. 849-870.
27. Dai, C., et al., *Spontaneous imbibition investigation of self-dispersing silica nanofluids for enhanced oil recovery in low-permeability cores*. Energy & Fuels, 2017. **31**(3): p. 2663-2668.
28. Wasan, D.T. and A.D. Nikolov, *Spreading of nanofluids on solids*. Nature, 2003. **423**(6936): p. 156-159.
29. Sedghi, M., M. Piri, and L. Goual, *Atomistic molecular dynamics simulations of crude oil/brine displacement in calcite mesopores*. Langmuir, 2016. **32**(14): p. 3375-3384.
30. Wu, H., J. Chen, and H. Liu, *Molecular dynamics simulations about adsorption and displacement of methane in carbon nanochannels*. The Journal of Physical Chemistry C, 2015. **119**(24): p. 13652-13657.
31. Sumer, Z. and A. Striolo, *Nanoparticles shape-specific emergent behaviour on liquid crystal droplets*. Molecular Systems Design & Engineering, 2020. **5**(2): p. 449-460.
32. Luu, X.C., J. Yu, and A. Striolo, *Nanoparticles adsorbed at the water/oil interface: coverage and composition effects on structure and diffusion*. Langmuir, 2013. **29**(24): p. 7221-8.
33. Luu, X.C., J. Yu, and A. Striolo, *Ellipsoidal Janus nanoparticles adsorbed at the water-oil interface: some evidence of emergent behavior*. J Phys Chem B, 2013. **117**(44): p. 13922-9.
34. Frost, D.S. and L.L. Dai, *Molecular dynamics simulations of charged nanoparticle self-assembly at ionic liquid-water and ionic liquid-oil interfaces*. The Journal of chemical physics, 2012. **136**(8): p. 084706.
35. Wang, X., et al., *Displacement of nanofluids in silica nanopores: influenced by wettability of nanoparticles and oil components*. Environmental Science: Nano, 2018. **5**(11): p. 2641-2650.

36. Marks, L. and L. Peng, *Nanoparticle shape, thermodynamics and kinetics*. Journal of Physics: Condensed Matter, 2016. **28**(5): p. 053001.
37. Talapin, D.V. and E.V. Shevchenko, *Introduction: nanoparticle chemistry*. Chemical Reviews, 2016. **116**(18): p. 10343-10345.
38. Heiligtag, F.J. and M. Niederberger, *The fascinating world of nanoparticle research*. Materials today, 2013. **16**(7-8): p. 262-271.
39. Husein, M., *Preparation of nanoscale organosols and hydrosols via the phase transfer route*. Journal of Nanoparticle Research, 2017. **19**(12): p. 1-18.
40. Foroozesh, J. and S. Kumar, *Nanoparticles behaviors in porous media: application to enhanced oil recovery*. Journal of Molecular Liquids, 2020. **316**: p. 113876.
41. Wong, K.V. and O. De Leon, *Applications of nanofluids: current and future*. Nanotechnology and Energy, 2017: p. 105-132.
42. Kostic, M.M. *Critical issues and application potentials in nanofluids research*. in *Multifunctional Nanocomposites and Nanomaterials International Conference*. 2006.
43. Green, D.W. and G.P. Willhite, *Enhanced oil recovery*. Vol. 6. 1998: Henry L. Doherty Memorial Fund of AIME, Society of Petroleum Engineers ....
44. Hendraningrat, L., S. Li, and O. Torsaeter. *Enhancing oil recovery of low-permeability Berea sandstone through optimized nanofluids concentration*. in *SPE enhanced oil recovery conference*. 2013. OnePetro.
45. Roustaei, A., et al. *An experimental investigation of polysilicon nanoparticles' recovery efficiencies through changes in interfacial tension and wettability alteration*. in *SPE international oilfield nanotechnology conference and exhibition*. 2012. OnePetro.
46. Fereidooni Moghadam, T. and S. Azizian, *Effect of ZnO nanoparticle and hexadecyltrimethylammonium bromide on the dynamic and equilibrium oil–water interfacial tension*. The Journal of Physical Chemistry B, 2014. **118**(6): p. 1527-1534.
47. Bizmark, N., M.A. Ioannidis, and D.E. Henneke, *Irreversible adsorption-driven assembly of nanoparticles at fluid interfaces revealed by a dynamic surface tension probe*. Langmuir, 2014. **30**(3): p. 710-717.
48. Powell, K.C. and A. Chauhan, *Interfacial tension and surface elasticity of carbon black (CB) covered oil–water interface*. Langmuir, 2014. **30**(41): p. 12287-12296.
49. Hua, X., M.A. Bevan, and J. Frechette, *Reversible partitioning of nanoparticles at an oil–water interface*. Langmuir, 2016. **32**(44): p. 11341-11352.
50. Zhang, Y., et al., *Computer simulation of liquid/liquid interfaces. I. Theory and application to octane/water*. The Journal of chemical physics, 1995. **103**(23): p. 10252-10266.
51. Vignati, E., R. Piazza, and T.P. Lockhart, *Pickering emulsions: interfacial tension, colloidal layer morphology, and trapped-particle motion*. Langmuir, 2003. **19**(17): p. 6650-6656.
52. Saleh, N., et al., *Oil-in-water emulsions stabilized by highly charged polyelectrolyte-grafted silica nanoparticles*. Langmuir, 2005. **21**(22): p. 9873-9878.
53. Pichot, R., F. Spyropoulos, and I. Norton, *Competitive adsorption of surfactants and hydrophilic silica particles at the oil–water interface*:

- Interfacial tension and contact angle studies*. Journal of colloid and interface science, 2012. **377**(1): p. 396-405.
54. SM, S.M., S. Tan, and N. Nguyen, *Temperature dependence of interfacial properties and viscosity of nanofluids for droplet-based microfluidics [J]*. Journal of Physics D: Applied Physics, 2008. **41**(8): p. 085502.
55. Giraldo, L.J. *Janus nanoparticles for enhanced oil recovery EOR: reduction of interfacial tension*. in *SPE annual technical conference and exhibition*. 2018. OnePetro.
56. Li, S., L. Hendraningrat, and O. Torsaeter. *Improved oil recovery by hydrophilic silica nanoparticles suspension: 2 phase flow experimental studies*. in *IPTC 2013: International Petroleum Technology Conference*. 2013. European Association of Geoscientists & Engineers.
57. Hendraningrat, L., S. Li, and O. Torsæter, *A coreflood investigation of nanofluid enhanced oil recovery*. Journal of Petroleum Science and Engineering, 2013. **111**: p. 128-138.
58. Abdallah, W., et al., *Fundamentals of wettability*. Technology, 1986. **38**(1125-1144): p. 268.
59. Moghadam, A.M. and M.B. Salehi, *Enhancing hydrocarbon productivity via wettability alteration: a review on the application of nanoparticles*. Reviews in Chemical Engineering, 2019. **35**(4): p. 531-563.
60. Seid Mohammadi, M., J. Moghadasi, and S. Naseri, *An experimental investigation of wettability alteration in carbonate reservoir using  $\gamma$ -Al<sub>2</sub>O<sub>3</sub> nanoparticles*. Iranian Journal of Oil and Gas Science and Technology, 2014. **3**(2): p. 18-26.
61. Negin, C., S. Ali, and Q. Xie, *Application of nanotechnology for enhancing oil recovery—A review*. Petroleum, 2016. **2**(4): p. 324-333.
62. Li, S. and O. Torsaeter. *The impact of nanoparticles adsorption and transport on wettability alteration of intermediate wet berea sandstone*. in *SPE Middle East Unconventional Resources Conference and Exhibition*. 2015. OnePetro.
63. Moslan, M.S., et al. *Wettability alteration of dolomite rock using nanofluids for enhanced oil recovery*. in *Materials Science Forum*. 2016. Trans Tech Publ.
64. Kondiparty, K., et al., *Wetting and spreading of nanofluids on solid surfaces driven by the structural disjoining pressure: statics analysis and experiments*. Langmuir, 2011. **27**(7): p. 3324-3335.
65. Wang, F.-C. and H.-A. Wu, *Enhanced oil droplet detachment from solid surfaces in charged nanoparticle suspensions*. Soft Matter, 2013. **9**(33): p. 7974-7980.
66. Sofla, S.J.D., L.A. James, and Y. Zhang. *Toward a mechanistic understanding of wettability alteration in reservoir rocks using silica nanoparticles*. in *E3S Web of Conferences*. 2019. EDP Sciences.
67. Li, S., et al., *Visualizing and quantifying wettability alteration by silica nanofluids*. ACS Applied Materials & Interfaces, 2021. **13**(34): p. 41182-41189.
68. Li, S., et al. *Investigation of Wettability Alteration by Silica Nanoparticles Through Advanced Surface-Wetting Visualization Techniques*. in *SPE Annual Technical Conference and Exhibition*. 2019. Society of Petroleum Engineers.
69. Wasan, D., A. Nikolov, and K. Kondiparty, *The wetting and spreading of nanofluids on solids: Role of the structural disjoining pressure*. Current Opinion in Colloid & Interface Science, 2011. **16**(4): p. 344-349.

70. Khalilnezhad, A., et al., *A Complete experimental study of oil/water interfacial properties in the presence of TiO<sub>2</sub> nanoparticles and different ions*. Oil & Gas Science and Technology—Revue d'IFP Energies nouvelles, 2019. **74**: p. 39.
71. DENG, W., et al., *Pickering emulsions stabilized by polysaccharides particles and their applications: a review*. Food Science and Technology, 2022. **42**.
72. Adil, M. and S.A. Onaizi, *Pickering nanoemulsions and their mechanisms in enhancing oil recovery: A comprehensive review*. Fuel, 2022. **319**: p. 123667.
73. Yoon, K.Y., et al., *Core flooding of complex nanoscale colloidal dispersions for enhanced oil recovery by in situ formation of stable oil-in-water pickering emulsions*. Energy & Fuels, 2016. **30**(4): p. 2628-2635.
74. Wang, Z., T. Babadagli, and N. Maeda. *Can we generate stable pickering emulsions activating naturally occurring nanoparticles in the reservoir for cost effective heavy-oil recovery?* in *SPE Western Regional Meeting*. 2021. OnePetro.
75. Ortiz, D.G., et al., *Current trends in Pickering emulsions: particle morphology and applications*. Engineering, 2020. **6**(4): p. 468-482.
76. Zhang, T., et al. *Nanoparticle-stabilized emulsions for applications in enhanced oil recovery*. in *SPE improved oil recovery symposium*. 2010. OnePetro.
77. Kumar, N. and A. Mandal, *Wettability alteration of sandstone rock by surfactant stabilized nanoemulsion for enhanced oil recovery—A mechanistic study*. Colloids and Surfaces A: Physicochemical and Engineering Aspects, 2020. **601**: p. 125043.
78. Jalilian, M., et al., *An experimental investigation of nanoemulsion enhanced oil recovery: Use of unconsolidated porous systems*. Fuel, 2019. **251**: p. 754-762.
79. Kumar, N., T. Gaur, and A. Mandal, *Characterization of SPN Pickering emulsions for application in enhanced oil recovery*. Journal of Industrial and Engineering Chemistry, 2017. **54**: p. 304-315.
80. Duffus, L.J., et al., *A comparative study on the capacity of a range of food-grade particles to form stable O/W and W/O Pickering emulsions*. Journal of colloid and interface science, 2016. **473**: p. 9-21.
81. Dudchenko, A.V., et al., *Coupling underwater superoleophobic membranes with magnetic pickering emulsions for fouling-free separation of crude oil/water mixtures: an experimental and theoretical study*. ACS nano, 2015. **9**(10): p. 9930-9941.
82. Binks, B.P., L. Isa, and A.T. Tyowua, *Direct measurement of contact angles of silica particles in relation to double inversion of pickering emulsions*. Langmuir, 2013. **29**(16): p. 4923-4927.
83. Binks, B.P., *Particles as surfactants—similarities and differences*. Current opinion in colloid & interface science, 2002. **7**(1-2): p. 21-41.
84. Low, L.E., et al., *Recent advances of characterization techniques for the formation, physical properties and stability of Pickering emulsion*. Advances in colloid and interface science, 2020. **277**: p. 102117.
85. Albert, C., et al., *Pickering emulsions: Preparation processes, key parameters governing their properties and potential for pharmaceutical applications*. Journal of Controlled Release, 2019. **309**: p. 302-332.
86. Yu, L., et al., *Plugging ability of oil-in-water emulsions in porous media: experimental and modeling study*. Industrial & Engineering Chemistry Research, 2018. **57**(43): p. 14795-14808.



87. Ding, B. and M. Dong, *Optimization of plugging high mobility zones in oil sands by injection of oil-in-water emulsion: Experimental and modeling study*. Fuel, 2019. **257**: p. 116024.
88. Soo, H. and C.J. Radke, *Flow mechanism of dilute, stable emulsions in porous media*. Industrial & engineering chemistry fundamentals, 1984. **23**(3): p. 342-347.
89. Liu, Z., et al., *Pore scale and macroscopic visual displacement of oil-in-water emulsions for enhanced oil recovery*. Chemical Engineering Science, 2019. **197**: p. 404-414.
90. Yu, L., et al., *Emulsification of heavy crude oil in brine and its plugging performance in porous media*. Chemical Engineering Science, 2018. **178**: p. 335-347.
91. Chen, Z., et al., *Effects of oil viscosity on the plugging performance of oil-in-water emulsion in porous media*. Industrial & Engineering Chemistry Research, 2018. **57**(21): p. 7301-7309.
92. Yu, L., et al., *Effects of interfacial tension and droplet size on the plugging performance of oil-in-water emulsions in porous media*. Industrial & Engineering Chemistry Research, 2017. **56**(32): p. 9237-9246.
93. Nguyen, C., et al., *Viscosity data for Al<sub>2</sub>O<sub>3</sub>-water nanofluid—hysteresis: is heat transfer enhancement using nanofluids reliable?* International journal of thermal sciences, 2008. **47**(2): p. 103-111.
94. Lee, S.W., et al., *Investigation of viscosity and thermal conductivity of SiC nanofluids for heat transfer applications*. International Journal of Heat and Mass Transfer, 2011. **54**(1-3): p. 433-438.
95. Naina, H.K., et al., *Viscosity and specific volume of TiO<sub>2</sub>/water nanofluid*. Journal of Nanofluids, 2012. **1**(2): p. 161-165.
96. Abdullah, A.M., et al., *Tailoring the viscosity of water and ethylene glycol based TiO<sub>2</sub> nanofluids*. Journal of Molecular Liquids, 2020. **297**: p. 111982.
97. Ke, H., M. Yuan, and S. Xia, *A review of nanomaterials as viscosity reducer for heavy oil*. Journal of Dispersion Science and Technology, 2022. **43**(9): p. 1271-1282.
98. Doryani, H., M. Malayeri, and M. Riazi, *Visualization of asphaltene precipitation and deposition in a uniformly patterned glass micromodel*. Fuel, 2016. **182**: p. 613-622.
99. Wu, C., et al., *The use of a nano-nickel catalyst for upgrading extra-heavy oil by an aquathermolysis treatment under steam injection conditions*. Petroleum Science and Technology, 2013. **31**(21): p. 2211-2218.
100. Nassar, N.N., A. Hassan, and P. Pereira-Almao, *Application of nanotechnology for heavy oil upgrading: Catalytic steam gasification/cracking of asphaltenes*. Energy & Fuels, 2011. **25**(4): p. 1566-1570.
101. Goh, C., et al. *Magnesium and Aluminium carbon nanotube composites*. in *Key Engineering Materials*. 2010. Trans Tech Publ.
102. Rapaport, D.C. and D.C.R. Rapaport, *The art of molecular dynamics simulation*. 2004: Cambridge university press.
103. Phan, A., D. Fan, and A. Striolo, *Fluid transport through heterogeneous pore matrices: Multiscale simulation approaches*. Physics of Fluids, 2020. **32**(10): p. 101301.
104. Liguori, N., et al., *Molecular dynamics simulations in photosynthesis*. Photosynthesis research, 2020. **144**(2): p. 273-295.

105. Kirch, A., et al., *Multiscale molecular modeling applied to the upstream oil & gas industry challenges*. Polytechnica, 2020. **3**(1): p. 54-65.
106. de Lara, L.S., M.F. Michelon, and C.R. Miranda, *Molecular dynamics studies of fluid/oil interfaces for improved oil recovery processes*. The Journal of Physical Chemistry B, 2012. **116**(50): p. 14667-14676.
107. Fu, L., et al., *Application of molecular simulation in tertiary oil recovery: A systematic review*. Journal of Petroleum Science and Engineering, 2022: p. 110196.
108. Fan, H. and A. Striolo, *Nanoparticle effects on the water-oil interfacial tension*. Physical Review E, 2012. **86**(5): p. 051610.
109. Luu, X.-C., J. Yu, and A. Striolo, *Nanoparticles adsorbed at the water/oil interface: coverage and composition effects on structure and diffusion*. Langmuir, 2013. **29**(24): p. 7221-7228.
110. de Lara, L.S., V.A. Rigo, and C.R. Miranda, *Functionalized silica nanoparticles within multicomponent oil/brine interfaces: a study in molecular dynamics*. The Journal of Physical Chemistry C, 2016. **120**(12): p. 6787-6795.
111. Fatemi, S.M. and S.J. Fatemi, *Current investigations in theoretical studies of nanostructure-liquid interfaces*. Chinese Journal of Physics, 2020. **65**: p. 93-107.
112. Zhao, G., et al., *Nanomixing effects in glycerol/dodecanol pickering emulsions for interfacial catalysis*. Langmuir, 2018. **34**(50): p. 15587-15592.
113. Frost, D.S., E.M. Nofen, and L.L. Dai, *Particle self-assembly at ionic liquid-based interfaces*. Advances in colloid and interface science, 2014. **206**: p. 92-105.
114. Cheung, D.L., *Molecular simulation of nanoparticle diffusion at fluid interfaces*. Chemical Physics Letters, 2010. **495**(1-3): p. 55-59.
115. Luo, M., Y. Song, and L.L. Dai, *Heterogeneous or competitive self-assembly of surfactants and nanoparticles at liquid-liquid interfaces*. Molecular Simulation, 2009. **35**(10-11): p. 773-784.
116. Song, Y., M. Luo, and L.L. Dai, *Understanding nanoparticle diffusion and exploring interfacial nanorheology using molecular dynamics simulations*. Langmuir, 2010. **26**(1): p. 5-9.
117. Gao, H.-M., et al., *Orientation and surface activity of Janus particles at fluid-fluid interfaces*. The Journal of Chemical Physics, 2014. **141**(13): p. 134907.
118. Fan, H., D.E. Resasco, and A. Striolo, *Amphiphilic silica nanoparticles at the decane-water interface: Insights from atomistic simulations*. Langmuir, 2011. **27**(9): p. 5264-5274.
119. Luu, X.C. and A. Striolo, *Ellipsoidal Janus nanoparticles assembled at spherical oil/water interfaces*. J Phys Chem B, 2014. **118**(47): p. 13737-43.
120. Li, W., et al., *Effects of salts and silica nanoparticles on oil-brine interfacial properties under hydrocarbon reservoir conditions: A molecular dynamics simulation study*. Journal of Molecular Liquids, 2020. **305**: p. 112860.
121. Wang, F. and H. Wu, *Molecular dynamics studies on spreading of nanofluids promoted by nanoparticle adsorption on solid surface*. Theoretical and Applied Mechanics Letters, 2013. **3**(5).
122. Wang, F.-C. and H.-A. Wu, *Enhanced oil droplet detachment from solid surfaces in charged nanoparticle suspensions*. Soft Matter, 2013. **9**(33).
123. Wu, J., et al. *Effect of nanoparticles on oil-water flow in a confined nanochannel: a molecular dynamics study*. in *SPE international oilfield nanotechnology conference and exhibition*. 2012. OnePetro.

- 
124. Wang, X., et al., *Effect of Nanoparticles on Spontaneous Imbibition of Water into Ultraconfined Reservoir Capillary by Molecular Dynamics Simulation*. Energies, 2017. **10**(4).
  125. Wang, X., et al., *Atomistic insights into the nanofluid transport through an ultra-confined capillary*. Phys Chem Chem Phys, 2018. **20**(7): p. 4831-4839.
  126. Wang, X., et al., *Transportation of Janus nanoparticles in confined nanochannels: a molecular dynamics simulation*. Environmental Science: Nano, 2019. **6**(9): p. 2810-2819.
  127. Wang, X., et al., *Insight into the pressure-induced displacement mechanism for selecting efficient nanofluids in various capillaries*. Environmental Science: Nano, 2020.
  128. Durrett, J., et al., *Superhydrophobic polymeric films with hierarchical structures produced by nanoimprint (NIL) and plasma roughening*. Applied Surface Science, 2018. **445**: p. 97-106.
  129. Wang, G., et al., *Kinetic Monte Carlo study on the evolution of silicon surface roughness under hydrogen thermal treatment*. Applied Surface Science, 2017. **414**: p. 361-364.
  130. Meng, Q., D. Chen, and G. Wu, *Microscopic Mechanisms for the dynamic wetting of a heavy oil mixture on a rough silica surface*. The Journal of Physical Chemistry C, 2018. **122**(43): p. 24977-24986.

## **Appendix A Appended papers**

**Paper I**

### **A.1 Paper I**

---

#### **Displacement dynamics of trapped oil in rough channels driven by nanofluids**

Authors: Yuanhao Chang, Senbo Xiao, Rui Ma, Xiao Wang, Zhiliang Zhang and Jianying He

Fuel, 2022, 314: 122760.

## **Displacement Dynamics of Trapped Oil in Rough Channels Driven by Nanofluids**

Yuanhao Chang <sup>a</sup>, Senbo Xiao <sup>a,1</sup>, Rui Ma <sup>a</sup>, Xiao Wang <sup>b</sup>, Zhiliang Zhang <sup>a</sup>, Jianying He <sup>a,2</sup>

<sup>a</sup> NTNU Nanomechanical Lab, Department of Structural Engineering,

Norwegian University of Science and Technology (NTNU), 7491 Trondheim, Norway

<sup>b</sup> School of Materials Science and Engineering, China University of Petroleum (East China),  
Qingdao, 266580 Shandong, China

### **Abstract**

It is well accepted that nanofluids have great potential in enhanced oil recovery (EOR). However, the EOR mechanisms by nanofluids largely remain elusive. In the study, the displacement dynamics of residual oil trapped in rough channels by different nanofluids under varied injection pumping forces are investigated by atomistic modeling. Our results indicate that both hydrophilic nanoparticles (NPs) and Janus NPs have highly obvious oil displacement effects. Specifically, hydrophilic NPs increase the viscosity and enlarge the sweeping scope of injected fluid, while Janus NPs favor either staying at the oil-water interface to reduce the interfacial tension or adsorbing onto the convex surface. Under the drag of the injecting flux, Janus NPs displace trapped oil molecules and alter the local surface wettability by sliding along the surface. In contrast, hydrophobic NPs are prone to migrate into the oil phase, which not only reinforces the trapping effect of the oil molecules by the rough surface but also poses a risk of channel blockage. Despite that the oil displacement effect of all the injection fluids is found to be less significant with low pumping force, the Janus NPs are able to maintain a stable

---

oil displacement performance under low pumping force thanks to their sufficiently long contact time with the oil phase. Furthermore, analysis on capillary number indicates that Janus NPs have outstanding application potentials in reservoirs under realistic flooding conditions. Our findings provide atomistic insights into the mechanism of nanofluids in EOR and shed light on the selection and optimization of NPs.

Keywords: enhanced oil recovery; displacement mechanism; nanoparticles; trapped oil; molecular dynamics;

## **1. Introduction**

Being the most widely used fossil fuel in the world, petroleum is the most important raw material in the modern industrial society [1, 2]. The aggressive exploration of petroleum via primary and secondary oil recovery has exhausted most of the oil fields global wide. Currently, there are urgent calls for new technologies of tertiary oil recovery, i.e. the enhanced oil recovery (EOR), for extracting the residual and more than 60% of the original oil in place (OOIP) [3, 4]. There are mainly three types of conventional EOR methods, namely thermal methods, gas injection, and chemical flooding [5]. Despite the ample research devoted to the thermal methods and gas injection, the corresponding applications are yet limited due to the harsh reservoir adaptation conditions and low economic benefits [6, 7]. The traditional EOR methods also encounter many challenges of high energy and chemicals cost and formation damage [8, 9]. Recently, EOR with nanofluids has attracted great attention and interest, thanks to the application potentials of nanoparticles (NPs), especially the high efficiency at low cost and their compatibility with environmental protection [10-12].

Compared with traditional chemical flooding ingredients, NPs have obvious advantages in improving both sweep efficiency and displacement efficiency. On the one hand, their small size allows them to transport into the small channels. On the other hand, their high surface energy and reactivity are conducive to modify the properties of fluids and rock surfaces, thereby improving oil displacement [13, 14]. So far, NPs have achieved highly encouraging results in both laboratory and field experiments [12]. There are multiple NPs-enabled EOR mechanisms proposed, including interfacial tension reduction [15], wettability alteration [16-18], viscosity adjustment [19, 20], pore channel plugging [21], and appearance of structural disjoining pressure [22-25]. Depending on specific experimental parameters (NPs properties, core properties, flooding rate, residual oil, etc.), different mechanisms may dominate EOR [26]. The multiple mechanisms proposed also indicate that EOR by NPs is a complex process, with many nanoscale behaviors remaining unclear. More fine-scale work is in desire for elucidating the mechanism of various NPs under different reservoir conditions.

Molecular dynamics (MD) simulations have been proven to be extremely effective tools for revealing the fundamentals of EOR mechanisms [27-29]. Firstly, MD simulations are able to decipher the key interactions among the chemical agent and oil and water that are key to the understanding of the EOR mechanism. MD simulations have been utilized to systematically unravel the interfacial activities and molecular interactions between crude oil components (mainly asphaltenes) and different types of surfactants [30-34]. For NPs specifically, MD simulations are widely used for clarifying their interfacial behaviors and characteristics in oil-water systems studied [25, 35-37]. Moreover, MD simulation can provide nanoscale dynamics of NPs in oil trapping channels and the underlying mechanisms of nanofluids in EOR, which is challenging to monitor with current experimental capability.

There are notable atomistic investigations considering the effects of rock surface properties on the transportation of NPs in the confined channels using MD simulations. Wu et.al simulated the flow behavior of nanofluids in confined clay channels filled with oil [38]. Wang et.al studied the spreading of nanofluids and the detachment process of the oil droplet [39, 40]. Wang et.al investigated the imbibition and displacement mechanism of NPs transportation [41-43]. The reported simulations were however all based on smooth channels, which cannot fully reflect the flow characteristics of nanofluids on rough rock surfaces in the reservoir [44-47]. Apparently, the motion pattern and the roles of NPs in EOR in the rough channel are different from the ideally smooth surface adopted in the previous studies. Furthermore, the displaced phase in previous studies consisted of only pure oil phase, which cannot present the residual oil distribution in most channels in the EOR period.

To reveal the realistic displacement dynamics of trapped oil, MD simulations of injecting various nanofluids into rough channels were carried out in this work, aiming to elucidate the EOR mechanisms enabled by different NPs (hydrophilic, hydrophobic, and Janus NPs). The displacement phenomena of trapped oil driven by nanofluids were compared, with the specific role of each NP type in EOR uncovered. Moreover, the influence of the injection driving force underlying the EOR effect is clarified. The results rationalize the basis of the EOR mechanism by NPs and provide guidance of NPs optimization in petroleum engineering.

## **2. Model and simulation details**

### **2.1 Model systems**

The aim of the modeling is to uncover the effects and mechanisms on the displacement of trapped oil in rough channels by nanofluids. Even at the nanoscale,



such a system might require scales in length and time beyond the limit of all-atom modeling. For example, a single nanoparticle with a diameter of 5nm already contains thousands of atoms, which needs an extremely large amount of computer resources for the corresponding simulations. In order to build a sufficiently large system containing a good number of nanoparticles, and at the same time achieve a meaningful time scale of oil displacement, approximations in the interatomic potentials are critically important. As such, coarse-grained model systems including inlet, channel, and outlet parts were constructed to feature injection of nanofluids in the EOR process, as shown in Fig. 1. For the sake of simplicity, all the model systems were built as semi-2D with a width of 25.34 Å in the y-axis (Fig. 1). The boundary conditions applied in the systems were periodic. The channel part contained residual oil/water/rough surfaces, mimicking the important characteristics of channels in the oil reservoir. The rough surface in the system consisted of pillars separated by even intervals, as dimensions given in Fig. 1. With the given hydrophobicity of the surface (atomistic parameters given in the following text), residual oil was trapped on the rough surface structure of the channel after primary water flooding. The detailed process to obtain the channel part with residual oil was given in the supporting information S1. The channel block in Fig. 1 consisted of 939 oil molecules and 9482 water molecules in total, with a volume size of  $200.97 \times 25.34 \times 120.82 \text{ \AA}^3$ .

The inlet of the systems included the displacing phase and the piston, with a length of 181.95 Å in the injection direction. There were four kinds of displacing phases: water (NP-free) and three types of nanofluids (with fifty hydrophilic, hydrophobic, or Janus NPs). The density of oil and water was correspondingly kept as  $659 \text{ kg/m}^3$  and  $1003 \text{ kg/m}^3$ , which are in excellent agreement with their experimental values[48, 49]. The rough surfaces and NPs shared the same diamond cubic crystalline lattice structure with

a lattice constant of 5.43 Å. The diameter of NPs was 7 Å. With the 50 NPs in each nanofluid, the NPs volume concentration was  $\sim 1.73\%$  in the systems. To enable the injection of the nanofluids into the channel, a piston was placed on the left side of the displacing phase (Fig. 1). The driving force was applied on the piston to mimic the applied pressure. The piston had the same cross-section area of the channel and a thickness of 10.86 Å, which was larger than the cutoff distance (10 Å) of non-bonded interactions to avoid mutual interference of possible interactions on both sides of the piston. The outlet part was built as the buffering space at the exit of the channel, and initially had a length of 50.12 Å as indicated in Fig. 1.

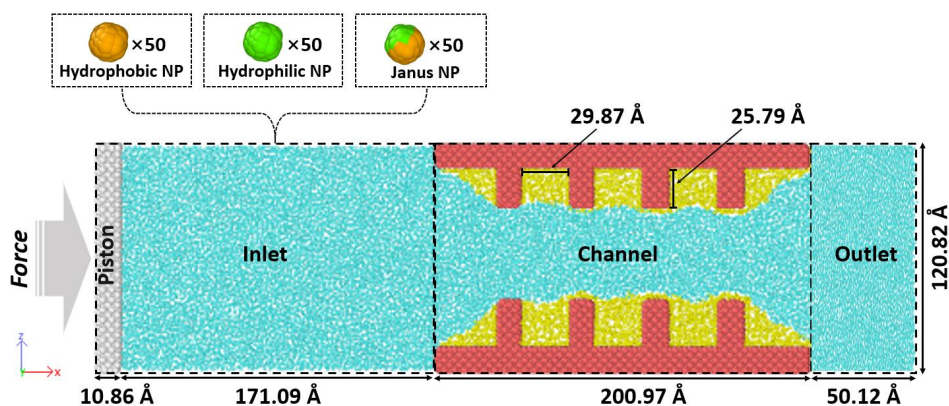


Figure 1. Representative of model systems containing inlet, channel, and outlet parts. The colors for different phases: piston (grey), water (cyan), rough surface (red), oil (yellow), hydrophobic NP (orange), hydrophilic NP (green), Janus NP (orange and green). The grey arrow indicates the direction of the applied force.

The choice of atomistic interaction parameters was the same as in the former study [25]. The mW water model was chosen for the water phase, while the Transferable Potentials for Phase Equilibria united-atom (TraPPE-UA) description of hexane was used for oil [49, 50]. The coarse-grained mW water model is famous for its accuracy,

including featuring hydrogen bonding, at less than 1% of the computational cost of other all-atom water models, while the TraPPE-UA force field has outstanding performances in realizing the appropriate properties of phase equilibrium of different materials, especially alkanes including hexane. The interaction of the water model mW followed the form of the Stillinger–Weber potential:

$$E = \sum_i \sum_{j>i} \varphi_2(r_{ij}) + \sum_i \sum_{j \neq i} \sum_{k>j} \varphi_3(r_{ij}, r_{ik}, \theta_{ijk}) \quad (1)$$

$$\varphi_2(r_{ij}) = 7.049556277\epsilon \left[ 0.602245584 \left( \frac{\sigma}{r_{ij}} \right)^4 - 1 \right] \exp\left( \frac{\sigma}{r_{ij}-1.8\sigma} \right) \quad (2)$$

$$\varphi_3(r_{ij}, r_{ik}, \theta_{ijk}) = 1.2\epsilon [\cos\theta - \cos 109.47^\circ]^2 \exp\left( \frac{1.2\sigma}{r_{ij}-1.8\sigma} \right) \exp\left( \frac{1.2\sigma}{r_{ik}-1.8\sigma} \right) \quad (3)$$

with characteristic interaction size  $\sigma = 2.3925 \text{ \AA}$ , and characteristic energy  $\epsilon_{ww} = 6.189 \text{ kcal/mol}$ . The pairwise non-bonded interactions in TraPPE-UA followed the Lennard-Jones (LJ) potential:

$$U_{LJ} = 4\epsilon_{ij} \left[ \left( \frac{\sigma_{ij}}{r_{ij}} \right)^{12} - \left( \frac{\sigma_{ij}}{r_{ij}} \right)^6 \right] \quad (4)$$

where the energy well depths for oil-oil and oil-water were  $\epsilon_{oo} = 0.0914 \text{ kcal/mol}$  and  $\epsilon_{ow} = 0.1191 \text{ kcal/mol}$ , respectively. A characteristic energy well  $\epsilon_{so}$  of 0.2 kcal/mol was given to the surface-oil interaction to enable the hydrophobic characteristic of the surfaces, as details provided in Fig. S2. A weak interaction 0.01 kcal/mol was applied between the piston and other types of molecules to minimize the influence of the piston on the flooding process. The overall interaction potentials between the NPs were provided in Table S1 [43]. All the atoms in the systems were free of charge.

## 2.2 Computational details

The LAMMPS package was adopted to carry out all the simulations [51]. First, all the systems were energy-minimized using the steepest descent method and then

equilibrated for 3 ns in the NVT ensemble using a simulation timestep of 3 fs. It should be noted here that the timestep with coarse-grained models like the mW coarse-grained water can be up to 10 fs [49, 50, 52]. In order to conserve the total energy of a large system stably and save the calculation costs, a timestep of 3 fs was chosen for all the simulations in this work. The temperature was controlled at 300 K by the Nosé–Hoover thermostat with a damping coefficient of 100 fs [53, 54]. As can be seen from Fig. S3, the total potential energy of the systems quickly reached a plateau in the equilibration. For enabling nanofluid injection, a constant force of  $10^{-4}$  kcal/mol/Å along the x-axis was applied on the piston, as depicted in Fig. 1. The displacement process in each simulation ended as the whole injected fluid volume was pushed into the channel, namely the piston was in close contact with the channel. The NPs were treated as rigid bodies to maintain the spherical shape. Meanwhile, the rough surfaces were fixed in position to speed up the simulation process. Ovito software was employed for the visualization and analysis [55].

### **3. Result and discussion**

#### **3.1 Displacement process**

##### **3.1.1 Displacement phenomenon**

The surface properties of NPs determined their transportation behaviors, which subsequently influenced the displacement of the trapped oil. As the snapshots of the displacement process at different stages shown in Fig. 2, the trapped oil was partially moved toward the outlet section by different extent as time increased in all the systems, including the reference NP-free system. In all the nanofluids, different types of NPs entered and passed through the rough channels efficiently from 0.6 to 2.3 ns. Nevertheless, there were differences in the behavior patterns of the three NPs during

the displacement. Particularly, Janus NPs were more likely to adsorb at the oil-water interface or stay near the top of the pillars, while most hydrophobic NPs were prone to enter and stay inside the oil, forming aggregated clusters. All the hydrophilic NPs stayed in the injected water phase, with the majority being displaced out of the channeling along with oil molecules.

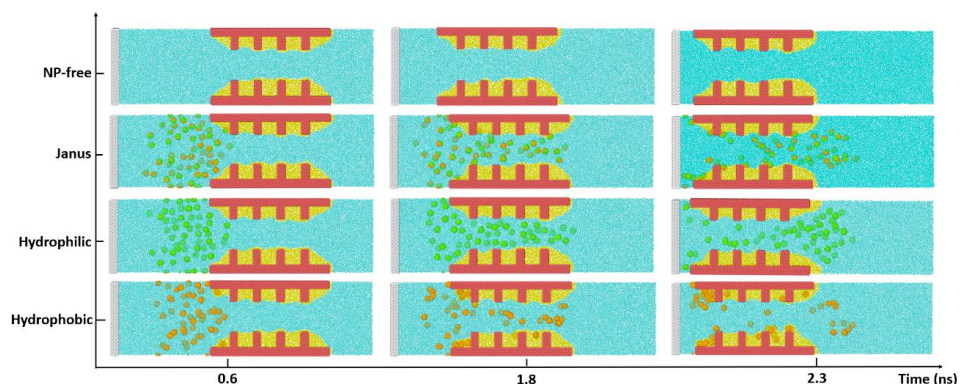


Figure 2. Representative snapshots of the displacement process in the four systems. The colors for different molecules can be found in Fig. 1.

The trapped oil in the four systems was displaced in different amounts by nanofluids. To further evaluate the flooding efficiency, residual oil molecules in the channel were recorded as shown in Fig. 3. In all the systems, the total amount of trapped oil molecules in the channel started to show a decreasing pattern at 1.5 ns and maintained such a trend to the end of the simulations (Fig. 3(a)). By comparing the number of oil molecules in the channel at the end of the simulations, the hydrophilic NPs had the best displacement effect (853 oil molecules left), followed by the Janus NPs (876 oil molecules left). Surprisingly, pure water flooding (905 oil molecules left) showed a better effect than that of the hydrophobic NPs (915 residual oil molecules). In detailing the displacement process, the channel was divided into three regions as indicated in Fig. 3 (b), with the change of the oil molecule number plotted in Fig. 3(c). It is known that it is difficult for

the trapped oil to be further extracted by pure water after initial water flooding, mainly due to the formation of the fixed water flow channels in reservoirs [56, 57]. Here, the pure water flooding (the NP-free system) still supplied the lateral friction on the trapped oil phase and enabled motions of certain oil molecules close to the oil-water interface. As showed in Fig. 3(c), the displacement effect was observed in each region of the NP-free system, signified by the decreasing number of oil molecules until the end of the simulation. For injection with nanofluids, there were obvious differences in the displacement effect owing to the different properties of NPs, especially in the region I and III as showed in Fig. 3(c). Particularly, nanofluids with Janus and hydrophilic NPs showed a great outperforming displacement effect in the region I and III, respectively. In contrast, injection of hydrophobic NPs yielded the least displaced oil molecules in all three regions of the channel, with nearly no effect at all in region I. This interesting result strongly suggests the application of Janus or hydrophilic NPs in the formulation of nanofluids. The motion behaviors of different NPs underlying this result were further analyzed in the following.

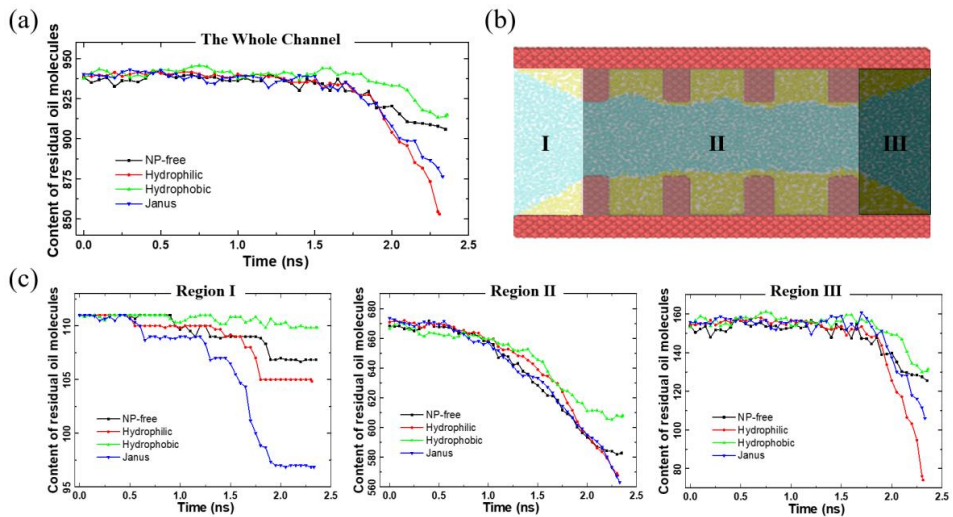


Figure 3. Displacement of trapped oil in the rough channel. (a) Oil molecules inside the whole channel in the displacement process; (b) The schematic diagram of different regions of the channel for displacement effect comparison; (c) Changes in the number of trapped oil molecules in the three regions of the channel in the displacement process.

### 3.1.2 Flow characteristics of the injection fluids

The atomic velocity of individual trapped oil molecules and the effective flow volume of injection fluids in the channel are the key factors to reflect the EOR effect. Taking the average of continuous 2-ps simulation trajectories with stable injection flux at 2 ns, the distribution of the instant atomic velocity of the oil molecules along the injection direction (velocity along X-axis), was shown in Fig. 4(a). In each case, the instant velocity distribution centered around zero speed. Because of the drag from the injecting flux, all four distributions showed an almost negligible right-skew pattern. Nevertheless, the oil molecules had the highest and the lowest average velocity with hydrophilic and hydrophobic NPs, respectively, as shown by the inset of Fig. 4(a). That is, oil in the hydrophilic case migrated fastest, while the presence of hydrophobic nanoparticles significantly hindered the flow of oil. The collective velocity of oil molecules, namely the total displacement in a certain period normalized by the corresponding time, further clarifies this difference. As shown by the collective velocity of a 20-ps period in Fig. S4, the collective velocity distribution of the oil molecules with the injection of hydrophobic NPs showed a second unique and distinctive peak at low velocity, which can be attributed to the oil molecules tightly bound to the hydrophobic NPs. The properties of the injected NPs indeed had profound effects on the displacement of the trapped oil molecules.

The effective flow volume ( $V_{\text{flow}}$ ) of the injection fluids characterizes the mobile volume of molecules in the channel. The absolute change of  $V_{\text{flow}}$  is thus approximately equal to the difference between the volume of fluids entering into ( $V_{\text{in}}$ ) and exiting from ( $V_{\text{out}}$ ) the rough channel, namely  $\Delta V_{\text{flow}} \approx V_{\text{in}} - V_{\text{out}}$ . The  $\Delta V_{\text{flow}}$  quantifies the change in the effective flow volume of the channel during the displacement process, which at the same time determines the difficulty of subsequent fluid injection. As shown in Fig. 4(b), the nanofluids with hydrophilic and Janus NPs, as well as the pure water (NP-free) injections increased the effective flow volume in the rough channel, with the hydrophilic NPs showing the best results. In contrast, the injection of hydrophobic NPs significantly decreased the effective flow volume, meaning it narrows the channel for the injection fluid in the displacement process. That is to say, injection of hydrophobic NPs into rough channels leads to an increase of injection pressure or even blockage of nanopores.

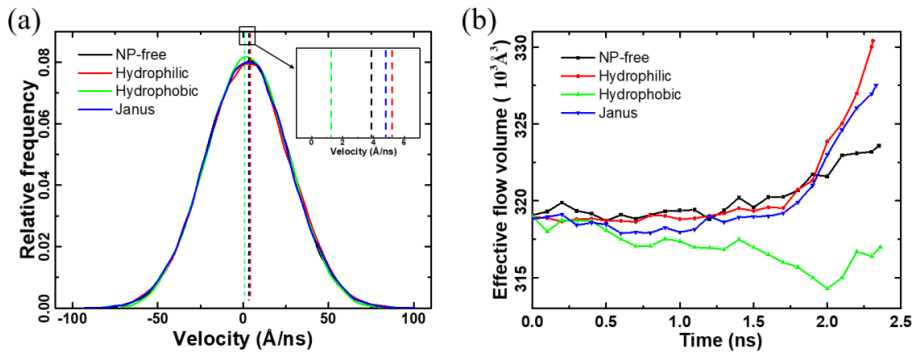


Figure 4. Flow characteristics of the injection fluids. (a) Atomic velocity distribution of the trapped oil under stable flux in the four systems along the direction of injection. The dotted lines in different colors represent the corresponding average value of the four distributions. (b) The effective flow volume of the injection fluids during the displacement process.



### 3.2 Mechanism of trapped oil displacement by NPs

The above results indicated that the occurrence of NPs directly affects the oil displacement in the rough channel. In the following sections, the displacement mechanism of different NPs on the trapped oil is analyzed by inspecting the specific micro behaviors of NPs.

#### 3.2.1 Mechanism by hydrophilic NPs

The hydrophilic NPs had led to the best displacement effect on trapped oil. Previous studies indicated that hydrophilic NPs cause the rearrangement of water molecules and affect the diffusion and properties of water molecules [41]. Here, all the hydrophilic NPs were found to disperse in the water phase during the displacement process, as shown in Fig. 2, which suggested that the hydrophilic NPs had altered the properties of the injected fluid. As the comparison of streamlines of water molecules depicted in Fig. 5, the hydrophilic NPs had a significant impact on the dynamics of their neighboring water molecules. In the pure water flooding, the main fluid streamline ran laterally, showing limited disturbances caused by the friction at the oil-water interface. With the occurrence of the hydrophilic NPs, water molecules closely bound to and migrated with the NPs due to the strong interaction forces. The diffusion of the hydrophilic NPs in the nanofluid led to disturbances of the local flow field and deviation of the streamlines from the main flow direction. This resulted in the strong friction to the oil at the oil-water interface and strengthening of the displacement effect. As the lowest mean square displacement (MSD) of water during the displacement shown in Fig. S5, the hydrophilic NPs obviously impeded water diffusion in the channel if compared with the three other systems. Since the viscosity of the injection fluids was negatively correlated with diffusion speed, the viscosity of the injected water was increased by hydrophilic NPs [58]. Consequently, the mobility ratio (the mobility of displacing fluid

divided by that of the displaced fluid) decreased as the viscosity of the injection phase increased [59]. As a result, the sweep efficiency increased, which led to the improvement of the EOR effect.

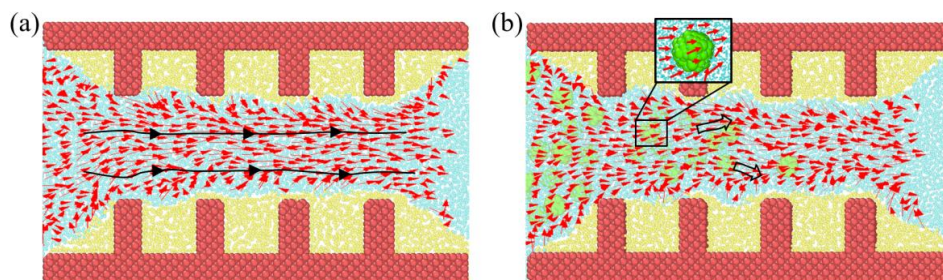


Figure 5. The streamlines of water at the stable injection state without NPs (a) and with hydrophilic NPs (b). The system snapshots were taken at 1.5 ns, where the injection fluid speed was stable. The black arrows in (a) and (b) showed the average running speed of water molecules for visualization effects. The inset in (b) showed the typical streamline distribution around a certain NP.

### 3.2.2 Mechanism by Janus NPs

In the flooding process, Janus NPs partially dispersed in the water phase and partially adsorbed at the oil-water interface. The impact of Janus NPs on the water diffusion was negligible, as indicated by the MSD results in Fig. S5. It is known that Janus NPs adsorbed at oil-water interfaces modify the interfacial tension [42]. The calculated interfacial tension for oil/water and Janus NPs/oil/water were 56.01 and 49.51 mN/m in this work, as the detailed modeling and calculation method listed in the Supporting information S6, which agreed with the known reduction of interfacial tension [60].

Given their amphiphilic surface properties, Janus NPs were able to strongly interact with different components in the channel, especially with the pillars of the rough solid

surface. At the end of the displacement process, the interfaces of oil-solid-water were populated with Janus NPs, as shown in Fig. 2 and 6. Interestingly, Janus NPs actively tangled with the pillar structure and altered the residence of the trapped oil. As the representative snapshots shown in Fig. 6, Janus NPs adsorbed on the backside of the pillar against the injection direction (Fig. 6(a)) in the displacement progresses, and gradually penetrated into the trapped oil along the surface. At the same time, water molecules entered the oil-trapping pocket with Janus NPs and drove the oil molecules outside by volume exclusion. In the process, the NPs migrated inward into the oil-trapping pocket along the solid wall, thanks to the injection flow and the interaction between the NPs and the surface. Meanwhile, the intrusion of water further forced Janus NPs to constantly adjust their orientation on the surface owing to their surface wettability characteristics. Because the hydrophilic parts of Janus NPs were exposed to the fluid, the local wettability of the total surface was thus altered to be more hydrophilic, highly beneficial for oil displacement [61]. Given the higher concentration of Janus NPs and the longer contact in reservoirs, it is expected that the accumulation of more Janus NPs at the three-phase contact area also has the potential to exert the structural disjoining pressure to detach the trapped oil from the surface [23, 25].

Janus NPs could also adsorb on the side of pillars facing the injection fluid. In such a situation, the position of Janus NPs was not stable, as illustrated in Fig. 6(b). Driven by the injected fluid, Janus NPs were pushed to slide over the pillars to the backside against the injection. In such a process, oil molecules were mobilized by the NPs, as depicted in Fig.6 (b) (T1-T5). Similarly, Janus NPs reached the top of the pillars were prone to be pushed forward by flooding, and eventually ended up on the backside of the pillars. The results were consistent with observations in experiments [62, 63], namely most NPs were found on the backside of the surface rough landscape against

injection fluid after displacement. Although the amount of oil carried by the movement of Janus NPs was limited, their associated effect on the trapped oil (extrusion, wettability alteration, and possible structural disjoining pressure) was intriguing. It is reasonable to speculate that in case the geometry of the oil-water interface becomes more abrupt, namely thin oil film covering rougher surface landscape, Janus NPs can be the right choice for their strong interactions with the three-phase contact area and their promising mechanism. Further verification certainly requires more atomistic modeling and experimental studies.

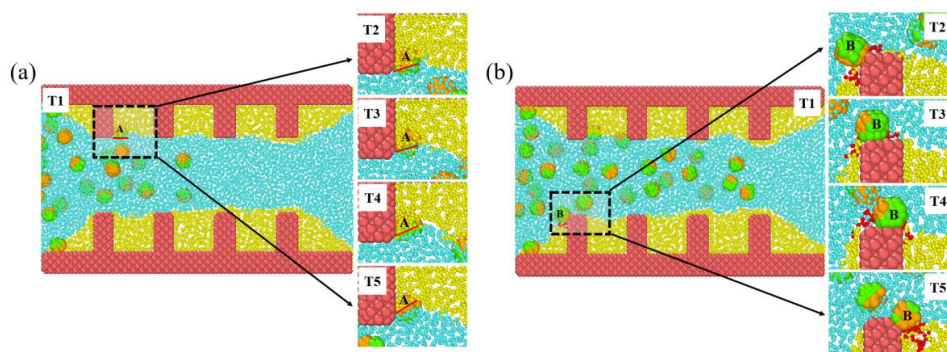


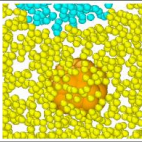
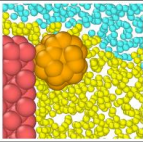
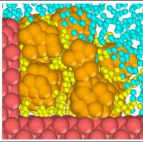
Figure 6. Migrations of Janus NPs in the channel. (a) A representative Janus NP (marked as A) adsorbed on the backside of the pillar against the injection direction. The location of the local oil-water interface in (a) is marked by the solid red line. (b) A representative Janus NP (marked as B) adsorbed on the front side of the pillar facing the injection fluid. Oil molecules migrated with Janus NP in (b) are highlighted in red. Sequential snapshots of the representative NPs over time are given and labeled with T2-5 in both (a) and (b).

### 3.2.3 Mechanism by hydrophobic NPs

As discussed above, hydrophobic NPs were likely to enter and stay in the trapped oil phase and yield the lowest displacement efficiency. The occurrence of hydrophobic

NPs in trapped oil after the displacement process was summarized in Table 1. Dispersed hydrophobic NPs can be immersed completely in the trapped oil phase or adsorbed on the pillar surface near the oil-water interface. Strikingly, the hydrophobic NPs could also aggregate tightly together in clusters on the solid surface. Due to the similar hydrophobicity, oil molecules also firmly adsorbed on hydrophobic NPs, as snapshots showed in Fig. S7. The average adsorption time of oil molecules on hydrophobic NPs was found to depend on the location of the NPs. For the hydrophobic NPs near the oil-water interface, oil molecules showed a relatively short adsorption time of 0.24 ns. In contrast, oil molecules were closely bound to the hydrophobic NPs immersed in the oil phase for a doubling average time of 0.43 ns. The adsorption time of oil molecules on aggregated NPs clusters was not high (0.29 ns), but when a cluster was taken as the calculation unit, there was a larger value (0.48 ns). Although the flow instability near the oil-water interface can decrease the oil molecule adsorption time, the addition of hydrophobic NPs reduced the mobility of the trapped oil phase, as the atomic velocities of the oil molecules shown in Fig. 4. The formed hydrophobic NP clusters potentially narrowed the flow channel. Slight displacement effect on the trapped oil was only observed close to the inlet region of the channel, owing to the limited volume exclusion effect of the hydrophobic NPs immersed in the trapped oil. For enhancing the displacement effect, a sufficient driving force was needed to separate the bound oil molecules from the hydrophobic NPs and the NP clusters. Furthermore, the hydrophobic NPs had the possibility to form channel blockage, suggesting their application potential in conformance control.

Table 1. Distribution of hydrophobic NPs after displacement processes. Three representative adsorption states are given, with the number of NPs and clusters as well as the adsorption time of oil molecules on the NPs and NP clusters.

State	Immerse deeply in oil	Stay near the interface	Aggregate in clusters
Diagram			
Number	6	5	14 (3)
Averaged adsorption time of oil molecules	0.43 ns	0.24 ns	0.29 ns (0.48 ns)

### 3.3 Effect of the pumping force

The injection pressure, controlled by the pumping force in this work, is known to have a crucial impact on the displacement process [43]. The pumping force was also found to influence the interaction of NPs with the trapped oil here. Although the major features of the final occurrence of NPs after displacement remained similar, increased pumping force can significantly reduce the contact of hydrophobic and Janus NPs with the trapped oil, as shown in Fig. S8. Higher pumping force led to a more obvious displacement effect, which was quantified by the ratio of the number of remaining oil molecules after the displacement to the total amount of the initial state in the channel, termed as EOR percentage in Fig. 7. By sampling pumping force covered two orders of magnitude ranging from 0.00005 to 0.001 kcal/mol/Å, all the injection fluids used in this work yielded a higher EOR percentage with high pumping force. This result was different from the findings on the displacement of oil in smooth channels in the previous study [43]. The reason was that the force used in this study was sufficiently low, which guaranteed the stability of the displacing front to achieve piston displacement like in the reservoir. Especially, the oil phase focused here was trapped in the surface roughness landscape of the channel rather than that filled the whole channel. The displacement effect observed relied on the drag at the oil-water interface between the trapped oil and the injection fluids, namely increased external pressure led to enhanced

interface squeezing. Because higher pumping force led to shorter displacement time, the probability of NPs contacting with the oil and the solid surface was also reduced. The change in the micro behaviors by hydrophobic and Janus NPs also had a significant impact on the displacement effect. Under higher pumping force, the hydrophobic NPs were more likely to rush through the channel with water instead of sticking into the oil phase (as shown in Fig. S9), which improved the EOR percentage as shown in Fig. 7. Interestingly, as the pumping force at the low level dropping from 0.0001 to 0.00005 kcal/mol/Å, the EOR percentage by Janus NPs remained steady and even surpassed hydrophilic NPs. In the light of the above analysis on Janus NPs, their displacement effect on trapped oil greatly depended on the interactions with the oil and surface. Under the low external force, the elongated displacement time and thus the enhanced contact probability had contributed to the positive impact of Janus NPs on the displacement effect.

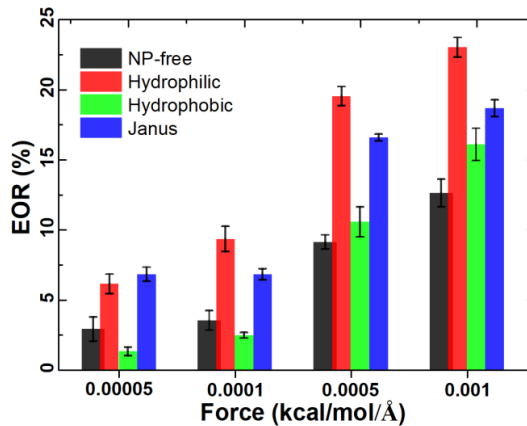


Figure 7. The EOR percentage by flooding with varied pumping forces.

The influence of pumping force on displacement effect can also be explained by the well-known capillary number [64]:

$$N_c = \frac{\text{viscous forces}}{\text{capillary forces}} = \frac{v\mu_w}{\sigma_{ow}\cos\theta} \quad (7)$$

where  $N_c$  is the capillary number,  $v$  is displacing velocity,  $\mu_w$  is the viscosity of the displacing phase,  $\sigma_{ow}$  is interfacial tension between trapped oil and nanofluids, and  $\theta$  is the water contact angle. The capillary number reflects the relative range of the driving force and resistance in the oil displacement effects [65] and relates residual oil saturation into three force-dominated regions. As capillary number increases, the residual oil saturation decreases and the three regions of oil displacement in sequence are capillary dominated, viscous-capillary coupling, and viscous dominated. Although the absolute quantitative results can differ under specific reservoir conditions, the qualitative description of the three oil displacement effect regions remains the same [64]. As the pumping force decreases, the displacing rate declines, and the capillary number drops. As a result, the EOR percentage lowers while the dominance of capillary force in the displacement gradually enhances [65, 66]. This phenomenon was well reproduced by Janus NPs under low pumping force, as their role in modifying the capillary force gradually became prominent. The results in this work were thus consistent with macroscopic conclusions. More importantly, almost all the reservoirs after water flooding are currently in a viscous-capillary coupling region or capillary force-dominated region [64, 67], which highlights the great EOR application potential for Janus NPs, compared to other types of NPs.

#### **4. Discussion**

This study provides nano-level information including the motion patterns of various NPs and the detailed interaction between components in a complex nanofluid system, which is formidable to obtain in large-scale oil displacement experiments. Such findings are essential for deepening the understanding of the mechanisms of EOR by NPs. In order to simulate a sufficiently large system at optimal computational costs, a



coarse-grained modeling approach was adopted for the fast sampling dynamics with a reduced degree of freedom of the different components in the system. The selected force field has been proven to successfully reproduce the nature of the components in nanofluid systems [25, 42, 49, 50]. The rough surface was represented by the rectangular groove as in the previous studies [68]. Thus, the designed model is simplified from real rough surfaces but is eligible for trapping a stable oil phase to be displaced by various NPs.

The oil displacement effect obtained by the lowest external force in this work is comparable with results by experiments. Although the Janus NPs are not as good as hydrophilic ones in EOR effect under external force larger than  $10^{-4}$  kcal/mol/Å (Fig. 7), their outperforming oil displacement results at low external force ( $5 \times 10^{-5}$  kcal/mol/Å) is striking. According to the previously known effect of the external force on the EOR, the results clearly suggested that the level of the lowest applied force in this work was close to the real conditions, where the EOR effect of Janus gradually became prominent. In other words, Janus NP, with their major oil displacement mechanism that relies on the interactions with both the oil phase and the solid surface, could have great potentials in recovery oil film on rock surfaces in the application.

It is important to note that the oil phase consisting of only hexane used in this work is a simplified model of the real crude oil. The purpose of such an oil phase model is only for the demonstration of the differences in the movement patterns and EOR mechanisms among various NPs. According to the previous studies [69], the polar molecules in crude oil, such as pyridine, asphaltene, prefer to accumulate at fluids interface and solid surface, which leads to the variation of the oil properties and could hinder the efficiency of the oil displacement process. However, the detailed chemical properties of different oil molecules do not counteract the EOR mechanism of different

NPs. Nevertheless, considering all the crude oil components in a single study, despite the foreseeable difficulty, could result in a more realistic oil phase in the reservoir, which would be an interesting step in future work. Moreover, only one single channel volume is considered in the work, which could potentially limit the possible contact between the NPs with the oil phase and the solid surface. It is thus highly beneficial to establish cyclic displacement simulation in different channel models for Janus NPs in future work for the in-depth analysis of EOR by nanofluids. Apart from that, water salinity, rock properties, both the size and concentration of NPs, and the system temperature and pressure, still await intensive investigations to establish the systematic theory for nanofluid EOR.

## **5. Conclusion**

This work revealed the displacement mechanisms of trapped oil in the rough channel by injection of nanofluids using MD simulations. The results completed the missing puzzle in the current literature that is dominated by modeling of oil displacement in smooth channels. The study indicated that hydrophilic and Janus NPs were able to drive significantly more trapped oil out of rough channels, while hydrophobic NPs had the lowest potential in trapped oil displacement with endangering probability of channel blockage. Specifically, hydrophilic NPs dispersed in water increased the viscosity of the injected fluid and disturbed the original stream field. As a result, the friction to the oil phase at the oil-water interface was enhanced and the sweeping scope of the displacing phase was enlarged. Janus NPs adsorbed not only at the oil-water interface to reduce the interfacial tension but also onto the roughness landscape (at two sides of the pillars). Driven by the injected flow, surface wettability, and possible structural disjoining pressure, Janus NPs can migrate along the solid

surface and into the trapped oil phase, and further exclude oil out of the trapping pockets and alter the local surface wettability. Moreover, the slippage of Janus NPs at the interface also contributed to the EOR effect. In contrast, hydrophobic NPs dispersed into the oil phase and further formed clusters, showing a negligible displacement effect. Higher pumping force was found to result in better oil displacement in all the systems. It's worth noting that Janus NPs showed outperforming EOR potential with low pumping force. Low force allowed for sufficient contact time between Janus NPs and trapped oil, which was beneficial for the EOR effect. Such phenomena were supported by the analysis of the capillary number, which suggested the EOR application potential of Janus NPs in actual reservoir conditions. The microscopic insights provided by this study are of great importance for the understanding of the oil displacement mechanism of different nanofluids and for the optimization and design of NPs in EOR.

### **Acknowledgments:**

This work was financially supported by the Research Council of Norway (Grant No. 234626) and the Chinese Scholarship Council. The supercomputer CPU hours were provided by the Norwegian Metacenter for Computational science (Project ID: NN9110K and NN9391K).

### **References**

1. Asif, M. and T. Muneer, *Energy supply, its demand and security issues for developed and emerging economies*. Renewable and sustainable energy reviews, 2007. **11**(7): p. 1388-1413.
2. Bradley, H.B., *Petroleum engineering handbook*. 1987.
3. Muggeridge, A., et al., *Recovery rates, enhanced oil recovery and technological limits*. Philosophical Transactions of the Royal Society A:

- Mathematical, Physical and Engineering Sciences, 2014. **372**(2006): p. 20120320.
4. Lyons, W.C. and G.J. Plisga, *Standard handbook of petroleum and natural gas engineering*. 2011: Elsevier.
  5. Zhang, N., et al., *Development of a hybrid scoring system for EOR screening by combining conventional screening guidelines and random forest algorithm*. Fuel, 2019. **256**: p. 115915.
  6. Shah, A., et al., *A review of novel techniques for heavy oil and bitumen extraction and upgrading*. Energy & Environmental Science, 2010. **3**(6): p. 700-714.
  7. Leonard, J., *Increased rate of EOR brightens outlook*. Oil Gas J.;(United States), 1986. **84**(15).
  8. Gurgel, A., et al., *A review on chemical flooding methods applied in enhanced oil recovery*. Brazilian journal of petroleum and gas, 2008. **2**(2).
  9. Sun, X., et al., *Enhanced heavy oil recovery in thin reservoirs using foamy oil-assisted methane huff-n-puff method*. Fuel, 2015. **159**: p. 962-973.
  10. Rezk, M.Y. and N.K. Allam, *Impact of Nanotechnology on Enhanced Oil Recovery: A Mini-Review*. Industrial & Engineering Chemistry Research, 2019. **58**(36): p. 16287-16295.
  11. Haruna, M.A., et al., *Nanoparticle modified polyacrylamide for enhanced oil recovery at harsh conditions*. Fuel, 2020. **268**: p. 117186.
  12. Sun, Y., et al., *Properties of Nanofluids and Their Applications in Enhanced Oil Recovery: A Comprehensive Review*. Energy & Fuels, 2020. **34**(2): p. 1202-1218.
  13. Alnarabiji, M.S. and M.M. Husein, *Application of bare nanoparticle-based nanofluids in enhanced oil recovery*. Fuel, 2020. **267**: p. 117262.
  14. Murshed, S.S. and C.N. De Castro, *Nanofluids: synthesis, properties, and applications*. 2014: Nova Science Publishers, Incorporated.
  15. Nowrouzi, I., A.K. Manshad, and A.H. Mohammadi, *Effects of TiO<sub>2</sub>, MgO, and  $\gamma$ -Al<sub>2</sub>O<sub>3</sub> nano-particles in carbonated water on water-oil interfacial tension (IFT) reduction in chemical enhanced oil recovery (CEOR) process*. Journal of Molecular Liquids, 2019. **292**: p. 111348.
  16. Al-Anssari, S., et al., *Effect of temperature and SiO<sub>2</sub> nanoparticle size on wettability alteration of oil-wet calcite*. Fuel, 2017. **206**: p. 34-42.
  17. Adil, M., H.M. Zaid, and L.K. Chuan, *Electromagnetically-induced change in interfacial tension and contact angle of oil droplet using dielectric nanofluids*. Fuel, 2020. **259**: p. 116274.
  18. Hendraningrat, L., S. Li, and O. Torsæter, *A coreflood investigation of nanofluid enhanced oil recovery*. Journal of Petroleum Science and Engineering, 2013. **111**: p. 128-138.
  19. Moldoveanu, G.M., et al., *Experimental study on viscosity of stabilized Al<sub>2</sub>O<sub>3</sub>, TiO<sub>2</sub> nanofluids and their hybrid*. Thermochemica Acta, 2018. **659**: p. 203-212.
  20. Nabil, M., et al., *An experimental study on the thermal conductivity and dynamic viscosity of TiO<sub>2</sub>-SiO<sub>2</sub> nanofluids in water: ethylene glycol mixture*. International Communications in Heat and Mass Transfer, 2017. **86**: p. 181-189.
  21. Sun, X., et al., *Application of nanoparticles in enhanced oil recovery: a critical review of recent progress*. Energies, 2017. **10**(3): p. 345.

22. Wasan, D., A. Nikolov, and K. Kondiparty, *The wetting and spreading of nanofluids on solids: Role of the structural disjoining pressure*. Current Opinion in Colloid & Interface Science, 2011. **16**(4): p. 344-349.
23. Wasan, D.T. and A.D. Nikolov, *Spreading of nanofluids on solids*. Nature, 2003. **423**(6936): p. 156-159.
24. Zhang, H., A. Nikolov, and D. Wasan, *Dewetting film dynamics inside a capillary using a micellar nanofluid*. Langmuir, 2014. **30**(31): p. 9430-9435.
25. Chang, Y., et al., *Nanomechanical characteristics of trapped oil droplets with nanoparticles: A molecular dynamics simulation*. Journal of Petroleum Science and Engineering, 2021. **203**: p. 108649.
26. Yakasai, F., et al., *Current Developments and Future Outlook in Nanofluid Flooding: A Comprehensive Review of Various Parameters Influencing Oil Recovery Mechanisms*. Journal of Industrial and Engineering Chemistry, 2020.
27. Sedghi, M., M. Piri, and L. Goual, *Atomistic molecular dynamics simulations of crude oil/brine displacement in calcite mesopores*. Langmuir, 2016. **32**(14): p. 3375-3384.
28. Li, C., Y. Li, and H. Pu, *Molecular simulation study of interfacial tension reduction and oil detachment in nanochannels by Surface-modified silica nanoparticles*. Fuel, 2021. **292**: p. 120318.
29. Zhao, J., et al., *Molecular dynamics investigation of substrate wettability alteration and oil transport in a calcite nanopore*. Fuel, 2019. **239**: p. 1149-1161.
30. Ahmadi, M. and Z. Chen, *Comprehensive molecular scale modeling of anionic surfactant-asphaltene interactions*. Fuel, 2021. **288**: p. 119729.
31. Ahmadi, M. and Z. Chen, *Spotlight onto surfactant–steam–bitumen interfacial behavior via molecular dynamics simulation*. Scientific reports, 2021. **11**(1): p. 1-33.
32. Ahmadi, M., et al., *Interfacial and molecular interactions between fractions of heavy oil and surfactants in porous media: Comprehensive review*. Advances in Colloid and Interface Science, 2020: p. 102242.
33. Ahmadi, M. and Z. Chen, *Molecular interactions between asphaltene and surfactants in a hydrocarbon solvent: application to asphaltene dispersion*. Symmetry, 2020. **12**(11): p. 1767.
34. Ahmadi, M. and Z. Chen, *Insight into the interfacial behavior of surfactants and asphaltenes: molecular dynamics simulation study*. Energy & Fuels, 2020. **34**(11): p. 13536-13551.
35. Miranda, C.R., L.S.d. Lara, and B.C. Tonetto. *Stability and mobility of functionalized silica nanoparticles for enhanced oil recovery applications*. in *SPE international oilfield nanotechnology conference and exhibition*. 2012. Society of Petroleum Engineers.
36. Fan, H. and A. Striolo, *Nanoparticle effects on the water-oil interfacial tension*. Physical Review E, 2012. **86**(5): p. 051610.
37. de Lara, L.S., V.A. Rigo, and C.R. Miranda, *Functionalized silica nanoparticles within multicomponent oil/brine interfaces: a study in molecular dynamics*. The Journal of Physical Chemistry C, 2016. **120**(12): p. 6787-6795.
38. Wu, J., et al. *Effect of nanoparticles on oil-water flow in a confined nanochannel: a molecular dynamics study*. in *SPE international oilfield nanotechnology conference and exhibition*. 2012. Society of Petroleum Engineers.

39. Wang, F. and H. Wu, *Molecular dynamics studies on spreading of nanofluids promoted by nanoparticle adsorption on solid surface*. Theoretical and Applied Mechanics Letters, 2013. **3**(5).
40. Wang, F.-C. and H.-A. Wu, *Enhanced oil droplet detachment from solid surfaces in charged nanoparticle suspensions*. Soft Matter, 2013. **9**(33).
41. Wang, X., et al., *Atomistic insights into the nanofluid transport through an ultra-confined capillary*. Phys Chem Chem Phys, 2018. **20**(7): p. 4831-4839.
42. Wang, X., et al., *Transportation of Janus nanoparticles in confined nanochannels: a molecular dynamics simulation*. Environmental Science: Nano, 2019. **6**(9): p. 2810-2819.
43. Wang, X., et al., *Insight into the pressure-induced displacement mechanism for selecting efficient nanofluids in various capillaries*. Environmental Science: Nano, 2020. **7**(9): p. 2785-2794.
44. Durret, J., et al., *Superhydrophobic polymeric films with hierarchical structures produced by nanoimprint (NIL) and plasma roughening*. Applied Surface Science, 2018. **445**: p. 97-106.
45. Savoy, E.S. and F.A. Escobedo, *Molecular simulations of wetting of a rough surface by an oily fluid: Effect of topology, chemistry, and droplet size on wetting transition rates*. Langmuir, 2012. **28**(7): p. 3412-3419.
46. Wang, G., et al., *Kinetic Monte Carlo study on the evolution of silicon surface roughness under hydrogen thermal treatment*. Applied Surface Science, 2017. **414**: p. 361-364.
47. Meng, Q., D. Chen, and G. Wu, *Microscopic Mechanisms for the dynamic wetting of a heavy oil mixture on a rough silica surface*. The Journal of Physical Chemistry C, 2018. **122**(43): p. 24977-24986.
48. Moulton, O.A., et al., *Atomistic molecular dynamics simulations of carbon dioxide diffusivity in n-hexane, n-decane, n-hexadecane, cyclohexane, and squalane*. The Journal of Physical Chemistry B, 2016. **120**(50): p. 12890-12900.
49. Molinero, V. and E.B. Moore, *Water modeled as an intermediate element between carbon and silicon*. The Journal of Physical Chemistry B, 2009. **113**(13): p. 4008-4016.
50. Martin, M.G. and J.I. Siepmann, *Transferable potentials for phase equilibria. I. United-atom description of n-alkanes*. The Journal of Physical Chemistry B, 1998. **102**(14): p. 2569-2577.
51. Plimpton, S., *Fast parallel algorithms for short-range molecular dynamics*. 1993, Sandia National Labs., Albuquerque, NM (United States).
52. Stillinger, F.H. and T.A. Weber, *Computer simulation of local order in condensed phases of silicon*. Physical review B, 1985. **31**(8): p. 5262.
53. Hoover, W.G., *Canonical dynamics: Equilibrium phase-space distributions*. Physical review A, 1985. **31**(3): p. 1695.
54. Nosé, S., *A unified formulation of the constant temperature molecular dynamics methods*. The Journal of chemical physics, 1984. **81**(1): p. 511-519.
55. Stukowski, A., *Visualization and analysis of atomistic simulation data with OVITO—the Open Visualization Tool*. Modelling and Simulation in Materials Science and Engineering, 2009. **18**(1): p. 015012.
56. Willhite, G.P., *Waterflooding*. 1986.
57. Craig, F.F., *The reservoir engineering aspects of waterflooding*. Vol. 3. 1971: HL Doherty Memorial Fund of AIME New York.

58. Thomas, J.A. and A.J. McGaughey, *Reassessing fast water transport through carbon nanotubes*. Nano letters, 2008. **8**(9): p. 2788-2793.
59. Speight, J.G., *Introduction to enhanced recovery methods for heavy oil and tar sands*. 2016: Gulf Professional Publishing.
60. Giraldo, L.J. *Janus nanoparticles for enhanced oil recovery EOR: Reduction of Interfacial Tension*. in *SPE annual technical conference and exhibition*. 2018. Society of Petroleum Engineers.
61. Eltoun, H., Y.-L. Yang, and J.-R. Hou, *The effect of nanoparticles on reservoir wettability alteration: a critical review*. Petroleum Science, 2020. **18**(1): p. 136-153.
62. Chang, B., et al., *Sliding droplets on hydrophilic/superhydrophobic patterned surfaces for liquid deposition*. Applied Physics Letters, 2016. **108**(15).
63. Zhang, P., et al., *Grooved organogel surfaces towards anisotropic sliding of water droplets*. Adv Mater, 2014. **26**(19): p. 3131-5.
64. Guo, H., K. Song, and R. Hilfer. *A Critical Review of Capillary Number and its Application in Enhanced Oil Recovery*. in *SPE Improved Oil Recovery Conference*. 2020. Society of Petroleum Engineers.
65. Guo, H., et al. *Review of capillary number in chemical enhanced oil recovery*. in *SPE Kuwait Oil and Gas Show and Conference*. 2015. Society of Petroleum Engineers.
66. Yiotis, A., et al., *Pore-scale effects during the transition from capillary-to viscosity-dominated flow dynamics within microfluidic porous-like domains*. Scientific Reports, 2021. **11**(1): p. 1-16.
67. Masalmeh, S.K. *Impact of capillary forces on residual oil saturation and flooding experiments for mixed to oil-wet carbonate reservoirs*. in *SCA*. 2012.
68. Fang, T., et al., *Oil extraction mechanism in CO<sub>2</sub> flooding from rough surface: Molecular dynamics simulation*. Applied Surface Science, 2019. **494**: p. 80-86.
69. Wang, X., et al., *Displacement of nanofluids in silica nanopores: influenced by wettability of nanoparticles and oil components*. Environmental Science: Nano, 2018. **5**(11): p. 2641-2650.

## Supporting Information

# Displacement Dynamics of Trapped Oil in Rough Channels Driven by Nanofluids

Yuanhao Chang <sup>a</sup>, Senbo Xiao <sup>a,1</sup>, Rui Ma <sup>a</sup>, Xiao Wang <sup>b</sup>, Zhiliang Zhang <sup>a</sup>, Jianying He <sup>a,2</sup>

<sup>a</sup> NTNU Nanomechanical Lab, Department of Structural Engineering,

Norwegian University of Science and Technology (NTNU), 7491 Trondheim, Norway

<sup>b</sup> School of Materials Science and Engineering, China University of Petroleum (East China), Qingdao, 266580 Shandong, China

### S1. The acquisition of trapped oil/water/rough surface system

In order to model the rough channel with trapped oil, a channel filled with oil phase was used to simulate the primary water flooding process. The initial system can be seen in Fig. S1(a). The size of the channel and the detailed structural parameters were given in the main text. A constant force ( $10^{-4}$  kcal/mol/Å) along the x-axis was applied on the piston for realizing the primary flooding. The simulation parameters of the primary flooding were the same as that of displacement simulations in the main text, as given in the Method section. The primary flooding ends as the injected water volume excludes the easy oil out of the channel, leaving the trapped oil in the rough channel, as shown in Fig. S1(b). The central channel part, as indicated by the dash-lined area, was used to build the simulation systems shown in Fig. 1.

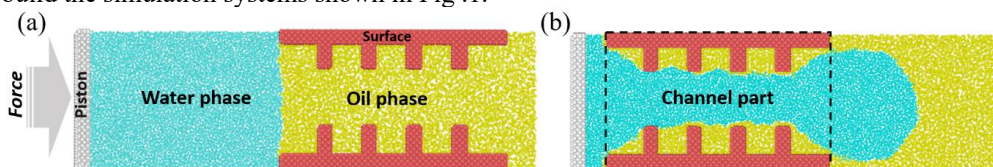


**Fig. S1** Primary flooding and preparation of trapped oil in the rough channel. (a) The side view of the initial displacement system with oil-filled channel and (b) the snapshot after primary flooding and 1-ns equilibration. The colors for different phases: piston (grey), water (light blue), rough surface (red), and oil (yellow). The dash-lined box represents the channel part of the system used for this study.

### S2. Atomistic interaction parameter validation

For maintaining stable trapped oil in the channel after the primary water flooding, a pre-test was carried out to determine the suitable atomistic potential parameters for



the hydrophobic surface. A smooth channel filled with oil was first built (Fig. S2(a)), with three flooding simulations carried out subsequently using different characteristic energy between surface and water (from 0.05 kcal/mol to 0.2 kcal/mol). In performing the simulations, all the other parameters are the same as given in the main text. The flooding simulations ended as the injected water volume was driven into the channel. All the simulations were equilibrated in the NVT ensemble for 3 ns. As the resulting system snapshots plotted in Fig. S2(b), the surfaces showed enhanced attraction to oil molecules with increasing characteristic energy  $\epsilon_{so}$ . With  $\epsilon_{so}$  reaching 0.1 kcal/mol, the surface starts to have residual oil molecules after flooding. As  $\epsilon_{so}$  reached 0.2 kcal/mol, there is the oil film left in the channel and the surface under this condition can be regarded as the hydrophobic channel. Therefore, characteristic energy  $\epsilon_{so}=0.2$  kcal/mol was chosen for the research.

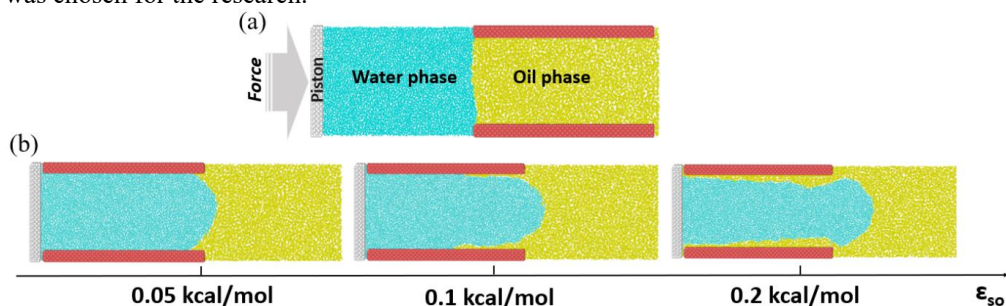


**Fig. S2** Atomistic parameter validation by flooding simulations. (a) The side view of the initial oil-filled system and (b) the snapshots after displacement and 1-ns equilibration. The x-axis represents the different characteristic energy.

### S3. The total potential energy of the systems in equilibration simulations

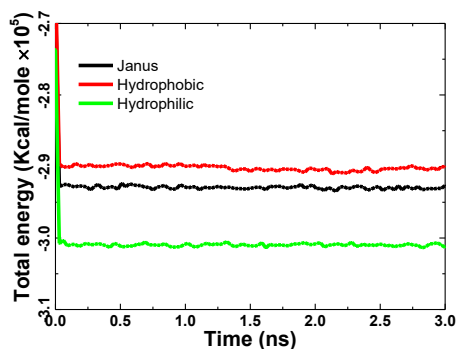


**Fig. S3** The total potential energy of the systems in the 3 ns equilibration simulation. The total potential energy of all the three systems quickly reached a plateau state and maintained stable till the end of the simulations.

### S4. The force fields parameters for NPs

Based on the previous study, the force field parameters for NPs with water, oil, surface, and itself are listed in Table S1 [1].

Table S1 Force fields parameters for NPs

Characteristic energy, kcal/mol	Water	Oil	Surface	Itself
Hydrophilic NPs	0.6	0.05	0.7	0.01
Janus NPs (hydrophilic part)	0.01	0.2		
Janus NPs (hydrophobic part)	0.4	0.01		
Hydrophobic NPs	0.05	0.6		

### S5. Collective velocity distribution of trapped oil along the x-axis

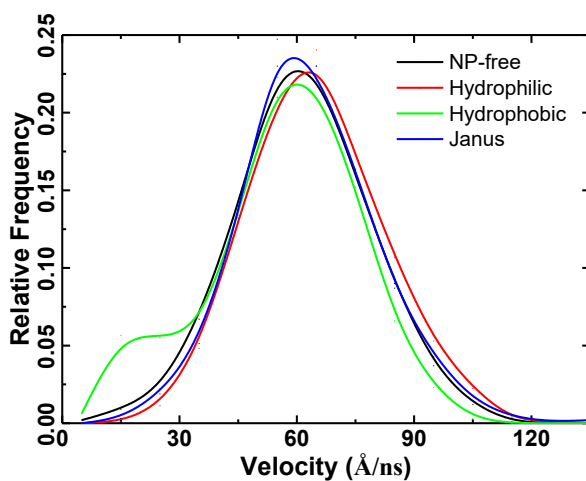


Fig. S4 Collective velocity distribution of the trapped oil in four systems along the direction of injection in a period of 20 ps.

### S6. The mean square displacement (MSD) of water molecules

The mean square displacement (MSD) curves of water molecules in the four systems calculated using a 1-ns equilibrium trajectory, as shown in Fig. S5.

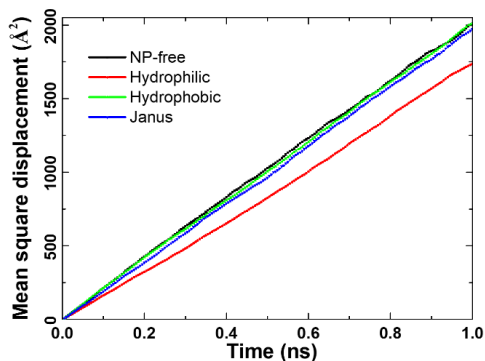


Fig. S5 MSD of water molecules in the four systems.

### S7. The modeling and calculation of interfacial tension

The oil/water/Janus NPs simulation system (Fig. S6(b)) containing four Janus NPs (the diameter is 7 Å) was built for obtaining the interfacial tension alteration by the appearance of Janus NPs. For comparison, the oil/water simulation system (Fig. S6(a)) was also constructed. All the simulation parameters and atomistic interaction potentials were the same as given in the main text. To obtain the surface tension, 5 ns equilibration was carried out in the NPT ensemble followed by another 5 ns equilibration in the NVT ensemble. Finally, an extra 1 ns trajectory of equilibration simulation in the NVT ensemble was performed for the interfacial tension calculation.

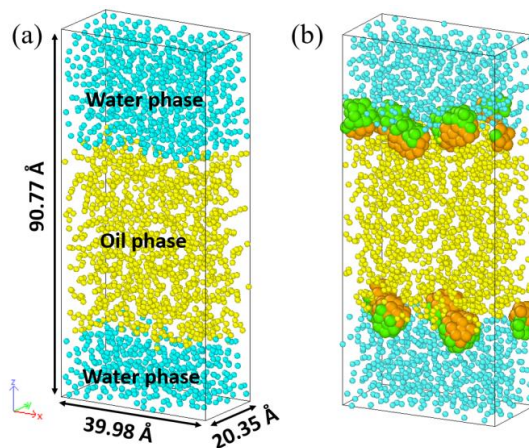


Fig. S6 Systems build for characterization of interfacial tension, namely the water/oil system (a) and the water/oil/Janus NPs system (b).

The interfacial tension of the systems (Fig. S6) consisting of two interfaces was calculated by subtracting mean tangential stress tensors from the normal one [2].

$$\gamma = \frac{1}{2} L_z [p_{zz} - \frac{1}{2} (p_{xx} + p_{yy})] \quad (1)$$

Where  $\gamma$  represents the interfacial tension,  $L_z$  is the length of the simulation box in the z-axis;  $p_{xx}$ ,  $p_{yy}$ ,  $p_{zz}$  are the stress tensors in the x-axis, y-axis, z-axis, respectively.

### S8. Adsorption of oil molecules on hydrophobic NPs

Bound oil molecules on a hydrophobic NP during the displacement process were recorded in Fig. S7. During the displacement process, these oil molecules were closely bound to and diffused with the NP.

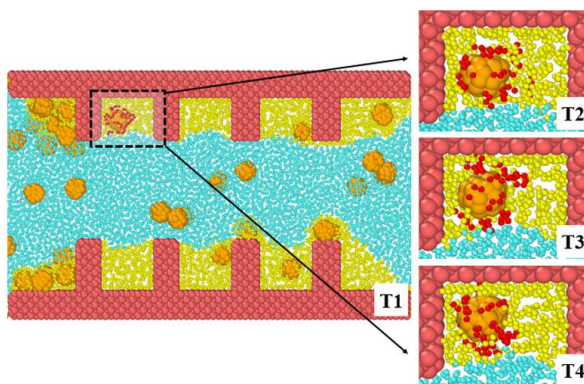


**Fig. S7** The representative snapshots for hydrophobic NPs in the displacement. The region in the dotted box included a hydrophobic NP with bound oil molecules. The corresponding sequential snapshots of the NP are given as insets, marked by T1-4. The bound oil molecules are highlighted in red to track their movement.

### S9. System snapshots after displacement under the varied applied force

After displacement with varied external force, system snapshots are collected and shown in Fig. S8. Compared to the results shown in the main text, the micro behavior pattern of the three types of nanofluids keeps similar. Specifically, Janus NPs were more likely to adsorb at the oil-water interface while hydrophobic NPs penetrated into the oil phase. With increasing pumping force, more Janus and hydrophobic NPs stayed in the water. The occurrence state of hydrophilic NPs in the system was not obviously affected by the increasing pumping force and kept staying in the water after the displacement.

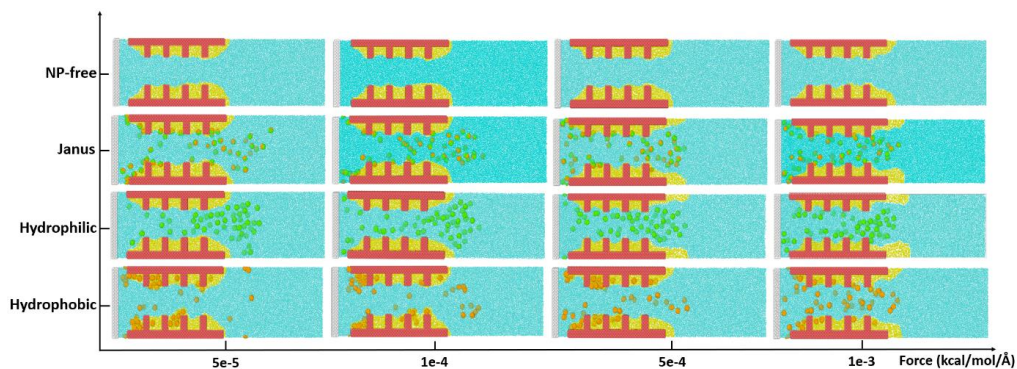


**Fig. S8** System snapshots after displacement under varied pumping force. The x-axis indicated the external force and the y-axis represents the types of injection fluids.

### S10. Oil sweeping by hydrophobic NPs under high pumping force

As detailed snapshots shown in Fig. S9, the movement of the two marked hydrophobic NPs was tracked under high pumping force applied on the injection fluid. The two NPs first migrated to the top of one pillar structure where oil molecules on the pillar bound to the NPs and subsequently being transported away.

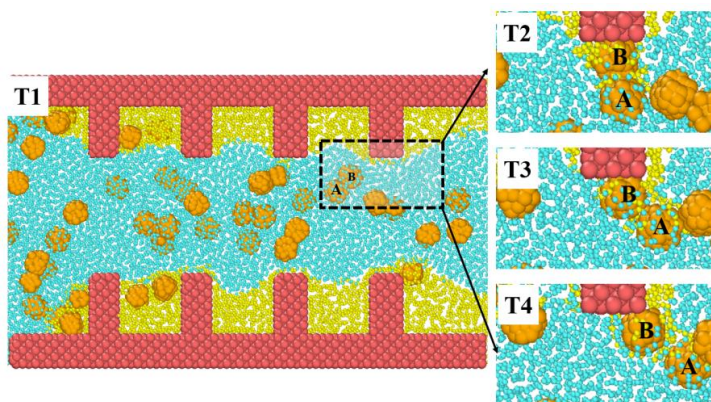


**Fig. S9.** The representative snapshots for hydrophobic NPs under high pumping force. The region in the dotted box includes the NPs of interest, with insets showing the sequential snapshots over time. The two NPs as the observation object are marked as A and B in the figure.

### References

1. Wang, X.; Zhang, Z.; Zhang, J.; He, J. Insight into the pressure-induced displacement mechanism for selecting efficient nanofluids in various capillaries. *Environmental Science: Nano* **2020**, *7*, 2785-2794.
2. Zhang, Y.; Feller, S.E.; Brooks, B.R.; Pastor, R.W. Computer simulation of liquid/liquid interfaces. I. Theory and application to octane/water. *The Journal of chemical physics* **1995**, *103*, 10252-10266.



## **A.2 Paper II**

---

### **Atomistic insight into oil displacement on rough surface by Janus nanoparticles**

Authors: Yuanhao Chang, Senbo Xiao, Rui Ma, Zhiliang Zhang and Jianying He  
Energy, 2022, 245: 123264.



**Atomistic Insight into Oil Displacement on Rough Surface by Janus  
Nanoparticles**

Yuanhao Chang <sup>a</sup>, Senbo Xiao <sup>a,1</sup>, Rui Ma <sup>a</sup>, Zhiliang Zhang <sup>a</sup>, Jianying He <sup>a,2</sup>

<sup>a</sup> Department of Structural Engineering, Norwegian University of Science and Technology (NTNU), 7491 Trondheim, Norway

**Abstract**

Janus nanoparticles (NPs) hold great potential in enhanced oil recovery (EOR), although the mechanism remains unclear. In the study, the displacement dynamics of trapped oil in the rough channel by Janus NPs are unraveled through atomistic modeling. The results indicate that Janus NPs with large polar faces significantly recover more oil from the nano-pocket (nano groove of the surface). The structure of adsorbed NPs on the wall of oil-trapping nano-pockets strongly causes the local wettability alteration, which ultimately determines the oil recovery. The crucial events in oil recovery by Janus NPs, termed ‘adsorption invasion process’, are identified, which comprise of anchoring onto the surface, pinning at the edge, and entering inside the pocket. The controlling factors are further detailed, including identification of the residual oil, displacement pressure, and the geometry of the oil-water interface inside nano-pockets. With the proposed analysis, the “huff-n-puff” mode is verified as the optimized application method for Janus NPs. For the first time, our results bring to light the dynamic wettability alteration on the rough surface by Janus NPs from atomistic insights. The findings reveal the intrinsic EOR mechanism of Janus NPs, which could guide the design and application of Janus NPs in EOR.

Keywords: Janus nanoparticles; oil recovery; molecular dynamics simulation; rough surface; wettability alteration

### Abbreviations

<b>Term</b>	<b>Meaning</b>
25JNP	Janus nanoparticle with nonpolar beads covering 25%
50JNP	Janus nanoparticle with nonpolar beads covering 50%
75JNP	Janus nanoparticle with nonpolar beads covering 75%
DPD	Dissipative particle dynamics
EOR	Enhance oil recovery
IFT	Interfacial tension
JNP	Janus nanoparticle
LJ	Lennard-Jones
mW	Monoatomic water
MD	Molecular dynamics
NEMD	Non-equilibrium molecular dynamics
PMF	Potential of mean force
SW	Stillinger–Weber
TraPPE-UA	The Transferable Potentials for Phase Equilibria united-atom

### 1. Introduction

It is expected that global energy consumption will increase by 30% or more by 2040, led mainly by fossil fuels [1]. Owing to the aggressive exploration of easily recoverable oil by the primary and secondary flooding, the current high cost and low efficiency in

oil recovery have been calling for the new generation of economical and effective enhanced oil recovery (EOR) technologies, for the purpose of extracting the huge amount of remaining oil in the available reservoirs [2-4]. Such desires are greatly driven by the huge challenges encountered by the traditional oil recovery methods, including but not limited to high energy and chemicals cost, gravity override, fingering and early breakthrough, formation damage, etc. [5-7]. On addressing the challenges, nanoparticles (NPs) are believed to possess promising potentials, thanks to their ultra-small size, high surface-to-volume ratio, low costs, and environmental friendliness [8-10]. Utilizing nanofluids, namely flooding liquids with NPs, has been a focus of interest in petroleum research and applications starting from the end of the last century [11-14].

The promising EOR effect of nanofluid flooding has been confirmed in multi-scale experiments [15, 16], and also in a number of field trials in Colombia, Saudi Arabia, and China [17-19]. Accordingly, multiple possible mechanisms for the nanofluid EOR, including wettability alteration, interfacial tension (IFT) reduction, structural disjoining pressure, and viscosity adjustment, have been proposed in different studies [9, 20]. However, because of the lack of knowledge on atomistic interactions among NPs, fluids, and rock surfaces, the intrinsic nanoscale basis for deciphering the nanofluid EOR mechanism is still missing. Furthermore, the published conclusions were obtained based on various experimental schemes, which complicated the understanding of the NP function in EOR [19]. Hence, more fundamental research inputs are urged to accelerate the wide-ranging oilfield applications for nanofluid EOR.

It is well accepted that the chemistry and distribution of functional groups on the surface determine the behavior of NPs [21, 22]. With the unique characteristic properties (polarity of two distinct hydrophobic and hydrophilic parts on the surface), Janus NPs were found to play a crucial role in EOR, with application potential proven

to significantly exceed unmodified NPs [23-27]. Particularly, there are a good number of studies devoted to uncovering the excellent performance of Janus NPs at the oil-water interface [27-32]. Janus NPs were proved to be more effective in the reduction of IFT if compared with other NPs with similar sizes [32]. Using dissipative particle dynamics simulations (DPD), A. Striolo et al. presented that the reduction of the IFT was determined by the surface coverage, shape, and ratio of polar/nonpolar beads of Janus NPs [29-31]. To the best of our knowledge, Wang X et al carried out the only reported molecular study on the interactions between Janus NPs, fluids, and solid substrate [28]. Their results indicated that Janus NPs were able to hinder the oil displacement and capillary pressure was found to be the crucial factor of the process. Nevertheless, the above results were obtained in smooth channels, which could potentially be deviating or even invalid in channels with rough surfaces in real reservoirs [33-35]. Elucidating the EOR mechanisms of displacing trapped oil on rough surfaces is highly desired [36], especially with the injection of Janus NPs.

Herein, molecular dynamics (MD) simulations were employed to investigate the displacement of residual trapped oil in the rough channel by Janus NPs. Specifically, oil recovery efficiency of Janus NPs with varied fractions of nonpolar beads on the surface was presented. The detailed motion characteristics of Janus NPs on anchoring onto the solid surface, sweeping trapped oil, pinning, and entering oil trapping pockets were revealed. Crucial parameters for optimizing the EOR effect of Janus NPs were proposed. The findings of the study open out the residual oil recovery mechanism on the rough surface and are thus desired by the design and application of Janus NPs in EOR.

## **2. Model and simulation details**

All the MD simulations were carried out using the LAMMPS package [37]. The visualization and analysis were implemented with the OVITO software [38]. As shown in Fig. 1, the atomic system representing the important feature of trapped oil on the rough surface was constructed. It had periodic boundaries and contained residual trapped oil in a nano-pocket and nanofluids. The grooved surface, namely the nano-pocket with the dimensions of  $100 \times 70 \times 51 \text{ \AA}^3$ , was created by removing the atoms in the solid substrate of silicon crystals. In order to eliminate periodic effects, the minimum height of the surface was set as  $11 \text{ \AA}$ , which was larger than the cutoff distance ( $10 \text{ \AA}$ ). The height of residual oil film on the upper surface was around  $5 \text{ \AA}$ . A number of 1004 hexane molecules were absorbed on the solid surface and in the nano-pocket to mimic the residual trapped oil after initial water flooding and had an oil density same as experiments. For the flooding phase, 48 spherical Janus NPs with a diameter of  $10 \text{ \AA}$  and 21399 water molecules were used for constructing the nanofluid with an NP concentration of 3.9%. The initial pressure was around 24.6 MPa. Three systems, with Janus NPs of the varied ratio of nonpolar beads covering 25%, 50%, and 75% of the surface areas, were built, respectively. The three corresponding Janus particle types were termed the 25JNP, the 50JNP, and the 75JNP in the following text if not otherwise specified.

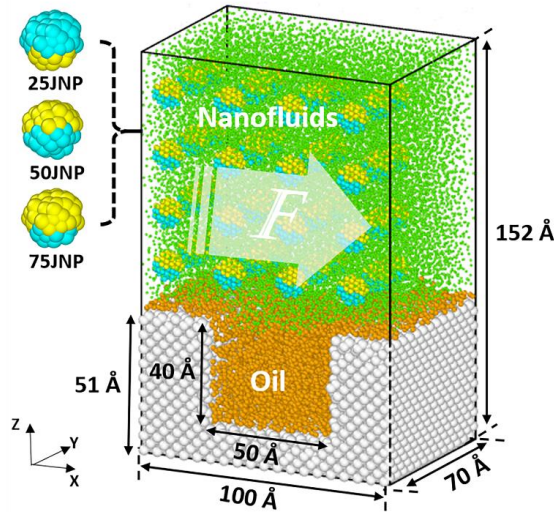


**Fig. 1.** The initial structure of the simulation system. The white arrow shows the flooding direction. The colors for different components: water (green), oil (orange), surface (white), the hydrophobic part (yellow), and the hydrophilic part of Janus NP (blue).

The mW water model was employed for the water molecules while the Transferable Potentials for Phase Equilibria united-atom (TraPPE-UA) description of hexane is chosen for oil molecules. The mW is able to reproduce the important properties of water (like energetics, density, and structure) with better accuracy than most other water models, at an extremely low computational cost [39]. The TraPPE-UA is well suitable for the phase separation process involving alkanes by using pseudo-atoms [40]. To be specific, the mW water model used the Stillinger–Weber (SW) potential to feature the many-body non-bonded interactions, while the water-oil and oil-oil non-bonded interactions adopted the standard pairwise 12-6 Lennard-Jones (LJ) potential. In our simulation, the main purpose is to study the displacement dynamics of the residual oil by JNPs on the oil-wet surface, rather than demonstrating a designed material of JNPs or the influence of the specific surface. Therefore, materials for the surface and JNPs were not specified in the work. Based on our previous study [41], the characteristic energy  $\varepsilon_{ws}$

(water-surface) was set as 0.3 kcal/mol to form a hydrophobic surface. The characteristic energy for interactions involved by Janus NPs was selected with reference to other previous studies [28, 42], with the specific values listed in supporting information Table S1.

In carrying out simulations, the systems were first energy-minimized using the steepest descent method and followed by a 0.5-ns equilibrium stage in the NVT ensemble at 350 K. The Nosé–Hoover thermostat with a coupling coefficient of 100 fs was used to maintain the aimed temperature [43, 44]. In order to mimic the nanofluid flooding process, another 60-ns non-equilibrium MD simulation (NEMD) was conducted in each system. A constant force along the x-axis (0.01 kcal/mol/Å in the reference system) was applied to each atom of water molecules. Besides, to speed up the simulation, Janus NPs were treated as the rigid body and the rough surface was positionally fixed. Five independent simulations were run for each system to improve the accuracy of results.

### **3. Result and discussion**

#### *3.1. Displacement of residual oil in nano pockets*

The inclusion of Janus NPs into the flooding significantly affected the displacement of the trapped oil in the nano-pocket. As the snapshots of residual oil in the nano-pocket shown in Fig. 2, pure water flooding (JNP-free) led to an almost non-observable displacement effect. In contrast, Janus NPs actively interacted with the solid substrate and the trapped oil during the flooding, not only adsorbing on the rough surface but also invading into the oil pocket depending on the surface nonpolar bead ratio. 25JNPs adsorbed on the solid substrate and were able to enter the nano-pocket along the solid wall. Thanks to the large area of the polar bead on the surface, 25JNPs also brought

water molecules into the nano-pocket and extracted a significant amount of oil molecules out of the pocket. The 50JNP also featured the behavior of the 25JNP in oil recovery. Furthermore, 50JNPs greatly altered the oil-water interface tension in the nano-pocket by stably dwelling at the oil-water interface [26]. 75JNPs entered the oil-trapping nano-pocket by immersion into the oil phase, thanks to the large portion of surface nonpolar beads. As such, a certain amount of oil molecules was displaced by 75JNPs due to volume exclusion in the nano-pocket.

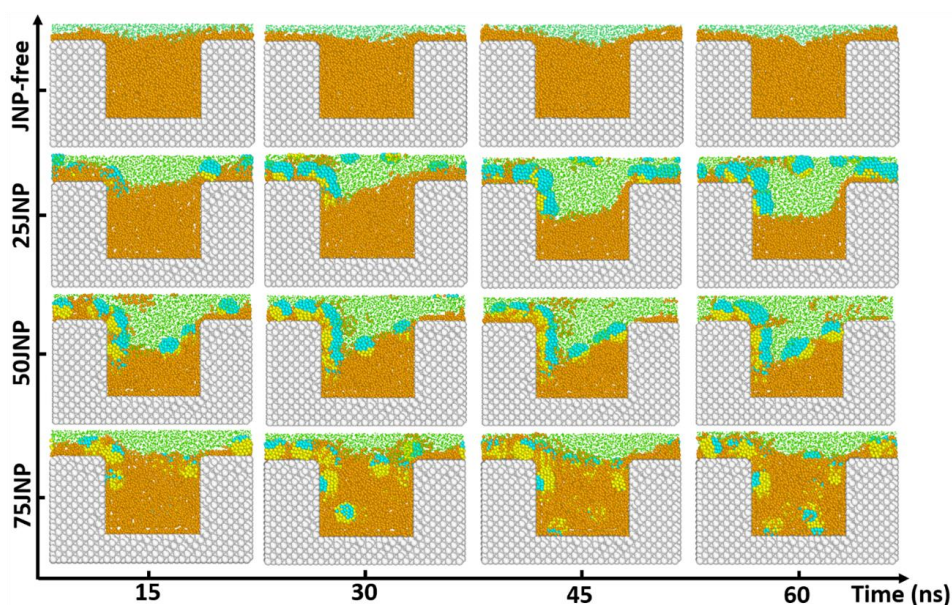


**Fig. 2.** System snapshots of the displacement process with different flooding. The x-axis indicates the simulation time, and the y-axis represents the types of injected Janus NPs. For better visualization, only the area near the nano-pocket was shown in the snapshots.

Because of the different behaviors of Janus particle types detailed above, the final performance of oil recovery varied correspondingly. The recovery efficiency defined by the percentage of oil molecules displaced out of the nano-pocket at the end of the simulations was shown in Fig. 3(a). The 25JNP and the 50JNP possessed the most obvious displacement effect, yielding a recovery efficiency of  $\sim 34.7\%$  and  $\sim 36.9\%$ ,



respectively. In comparison, the 75JNP showed a much lower recovery efficiency of  $\sim 8\%$ . Pure water flooding resulted in the lowest recovery efficiency ( $\sim 1.7\%$ ) as expected given that the mobility of residual trapped oil was known to be highly limited after primary and secondary flooding [45, 46]. The surface properties of the Janus NPs determined their final distribution in the nano-pocket after flooding. As shown in Fig. 3(b, left panel), all the Janus NPs favored accumulating on the left-side wall of the nano-pocket. Both 50 JNPs and 75JNPs appeared in the center of the nano-pocket, as they either adsorbed at the oil-water interface or immersed into the oil phase. In contrast, there were almost no 25JNPs in the center of the nano-pocket. The three kinds of Janus NPs also exhibited varied migration depth into the nano-pocket, as depicted in Fig. 3(b, right panel). The bigger the surface nonpolar area, the deeper invasion of the NPs into the nano-pocket, given the same flooding condition. Obviously, the distinct motion patterns and adsorption positions of Janus NPs underlay the displacement mechanism and subsequently the recovery efficiency, which will be discussed in detail in the following sections.

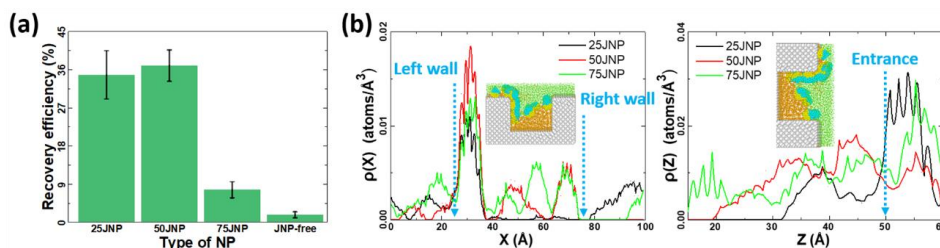


**Fig. 3.** Oil recovery efficiency and NPs distribution. (a) Recovery efficiency with different types of Janus NPs; (b) Distribution of NPs, quantifying by the density profiles of the atoms belong to the Janus NPs along the flooding direction ( $x$ -axis, left panel) and the depth of the nano-pocket ( $z$ -axis, right panel), respectively. The position of the walls and the entrance of the nano-pocket were marked in the figure. Representative system snapshots were shown as the inset with different perspectives for visualization.

### 3.2. Migration characteristics of Janus NPs

### 3.2.1 The structure of adsorbed NPs on the wall of the nano-pocket

The migration of Janus NPs into the nano-pocket along the solid wall underpinned recovery of trapped oil, either by leading invasion of water, alteration of the oil-water interface, or simply volume exclusion as discussed above. Hence, it is of great importance to further characterize the linkage between the dynamic oil recovery, illustrated by the real-time oil molecule numbers in Fig. 4(a), and the change in the distribution and the behavior of the NPs in the nano-pocket in Fig. 4(c). Three quantities were adopted here for the analysis of the NPs' structure, namely the surface coverage  $\phi$  of the pocket wall, the average centroid depth  $D$ , and the ratio of hydrophilicity  $R_{hydrophilic}$ . The detailed definitions of the three quantities were given below, with the sketch given by the snapshot in Fig. 4(b).

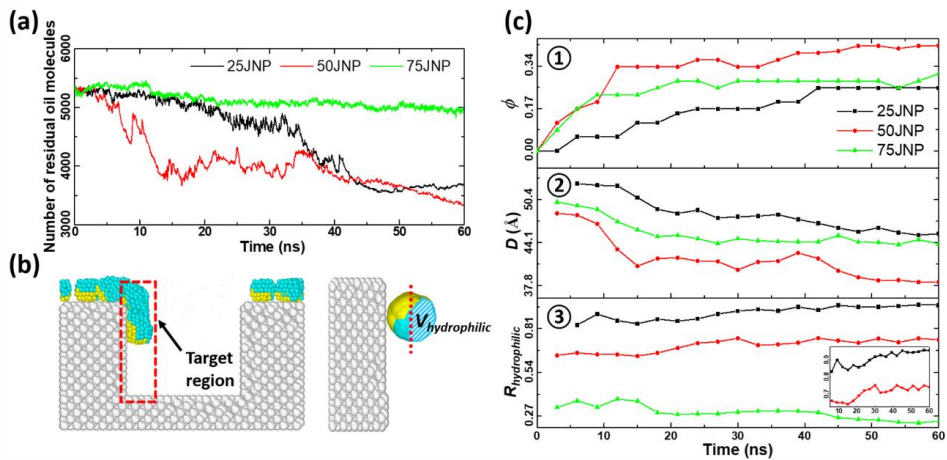


**Fig. 4.** Oil recovery and the underpinning behaviors of Janus NPs. (a) The number of oil molecules inside the nano pocket during the displacement. (b) Adsorption and migration of NPs on the wall of the nano-pocket and sketch of the  $V_{hydrophobic}$  definition. The snapshot on the left indicated the specific NPs of interest for the analysis, and the example on the right indicated the volume of hydrophilic beads in a Janus NP used for the calculation; (c) Changes in three important quantities of the Janus NPs migrating into the nano-pocket, namely ① surface coverage, ② average centroid depth, and ③ the ratio of hydrophilicity from top to bottom.

The surface coverage  $\phi$  reflects the adsorption quantity of the NPs on the wall of the nano-pocket (Fig. 4(c, ①)), which is calculated as:

$$\phi = \frac{N \times \pi d^2}{4A} \quad (1)$$

where  $N$  is the number of adsorbed NPs,  $d$  is the diameter of NPs and  $A$  is the surface area of the wall (dotted area in Fig. 4(c)). The higher the  $\phi$  value, the more NPs adsorbed and migrated on the solid wall inside the nano-pocket. For all the Janus NPs,  $\phi$  featured an obvious increasing pattern during the displacement process, with the 50JNP being the most outperforming in reaching a saturated plateau and in the number of absorbed NPs (Fig. 4(c, ①)). The depth of the adsorbed NPs directly quantifies the migration of the NPs along the solid wall into the nano pocket, which was characterized by the average centroid depth  $D$ . As shown by Fig. 4(c, ②), all the Janus NPs gradually moved down inside the nano-pocket during the displacement. 50JNPs were able to migrate the deepest distance at the end of the displacement. Interestingly, the 50JNP took the shortest time to reach the deepest position in the nano-pocket (Fig.4 (c, ②)) and the highest  $\phi$  value (Fig. 4(c, ①)), which directly resulted in the highly effective oil displacement (Fig. 4(a)). The orientation of the NPs adsorbed on the solid wall directly caused the local surface wettability alteration. The solid substrate was parameterized to be relatively hydrophobic in this work. As such, adsorbed Janus NPs with their polar faces toward the liquid phase resulted in an increase of hydrophilicity of the surface, namely making the surface more water-like. The contribution of the Janus NPs in wettability alteration was indicated by the ratio of hydrophilicity  $R_{hydrophilic}$ , which is defined as:

$$R_{hydrophilic} = \frac{V_{hydrophilic}}{V_{half}} \quad (2)$$

As sketched in Fig. 4(b),  $V_{hydrophilic}$  accounts for the volume of the hydrophilic (polar) beads in the half of NPs,  $V_{half}$ , away from the solid wall. Taking the 50JNP for example, the  $R_{hydrophilic}$  would have a value of 0 or 1 if the polar and nonpolar faces cross-section surface was parallel to the solid wall and the polar faces were facing to or against the solid wall, respectively. Otherwise, the  $R_{hydrophilic}$  had a value between 0 and 1. Given that the 25JNP and the 75JNP were not symmetric in surface polarity like the 50JNP, the absolute value of  $R_{hydrophilic}$  was not the only focus of interest for comparison but also the pattern of changes. As shown in Fig 4(c, ③), the adsorbed 25JNPs had the highest  $R_{hydrophilic}$  as expected, given their highest portion of polar beads in the NP. 50JNPs also exhibited a high value of  $R_{hydrophilic}$ , indicating their effectiveness in converting their adsorbing surface area into hydrophilic. Both the 25JNP and the 50JNP featured a common slowing increase pattern of  $R_{hydrophilic}$  during the displacement. Despite that the 50JNP yielded an obvious lower  $R_{hydrophilic}$  (0.68) than the 25JNP (0.95), their oil recovery efficiency was still superior (Fig. 4(a)), which could be attributed to more adsorbed 50JNPs on the sidewall (i.e. higher  $\phi$  and lower  $D$ ). The 75JNP had the lowest and a decreasing pattern of  $R_{hydrophilic}$  in the three Janus NPs, owing to their relatively small polar faces. As a result, the 75JNP did not show significance in surface wettability alteration, which could be a reason for their low oil recovery (Fig. 2).

### 3.2.2 Motion pattern of adsorbed Janus NPs

The motion pattern of Janus NPs on the surface is the key to elaborate the mechanism of oil recovery. The Janus NPs were able to slide on the substrate and spontaneously invade into the nano-pocket, which suggested an underlying special energy landscape.

To verify this phenomenon, the potential of mean force (PMF) was calculated using umbrella sampling. The PMF quantified the energy differences of one adsorbed Janus NP at different positions on the surface with the oil film without external flooding force, as the calculation system can be seen in Fig. S1. Similar to the umbrella sampling in other studies [28], the NP was anchored to positions with constant interval distances along the oil film plane by a harmonic potential for sampling in equilibration simulations. The displacement distance of the NP from its original position and the corresponding force from the harmonic potential were recorded and processed using the WHAM algorithm [47, 48]. Due to the symmetry of the system, the calculation only covered the first half of the system in the x-direction. As shown in Fig. 5(a), the PMF featured fluctuations at different positions on the solid substrate and flattened out at the oil-water interface over the nano-pocket. The fluctuations of the PMF were attributed to the lattice structure effect of the substrate, namely the matching atomic structure between the Janus NPs and the surface. Good matching can lead to low energy valley of the PMF. If the atomic radius of the solid substrate increased, thus smoother surface, the amplitude of fluctuation decreased, as confirmation results showed in Fig. S2. Interestingly, there was the minimized energy at the entrance of the nano-pocket, and a subsequent high energy barrier for the Janus NPs to directly migrate along the oil-water interface over the nano-pocket, as highlighted in Fig. 5(a). Correspondingly, as indicated in Fig. 5(a), the Janus NP was stably pinned at the edge of the solid substrate. Taking the applied flooding force into consideration, such pinning effect enabled the further downward invasion of the Janus NPs into the nano-pocket and oil recovery. Without the pinned Janus NPs, the flow direction of pure water displacement at the edge of the surface didn't change much from the flooding direction. In comparison to the local streamlines of water plotted in Fig. 5(b), the adsorbed Janus NPs at the edge of the

substrate altered the local wettability and resulted in the transformation of the waterflood direction. In other words, adsorbed Janus NPs on the plane solid surface and slid by the external flooding force were highly likely to stay at the rough edges of the surface and further migrate into the rough structures, which has been observed and confirmed in the experiments [49, 50].

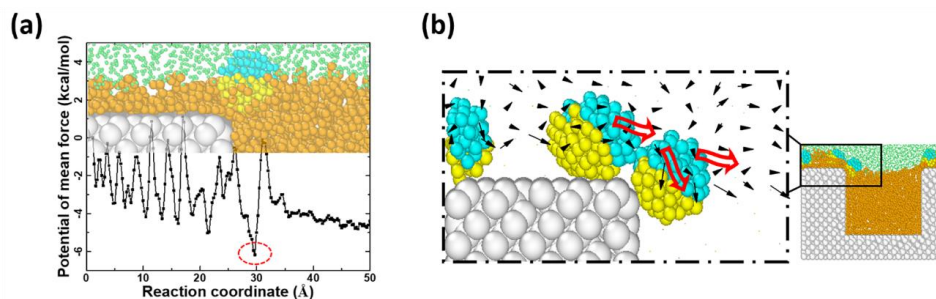


**Fig. 5.** Motion pattern of adsorbed Janus NPs. (a) The PMF of an NP transporting from the left side of the surface to the middle of the nano-pocket along the oil-water interface. The energy well resulting in pinning effects of Janus NPs is highlighted in the figure. (b) Local streamlines of water molecules around adsorbed Janus NPs. The red arrows indicated the motion of Janus NPs at the entrance of the nano-pocket for better visualization.

With the above analysis, the key events in the motion of Janus NPs adsorbed on the solid surface can be summarized as Fig. 6. There were four stages involved in the ‘adsorption invasion process’, namely oil-water interface identification and surface adsorption, edge pinning, invasion, and collision and pushing. More specifically, the Janus NPs were able to identify the oil-water interface and further adsorbed on the solid surface relying on their hydrophobic face. Driven by the flooding flow, the Janus NP slid on the surface and pinned stably at the edge of the substrate owing to the local deep energy well, termed pinning effect. Impelled by the local flooding currents, the NP initially invaded into the entrance of the nano-pocket along the solid wall. With given more Janus NPs adsorbing on the substrate and following the above route, multiple

Janus NPs entered the nano-pocket and pushed the NPs in front to move down inside the nano-pocket. Owing to the unique surface wettability polarity, the Janus NPs can rotate and adjust their position in this process and alter the wettability of the solid wall. Such motion pattern resembled the appearance and growth of climbing film observed in the previous experiment [27], and provided atomistic details for a better understanding.

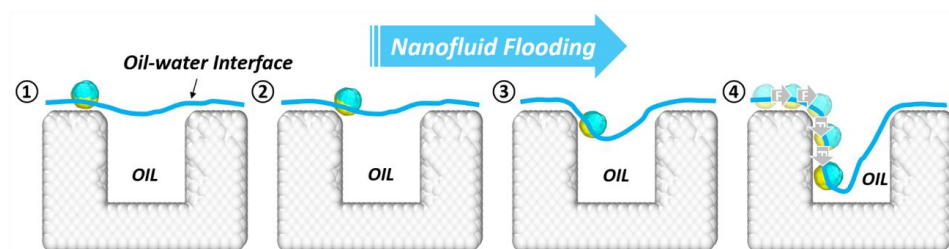


**Fig. 6.** Schematic diagram of the ‘adsorption invasion process’ of Janus NPs in the flooding. From left to right are ① oil-water interface identification and surface adsorption, ② edge pinning, ③ invasion, and ④ collision and pushing.

### 3.3. Controlling factors analysis

The representative motion pattern of Janus NPs on the solid surface can be specifically termed the ‘adsorption invasion process’ here (Fig. 6), which determined the arrangement of NPs inside the nano pocket and greatly influenced the amount of extracted oil. For a given rough surface of similar nature, three factors dominate the ‘adsorption invasion process’: identification of the residual oil, the driving force for migration, and geometry of oil-water interface inside the pocket.

The 25JNP and the 50JNP behaved effectively in oil displacement, as indicated by Fig. 4, and were taken for illustrating the “adsorption invasion process” in detail. Firstly, the more Janus NPs adsorbed onto the flat substrate, the higher probability of gathering of NPs inside the nano-pocket and the higher the oil recovery. As the surface

coverage of Janus NPs on the flat substrate monitored in Fig. 7(a), 50JNPs were able to adsorb and populate swiftly at the beginning of the displacement process, namely to fast identify the residual oil, which led to the fast recovery of a large number of oil molecules from the nano-pocket (Fig. 4(a)). In comparison, the 25JNP took a much longer time to populate the flat substrate area, which resulted in slower oil recovery (Fig. 4(a)). The fast adsorption of the 50JNP can be attributed to the strong interaction potential of their nonpolar faces with the oil molecules, as shown in Fig. S3. Adsorption of the 50JNP resulted in the fast decrease of the system's total energy, which was energetically favorable. In contrast, adsorption of the 25JNP led to a much less obvious contribution of system energy minimization owing to the much smaller nonpolar faces on NPs. Sufficient surface coverage of the 25JNP only happened in the later stage of displacement and subsequently the effective ongoing events of the “adsorption invasion process”. Nevertheless, the high surface coverage of NPs either by the 25JNP or the 50JNP increased the collision and pushing of the fourth stage in Fig. 6, and so forth oil recovery. The encouraging result of residual oil recovery highlighted the importance of the identification of the residual oil by the Janus NPs.

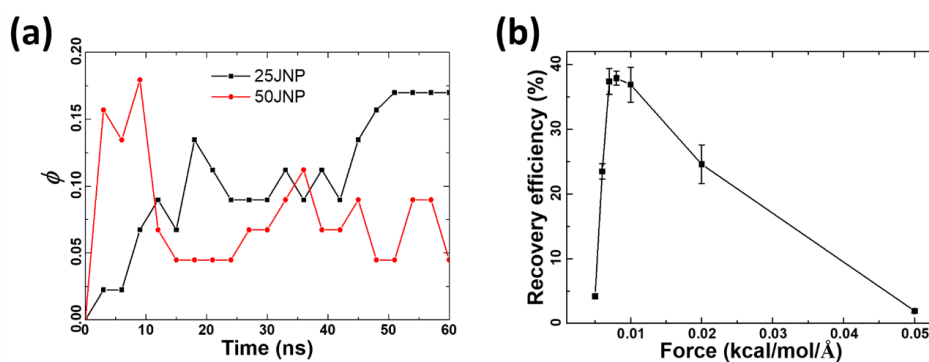


**Fig. 7.** Key factors determining oil recovery. (a) Dynamic surface coverage  $\phi$  by the 25JNP and the 50JNP on the flat substrate in the displacement. (b) The recovery efficiency by the varied applied force. The sketch solid line in the plot is for visualization.



The main driving force interplayed with other factors for the migration of Janus NPs, i.e., the displacement force, was also essential to oil recovery. There was an optimal threshold range of driving force, neither monotonically high nor low, for the highest oil recovery efficiency. The relationship between the applied external force and the recovery efficiency (ratio of the reduced oil molecules to the total) was recorded in Fig. 7(b), with the final system snapshots under the corresponding forces provided in Fig. S4. Under low driving forces, the Janus NPs diffused slowly and had a sufficient time to adsorb on the flat substrate. Meanwhile, the Janus NPs gained low pushing force at the pinning position at the edge of the substrate to enter the nano-pocket. On the other hand, the excessive driving force was more likely to overpower the pinning effect and forward push the NPs over the nano-pocket, in addition to decreasing the possibility of NPs adsorbing on the flat substrate. This was highly detrimental to the accumulation of NPs on the solid wall of the nano-pocket. As such, only the suitable displacement force enabled the promotion and acceleration of the ‘adsorption invasion process’ (Fig. 7(b)).

The alteration of the oil-water interface in the nano-pocket by the Janus NPs is worth further noting. As presented in Fig. 2, the 50JNP led to the tilted oil-water interfaces inside the nano-pocket, of which the 25JNP resulted in horizontal ones. Given the same invasion depth of Janus NPs, the horizontal oil-water interface means more oil recovery. By the analysis shown in Fig. 4(c), the most obvious wettability alteration by 25JNPs also contributed to the horizontal oil-water interface, as the large polar faces of the invaded 25JNPs encouraged more water molecules to enter the nano-pocket. It is also important to mention that the 50JNP could potentially raise NPs jamming effect in the nano-pocket. There were a considerable number of 50JNPs stably adsorbed at the oil-water interface and even at the exit edge of the nano-pocket. The accumulation of 50JNPs could further prevent the intrusion of the nearby water molecules into the nano-

pocket. The less stability of the 25JNP at the oil-water interface greatly eliminated such effects.

### 3.4. Optimization demonstration

The results and analysis above opened rational avenues for the optimization of oil recovery. Taking the 25JNP for example, enhancing the initial adsorptions of Janus NPs on the flat substrate can improve their performance in oil recovery under the previously applied force. For demonstration, a new displacement process with the 25JNP was carried out with a 30-ns equilibration simulation for adsorption of as many 25JNPs onto the flat substrate as possible prior to applying external force. The reason for employing no external driving force in the initial stage (equilibrium stage) was that low to no displacement force contributed to the increased recognition probability of residual oil by NPs. In other words, the displacement working mode of the simulation changes from constant flooding to a cycle of “huff-n-puff”. Following such an optimized flooding approach, the oil recovery effect was greatly elevated, as results shown in Fig. 8.

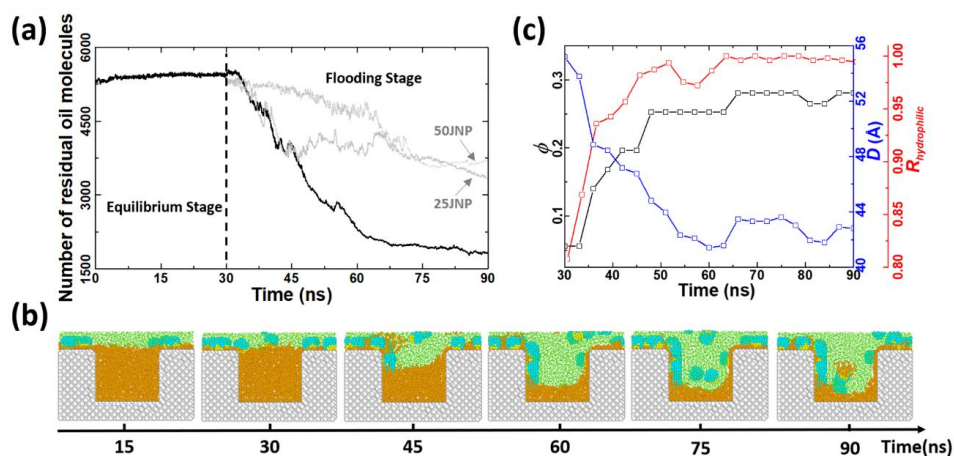


**Fig. 8.** The optimization approach for outperforming oil recovery. (a) The number of residual oil molecules in the nano-pocket with the injection of 25JNPs with the optimized displacement process. Performance by the 25JNP and the 50JNP in the original displacement process is shown (grey curves)

for comparison. (b) System snapshots of oil exaction after optimized displacement process; (c) Dynamic surface coverage  $\phi$ , centroid depth  $D$ , and the ratio of hydrophilicity  $R_{hydrophilic}$  following the optimized flooding.

As shown by the change in the amount of residual oil in the nano pocket in Fig. 8(a), the optimized flooding approach promisingly increased the final oil recovery efficiency to almost 70%. For the same given flooding time under the same driving force, the optimized approach also extracted more oil than the original flooding cases. Besides the excellent oil recovery effect, the system snapshots during the displacement process shown in Fig. 8(b) further confirmed more NPs adsorbed on the flat substrate after the equilibrium simulation. Furthermore, the optimized flooding resulted in higher values of  $\phi$  and  $R_{hydrophilic}$  and at the same time, lower value of  $D$  by adsorbed Janus NPs (Fig. 8(c)) if compared with the original flooding (Fig. 4(c)). The results suggested that the introduction of an extra equilibration was highly beneficial for promoting the ‘adsorption invasion process’, which made the solid wall in the nano-pocket more hydrophilic and led to more oil recovery. The demonstration carried out using the 25JNP should apply to other Janus NPs. The “huff-n-puff” flooding approach could be a favorite operating mode for such trapped residual oil in the reservoir. As such enhancing the ‘adsorption invasion process’ can be a key consideration in the design of Janus NPs and the modification of flooding working mode.

## 5. Discussion

Atomic modeling and MD simulation provide nano-level information, especially the detailed interaction between components in the complex nanofluid system, which is formidable to obtain in large-scale oil displacement experiments. Such knowledge is essential for the design and application of JNP in nano-enabled petroleum engineering.

This work adopts the coarse-grained modeling approach to achieve faster sampling by reducing the degree of freedom of the system. The selected force field has been proven to successfully reproduce the nature of the components in nanofluid systems, including physical characteristics of the fluid, the amphiphilicity of JNP, and the hydrophobicity of the surface. The modelled topography of the rough surface, here represented by the rectangular groove as in the previous studies, is able to serve the purpose of stably trapping residual oil. The periodic boundaries of the simulation systems enable an infinitely long rough surface with the trapped oil film, which is beneficial to the continuous capture and investigation of the displacement behavior of JNPs. Thus, the designed model is eligible to be a basic case for the study of the displacement of nanoscale trapped oil by JNPs, which corresponds to the nanoscale locations in the rough throats or in the internal channel of nanopores in the actual reservoir.

Unlike the previous atomistic simulations focusing on smooth channels [28], the result is more relevant to the experimental results [23-25] on deciphering the excellent EOR effect of JNP. Regarding the understanding of the EOR mechanism of JNP, previous experiments have confirmed the IFT reduction and wettability alteration caused by JNP without evaluating their contributions in the process. Giraldo et al. believe that reducing IFT is the decisive factor in this process rather than the wettability alteration [25, 26]. The present work further details the dominating contribution of wettability alteration in the nanoscale oil film displacement effect. The simulations provide atomistic resolution for observing key steps of JNPs dynamics in the process of the oil-film type of residual oil displacement. Such resolution is obviously missing in the experiment where it is impossible to distinguish the specific role played by JNP for various remaining oil types (clustered, columnar, droplet, etc. [51]). As such, simulations of this kind provide the possibility for the refined interpretation of the EOR

mechanism of JNP. Furthermore, this work reveals the dynamics of wettability alteration (ie, the 'adsorption invasion process'), which is highly valuable to nanoparticle design in EOR. Interestingly, the 'adsorption invasion process' observed in this work features the previous proposed 'climbing film' of Janus nanosheets [27]. However, the intrinsic mechanisms of the two are different. As the so-called Marangoni stress is the key to 'climbing film', the pinning effect driven by local energy minimum governs the 'adsorption invasion process' in the migration of JNP on the solid surface and into the nano-pores.

It should be noted that this work focuses on the displacement of oil film by JNPs on a rough surface with simplified parameter sets. Key factors such as oil type properties, water salinity, rock properties, the concentration of JNPs, pore geometries and size, and system temperature and pressure, await intensive investigation and discussion. Nevertheless, it is foreseeable that some of these factors have their synergy to the 'adsorption invasion process' of JNP on the EOR. Further extensive atomistic modeling and simulations are needed for answering such questions. Lastly, upscaling the results and eventually bridging them to the reservoir scale is the ultimate goal in future work. It's undeniable that the obtained motion pattern and the optimal fraction of hydrophilic parts for JNP can qualitatively guide the design and fabrication of JNP in EOR. What's more, the results can provide a design basis of the bottom layer parameters for the final effect prediction at the reservoir scale. As illustrated in the framework of the multiscale EOR research method (Fig. 9), the work contributes to the fine-tuning of the parameters for microscale experiments or fluid simulations such as roughness and JNP properties. Based on this, the microscopic study can verify the displacement effect of JNP and further extend the displacement characteristics to the core scale. Finally, the prediction of the displacement effect of JNP under actual reservoir conditions is carried out in the

reservoir numerical simulation with the help of the evaluation of the performance of JNP in core flooding. Besides, combined with the increasingly mature machine learning technology, a large number of MD simulation results can also be adopted to construct a screening chart of JNP properties and displacement effects, which can be directly utilized in the design of EOR applications.

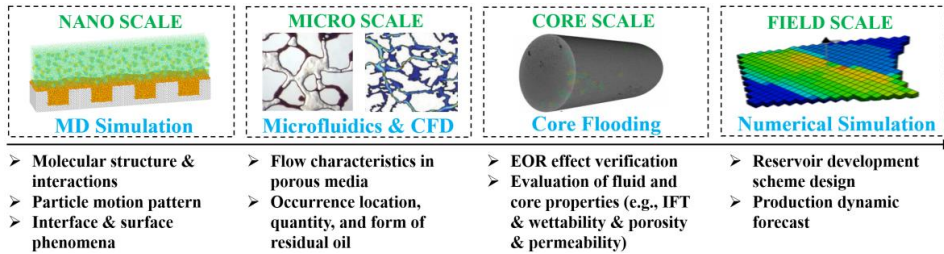


**Fig. 9.** The framework of the multiscale EOR research techniques. The CFD is short for Computational Fluid Dynamics.

## 6. Conclusions

Oil recovery from the rough surface by displacement of Janus NPs was investigated using atomistic modeling and MD simulations. The study found that Janus NPs with larger polar faces (25JNPs and 50JNPs) achieved a more notable oil recovery effect than those with smaller polar faces (75JNPs) or pure water (JNP-free). The structure of adsorbed NPs on the wall of the nano-pockets strongly affected oil recovery efficiency. Altering the solid wall to be more hydrophilic by adsorbed Janus NPs can lead to deeper migration of the NPs into the nano-pocket and more oil recovery. Furthermore, an ‘adsorption invasion process’ was identified in this work, highlighting the key mechanism of the oil recovery effect of Janus NPs. Specifically, Janus NPs adsorbed on the solid surface by first identifying the oil-water interface. Constrained by the pinning effect, the adsorbed Janus NPs slid and stayed on the edge before entering oil

trapping nano-pockets. Under the impelling local water flow, the pinned Janus NPs were forced into the nano-pocket along the solid wall. With the continuous collisions and pushing, more Janus NPs could further migrate deep into the nano-pockets. Moreover, controlling factors, including identification of the residual oil, displacement pressure, and the geometry of the oil-water interface inside nano-pockets, were proposed for the ‘adsorption invasion process’. Utilizing the new results and analysis, an optimization flooding approach, namely the “huff-n-puff” working mode, was proposed, which yielded outstanding oil recovery performance. The findings of this work directly correlated critical factors with oil recovery on the rough surface by Janus NPs for the first time and shed light on the intrinsic EOR mechanism of Janus NPs. The results provided guidance not only for designing the suitable Janus NPs, but also for modifying the targeted displacement strategy in the practical applications of EOR.

**CRedit authorship contribution statement:**

**Yuanhao Chang:** Conceptualization, Writing-original draft. **Senbo Xiao:** Methodology, Software. **Rui Ma:** Software. **Zhiliang Zhang:** Writing-review & editing, Supervision. **Jianying He:** Validation, Writing-review & editing.

**Acknowledgments:**

This work was financially supported by the Research Council of Norway (Grant No. 234626) and the Chinese Scholarship Council. The supercomputer CPU hours were

provided by the Norwegian Metacenter for Computational science (Project ID: NN9110K and NN9391K).

### Appendix A. Supplementary data:

Supplementary data to this article can be found online.

### References

1. Newell, R., D. Raimi, and G. Aldana, *Global Energy Outlook 2019: The next generation of energy*. Resources for the Future, 2019: p. 8-19.
2. Bai, B., *Overview: eOR/IOR (January 2008)*. Journal of Petroleum Technology, 2008. **60**(01): p. 42-42.
3. Richards, P.W., R. Frankham, and R. Walsh, *The tropical rain forest: an ecological study*. 1996: Cambridge university press.
4. Lyons, W.C. and G.J. Plisga, *Standard handbook of petroleum and natural gas engineering*. 2011: Elsevier.
5. Sun, X., et al., *Enhanced heavy oil recovery in thin reservoirs using foamy oil-assisted methane huff-n-puff method*. Fuel, 2015. **159**: p. 962-973.
6. Ahmadi, Y., et al., *Comprehensive Water–Alternating-Gas (WAG) injection study to evaluate the most effective method based on heavy oil recovery and asphaltene precipitation tests*. Journal of Petroleum Science and Engineering, 2015. **133**: p. 123-129.
7. Olajire, A.A., *Review of ASP EOR (alkaline surfactant polymer enhanced oil recovery) technology in the petroleum industry: Prospects and challenges*. Energy, 2014. **77**: p. 963-982.
8. Haruna, M.A., et al., *Nanoparticle modified polyacrylamide for enhanced oil recovery at harsh conditions*. Fuel, 2020. **268**: p. 117186.
9. Almahfood, M. and B. Bai, *The synergistic effects of nanoparticle-surfactant nanofluids in EOR applications*. Journal of Petroleum Science and Engineering, 2018. **171**: p. 196-210.
10. Sun, X., et al., *Application of nanoparticles in enhanced oil recovery: a critical review of recent progress*. Energies, 2017. **10**(3): p. 345.
11. Chaturvedi, K.R., et al., *Experimental investigations to evaluate surfactant role on absorption capacity of nanofluid for CO<sub>2</sub> utilization in sustainable crude mobilization*. Energy, 2021. **225**: p. 120321.
12. Yang, X., et al., *Nanoparticle plugging prediction of shale pores: A numerical and experimental study*. Energy, 2020. **208**: p. 118337.
13. Khalil, M., et al., *Advanced nanomaterials in oil and gas industry: design, application and challenges*. Applied energy, 2017. **191**: p. 287-310.
14. Murshed, S.S. and C.N. De Castro, *Nanofluids: synthesis, properties, and applications*. 2014: Nova Science Publishers, Incorporated.
15. Li, K., D. Wang, and S. Jiang, *Review on enhanced oil recovery by nanofluids*. Oil & Gas Science and Technology–Revue d'IFP Energies nouvelles, 2018. **73**: p. 37.



16. Kazemzadeh, Y., et al., *Review on application of nanoparticles for EOR purposes: A critical review of the opportunities and challenges*. Chinese Journal of Chemical Engineering, 2019. **27**(2): p. 237-246.
17. Wilson, A., *Field Trials of Reservoir Nanoparticles Reveal Stability, High Rates of Recovery*. Journal of Petroleum Technology, 2012. **64**(11): p. 92-99.
18. Kanj, M.Y., M. Rashid, and E. Giannelis. *Industry first field trial of reservoir nanoagents*. in *SPE Middle East oil and gas show and conference*. 2011. Society of Petroleum Engineers.
19. Yakasai, F., et al., *Current Developments and Future Outlook in Nanofluid Flooding: A Comprehensive Review of Various Parameters Influencing Oil Recovery Mechanisms*. Journal of Industrial and Engineering Chemistry, 2020.
20. Idogun, A.K., et al. *A review study of oil displacement mechanisms and challenges of nanoparticle enhanced oil recovery*. in *SPE Nigeria annual international conference and exhibition*. 2016. OnePetro.
21. Ruhland, T.M., et al., *Janus cylinders at liquid–liquid interfaces*. Langmuir, 2011. **27**(16): p. 9807-9814.
22. Laredj-Bourezg, F., et al., *Emulsions stabilized with organic solid particles*. Colloids and Surfaces A: Physicochemical and Engineering Aspects, 2012. **413**: p. 252-259.
23. Wu, H., et al., *Silica-based amphiphilic Janus nanofluid with improved interfacial properties for enhanced oil recovery*. Colloids and Surfaces A: Physicochemical and Engineering Aspects, 2020. **586**: p. 124162.
24. Liu, P., et al., *Functional Janus-SiO<sub>2</sub> Nanoparticles Prepared by a Novel “Cut the Gordian Knot” Method and Their Potential Application for Enhanced Oil Recovery*. ACS applied materials & interfaces, 2020. **12**(21): p. 24201-24208.
25. Giraldo, L.J., et al., *Enhanced waterflooding with NiO/SiO<sub>2</sub> 0-D Janus nanoparticles at low concentration*. Journal of Petroleum Science and Engineering, 2019. **174**: p. 40-48.
26. Giraldo, L.J. *Janus nanoparticles for enhanced oil recovery EOR: reduction of interfacial tension*. in *SPE annual technical conference and exhibition*. 2018. Society of Petroleum Engineers.
27. Luo, D., et al., *Nanofluid of graphene-based amphiphilic Janus nanosheets for tertiary or enhanced oil recovery: High performance at low concentration*. Proceedings of the National Academy of Sciences, 2016. **113**(28): p. 7711-7716.
28. Wang, X., et al., *Transportation of Janus nanoparticles in confined nanochannels: a molecular dynamics simulation*. Environmental Science: Nano, 2019. **6**(9): p. 2810-2819.
29. Luu, X.C. and A. Striolo, *Ellipsoidal Janus nanoparticles assembled at spherical oil/water interfaces*. J Phys Chem B, 2014. **118**(47): p. 13737-43.
30. Luu, X.C., J. Yu, and A. Striolo, *Nanoparticles adsorbed at the water/oil interface: coverage and composition effects on structure and diffusion*. Langmuir, 2013. **29**(24): p. 7221-8.
31. Luu, X.C., J. Yu, and A. Striolo, *Ellipsoidal Janus nanoparticles adsorbed at the water-oil interface: some evidence of emergent behavior*. J Phys Chem B, 2013. **117**(44): p. 13922-9.
32. Glaser, N., et al., *Janus particles at liquid– liquid interfaces*. Langmuir, 2006. **22**(12): p. 5227-5229.

33. Chang, Y., et al., *Displacement dynamics of trapped oil in rough channels driven by nanofluids*. Fuel, 2021: p. 122760.
34. Toghraie, D., et al., *Molecular dynamics simulation of Couette and Poiseuille Water-Copper nanofluid flows in rough and smooth nanochannels with different roughness configurations*. Chemical Physics, 2019. **527**: p. 110505.
35. Alipour, P., et al., *Molecular dynamics simulation of fluid flow passing through a nanochannel: effects of geometric shape of roughnesses*. Journal of Molecular Liquids, 2019. **275**: p. 192-203.
36. Fang, T., et al., *Oil extraction mechanism in CO<sub>2</sub> flooding from rough surface: Molecular dynamics simulation*. Applied Surface Science, 2019. **494**: p. 80-86.
37. Plimpton, S., *Fast parallel algorithms for short-range molecular dynamics*. Journal of computational physics, 1995. **117**(1): p. 1-19.
38. Stukowski, A., *Visualization and analysis of atomistic simulation data with OVITO—the Open Visualization Tool*. Modelling and Simulation in Materials Science and Engineering, 2009. **18**(1): p. 015012.
39. Molinero, V. and E.B. Moore, *Water modeled as an intermediate element between carbon and silicon*. The Journal of Physical Chemistry B, 2009. **113**(13): p. 4008-4016.
40. Martin, M.G. and J.I. Siepmann, *Transferable potentials for phase equilibria. I. United-atom description of n-alkanes*. The Journal of Physical Chemistry B, 1998. **102**(14): p. 2569-2577.
41. Chang, Y., et al., *Nanomechanical Characteristics of Trapped Oil Droplets with Nanoparticles: A Molecular Dynamics Simulation*. Journal of Petroleum Science and Engineering, 2021: p. 108649.
42. Wang, X., et al., *Insight into the pressure-induced displacement mechanism for selecting efficient nanofluids in various capillaries*. Environmental Science: Nano, 2020. **7**(9): p. 2785-2794.
43. Nosé, S., *A unified formulation of the constant temperature molecular dynamics methods*. The Journal of chemical physics, 1984. **81**(1): p. 511-519.
44. Hoover, W.G., *Canonical dynamics: Equilibrium phase-space distributions*. Physical review A, 1985. **31**(3): p. 1695.
45. Craig, F.F., *The reservoir engineering aspects of waterflooding*. Vol. 3. 1971: HL Doherty Memorial Fund of AIME New York.
46. Willhite, G.P., *Waterflooding*. 1986.
47. Choudhary, N., et al., *Effect of polyvinylpyrrolidone at methane hydrate-liquid water interface. Application in flow assurance and natural gas hydrate exploitation*. Fuel, 2016. **186**: p. 613-622.
48. Beckmann, A., et al., *A fast recoiling silk-like elastomer facilitates nanosecond nematocyst discharge*. BMC biology, 2015. **13**(1): p. 1-16.
49. Zhang, P., et al., *Grooved organogel surfaces towards anisotropic sliding of water droplets*. Adv Mater, 2014. **26**(19): p. 3131-5.
50. Chang, B., et al., *Sliding droplets on hydrophilic/superhydrophobic patterned surfaces for liquid deposition*. Applied Physics Letters, 2016. **108**(15).
51. Mi, L., et al. *Microscopic oil and water percolation characteristic investigation of water flood reservoir in ultrahigh water cut period*. in *SPE Trinidad and Tobago Section Energy Resources Conference*. 2016. OnePetro.

*Supporting Information*

## Atomistic Insight into Oil Displacement on Rough Surface by Janus Nanoparticles

Yuanhao Chang <sup>a</sup>, Senbo Xiao <sup>a,1</sup>, Rui Ma <sup>a</sup>, Zhiliang Zhang <sup>a</sup>, Jianying He <sup>a,2</sup>

<sup>a</sup> Department of Structural Engineering, Norwegian University of Science and Technology (NTNU), 7491 Trondheim, Norway

**Table. S1.** Energy well depth (characteristic energy, kcal/mol) of interaction Lennard-Jones potential between the hydrophilic/hydrophobic parts of the Janus NPs with the other components of the simulation systems.

Characteristic energy, kcal/mol	Water	Oil	Surface
Hydrophilic part of NPs	0.4	0.01	0.7
Hydrophobic part of NPs	0.01	0.2	

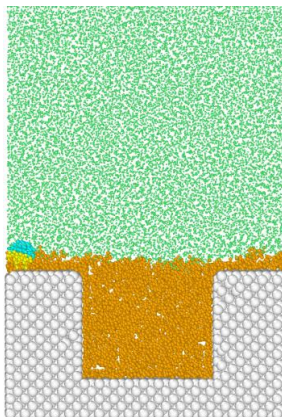


**Fig. S1.** The side view of the calculation system for the potential of mean force. The Janus NP was anchored by a harmonic potential at different positions with constant interval distances along the water-oil interface. The force constant of the harmonic potential is  $2 \text{ kcal/mol/\AA}^2$ . The displacement distance of the NP from its original position and the experienced force from the harmonic potential were recorded and analyzed by the WHAM algorithm. The colors for different components: water (green), oil (orange), surface (white), hydrophobic part of Janus NP (yellow), and hydrophilic part of Janus NP (blue).

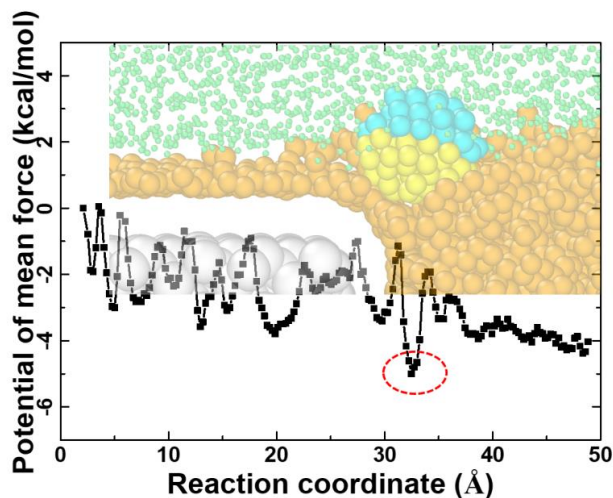


**Fig. S2.** The potential of mean force of a Janus NP transporting from the left side of the surface to the middle of the system with the smoother substrate surface. The atoms comprising the surface had atom sizes, namely a larger sigma value of  $7 \text{ \AA}$ . The result from this system is only for comparison with PMF given in the main text, and for clarifying the effect of atomic structure on the fluctuation of the PMF.

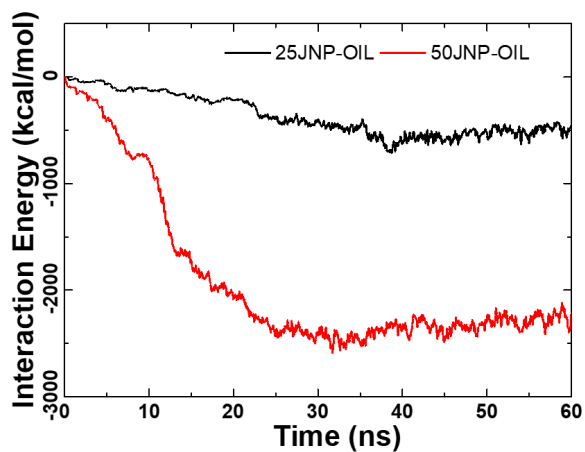


Fig. S3. Interaction potential between the two Janus NPs (25JNP and 50JNP) with the oil phase during the flooding.

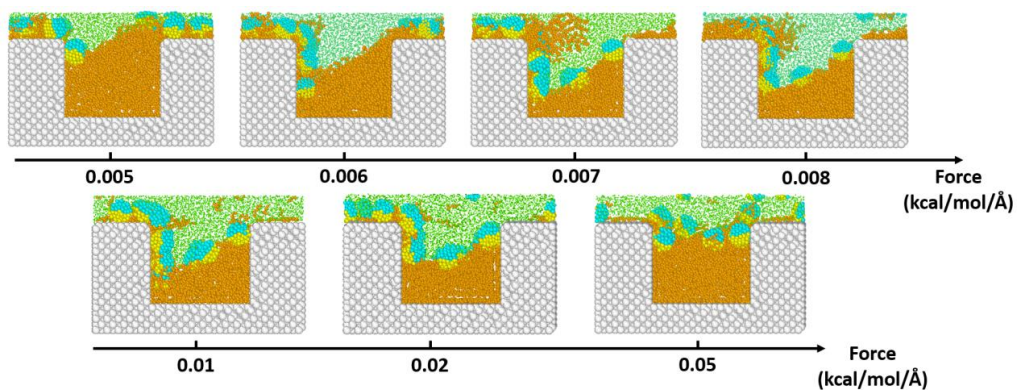


Fig. S4. The final system snapshots of displacement varied external forces ranging from 0.005 to 0.05 kcal/mol/Å.

### **A.3 Paper III**

---

## **Unraveling the Influence of Surface Roughness on Oil Displacement by Janus Nanoparticles**

Authors: Yuanhao Chang, Senbo Xiao, Rui Ma, Zhiliang Zhang and Jianying He  
Petroleum Science, 2023.02.

## Unraveling the Influence of Surface Roughness on Oil Displacement by Janus Nanoparticles

Yuanhao Chang <sup>a</sup>, Senbo Xiao <sup>a,1</sup>, Rui Ma <sup>a</sup>, Zhiliang Zhang <sup>a</sup>, Jianying He <sup>a,2</sup>

<sup>a</sup> Department of Structural Engineering, Norwegian University of Science and Technology (NTNU), 7491 Trondheim, Norway

### Abstract

Janus nanoparticles (JNPs) possess great potential in recovering the residual oil from reservoirs, however, the fundamental interaction mechanisms among nanoparticles, the oil, and reservoir wall characteristics remain to be elucidated. In this work, models of oil trapping grooves with different geometric features are subjected to molecular dynamics simulations for investigating the influences of roughness parameters on oil displacement dynamics by JNPs. Four key surface geometry parameters and different degrees of surface hydrophobicity are considered. Our results indicate that JNPs hold an outstanding performance in displacing residual oil on weakly to moderately hydrophobic surfaces. Overall, smaller entry and exit angles, the larger aspect ratio of the oil trapping grooves, and a bigger tip length of the rough ridges lead to superior oil recovery. Among the key geometric parameters, the aspect ratio of the oil trapping grooves plays the dominant role. These insights about the interaction of surface properties and JNPs and the resulting trapped oil displacement could serve as a theoretical reference for the application of JNPs for targeted reservoir conditions.

Keywords: Janus nanoparticles; oil displacement; enhanced oil recovery, molecular dynamics simulation; rough surface

### 1. Introduction

Being the greatest part of global energy, the demand for fossil fuels will grow by more than 30% in 20 years (Qian and Li, 2018). Since most oil fields have reached the economic limit of the secondary oil recovery stage, the implementation of enhanced oil recovery (EOR) measures is the key to meeting the oil consumption demand (Jia, 2020;

Li et al., 2000). Taking Norway as an example, a merely 1% recovery increase in the EOR stage will translate into more than 300 billion Norwegian kroner in revenue. Currently, the traditional EOR technology has entered a bottleneck period due to challenges like high cost, eco-unfriendliness, and gravity override (Chang et al., 2016; Kang et al., 2020; Sun et al., 2015). In the meanwhile, nanoparticles have been widely accepted to have great potential to be a breakthrough in EOR (Liang et al., 2021; Sun et al., 2021; Zhang et al., 2022). In particular, there is growing interest in the EOR application of Janus nanoparticles (JNPs) whose surfaces have two distinct wettability (Jia et al., 2021; Shi et al., 2019; Wu et al., 2020b).

There is a bulk of encouraging results indicating that JNPs exhibit significantly better performance and greater application potentials than conventional homogeneous nanoparticles in the EOR process (Giraldo et al., 2019; Li et al., 2020; Liang et al., 2017; Liu et al., 2020; Luo et al., 2016; Wu et al., 2020a; Yin et al., 2019). Through experimental studies, JNPs were found to contribute to water viscosity increment (Giraldo et al., 2019), interfacial tension reduction (Wu et al., 2020a; Yin et al., 2021), and surface wettability alteration (Giraldo et al., 2019; Wu et al., 2020a) in the EOR process. Moreover, JNPs exhibited a special dynamic displacement mechanism of climbing film growth and slug-like displacement that was not observed in other homogeneous nanoparticles (Luo et al., 2016). What's more, the simulation study provides the theoretical fundamentals of JNPs in EOR technology (Ahmadi and Chen, 2021; Zhao et al., 2019), which effectively compensates for the current limitation of experimental conditions at the nanoscale. For example, the interfacial activities of JNPs at the oil-water interface were explored by dissipative particle dynamics (DPD) simulations, yielding results for the design of the Pickering emulsion (Luu and Striolo, 2014). The self-assembly and characteristics of JNPs at the oil-water interface were studied by molecular dynamics (MD) simulations, which supplied the basis of JNP applications in practice (Xiang et al., 2017). Due to the size limitation of these simulation systems, only a limited number of nanofluid flooding systems involving solid surfaces exist. Unexpected results of JNPs impeding oil displacement were observed in capillary pressure-dominated smooth nano-channels (Wang et al., 2019). The great potential of JNPs in displacing residual oil from rough channels was also newly reported (Chang et al., 2022a). Moreover, the outstanding performance of JNPs and their unique dynamics of the wettability alteration process (namely, the 'adsorption invasion process') were revealed (Chang et al., 2022b). Obviously, these limited works



are far from the complete understanding of displacing trapped oil in reservoir pores and throats with JNPs.

It is worth noting that the significantly different results in smooth and rough nanochannels highlight the influence of roughness in oil displacement dynamics (Niu and Tang, 2014; Wang et al., 2019; Zhang, 2016). Besides, differences in flow and wetting characteristics of nanofluids on smooth and rough surfaces have been confirmed in studies in varied research fields (Durret et al., 2018; Savoy and Escobedo, 2012; Wang et al., 2017). Hence, only by taking into account the roughness effect of solid surfaces (the actual reservoir situation), the motion law of JNPs, the oil displacement effect, and the EOR mechanism can be more truly manifested. Considering the size limitation of molecular simulation systems, it is nevertheless challenging to construct the real rough topography in the oil reservoir. Generally, surface roughness is featured by grooves with regular shapes in MD simulations (Fang et al., 2019; Yaghoubi and Foroutan, 2018). By modifying the geometric parameters of the grooves, the influence of the surface roughness on fluid dynamics or wetting can be effectively elucidated (Fang et al., 2019; Song et al., 2018; Xie and Cao, 2016). Regrettably, there are seldom molecular simulation studies on the influence of nanochannel roughness on oil displacement.

Herein, the effects of surface geometric parameters on displacing oil from nano-pockets are investigated. Specifically, the tip length of the ridge (**S**), entry angle ( **$\alpha$** ), exit angle ( **$\beta$** ), and the aspect ratio (**A**) of the groove width (**L**) to depth (**H**) (that is, **A=L/H**), as shown in Fig. 1, are chosen as the focused roughness parameters. As the most common geometric parameters in research on the rough surface (Fang et al., 2019; Lalegani et al., 2018), their combinations are able to cover almost all the rough surface geometry. By monitoring the formation of JNPs adsorption film on the sidewall of the grooves and comparing the final oil displacement results, the EOR effect of each surface geometric parameter is quantitatively analyzed and clarified. Moreover, an in-depth discussion on the possible interactive influence among the geometric parameters and the limitation of this work is conducted. The results broaden the understanding of the adaptability of JNPs in displacing residual oil on rough surfaces and are thus desired by the application of JNPs in EOR.

## **2. Model and simulation details**

### *2.1. Molecular model*

The model systems are constructed with the aim to capture the key features of rough surfaces with trapped oil for displacement by the injection of JNPs, as one representative example shown in Fig. 1. Following previous studies and for the sake of simplicity (Chang et al., 2022b), the model systems hold a dimension of  $100 \times 70 \times 151 \text{ \AA}^3$  with periodic boundary conditions. The rough surface is created by removing atoms from an initially smooth silicon crystal to result in a groove, as represented by a rectangular groove in Fig. 1. The hydrophobicity of such surface is controlled by its inter-atomic interactions with the water and oil phase, namely the force-field parameters, which could capture the wetting features of common types of rocks found in actual reservoirs (Harrison et al., 2014; Kondratyuk et al., 2005). To avoid artificial molecular interactions across the solid surface because of the periodic boundary condition, the minimum height at the bottom of the groove in the surface ( $11 \text{ \AA}$ ) is set to be larger than the cutoff distance of the non-bonding interactions ( $10 \text{ \AA}$ ). The crucial geometric parameters of the surface roughness, namely the tip length of the ridge ( $\mathbf{S}$ ), entry angle ( $\boldsymbol{\alpha}$ ), exit angle ( $\boldsymbol{\beta}$ ), and the aspect ratio of the groove ( $\mathbf{A}$ ) as depicted in the figure, are altered in surface modeling, with the chosen values listed in Table 1. As such, multiple systems with varied rough surfaces are obtained for the oil displacement simulations. It is worth noting here that the system containing a rough surface with  $\mathbf{S} = 50 \text{ \AA}$ ,  $\boldsymbol{\alpha} = 270^\circ$ ,  $\boldsymbol{\beta} = 270^\circ$  and  $\mathbf{A} = 1.25$  is taken as the reference for result comparison, as highlighted in the bold text in Table 1. For the fluid of the model systems, hexane (model density  $640 \text{ kg/m}^3$ ), water, and spherical JNPs with diameters of  $10 \text{ \AA}$  ( $d = 10 \text{ \AA}$ ) are used. As an example, the reference system contains 1001 oil molecules, 21400 water molecules, and 48 JNPs with a nanoparticle volume concentration of 3.9%. The JNPs are evenly distributed in the solution before flooding simulation in an equilibrium state.

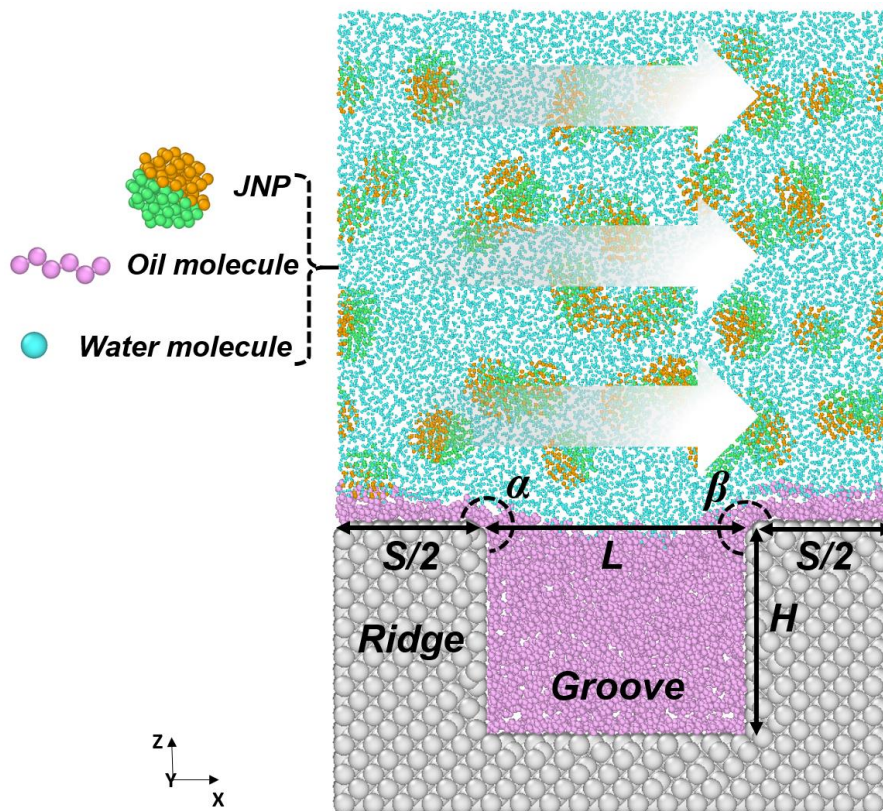


**Fig. 1.** Representative structure of the simulation system. The white arrows indicate the flooding direction in the periodic simulation box. The colors for different components in the system: water (light blue), oil (pink), surface (grey), hydrophobic part (orange), and hydrophilic part (green) of Janus NPs. The key geometric parameters, the tip length of the ridge ( $S$ ), entry angle ( $\alpha$ ), exit angle ( $\beta$ ), groove width ( $L$ ), and depth ( $H$ ) are illustrated in the figure.

**Table 1.** The selected geometric values in modeling the rough surfaces. The bold values are the parameters of the reference model.

Geometric Parameters	Designed Value						
Tip Length of the Ridge ( $S$ ) ( $d=10\text{\AA}$ )	$2.5d$	$3d$	$4d$	<b><math>5d</math></b>	$7.5d$	$10d$	
Entry Angle ( $\alpha$ )	$210^\circ$	$225^\circ$	$240^\circ$	<b><math>270^\circ</math></b>	$300^\circ$	$315^\circ$	
Exit Angle ( $\beta$ )	$210^\circ$	$225^\circ$	$240^\circ$	<b><math>270^\circ</math></b>	$300^\circ$	$315^\circ$	
Aspect Ratio of the groove ( $A$ )	0.625	<b>1.250</b>	1.875	2.500	3.125	3.750	5.000

## 2.2. Force field

The atomistic interaction parameters are selected following previous studies. Specifically, the monoatomic water (mW) model is adopted for the water phase, while the Transferable Potentials for Phase Equilibria united-atom (TraPPE-UA) description of hexane is employed for oil (Martin and Siepmann, 1998; Molinero and Moore, 2009). The mW water models interact via the 3-body Stillinger–Weber (SW) potential to account for the hydrogen bonding in water. The water-oil and oil-oil non-bonded interactions follow the standard pairwise 12-6 Lennard-Jones (LJ) potential. The combination of the water and oil models is found to appropriately capture the fluid properties at minimal computational costs (Chang et al., 2021). The interactions between the surface with water and oil are also parameterized by LJ potentials, with the oil droplet contact angle on the surface controlled by the characteristic energy  $\epsilon_{ws}$  (water-surface), as depicted in Fig. S1. Since the focus is the influence of the morphology of rough surface rather than the specific materials of the surface, the choice of the  $\epsilon_{ws}$  is to guarantee the oil phase is trapped in the groove on the surface for flooding, as detailed in the follow sections. The characteristic energy for interactions involved the JNPs is selected from the previous studies (Chang et al., 2022b), with the values given in the supporting information (Table S1). Although the atoms in the systems are free of charge, the effect of coulombic interactions in the system, especially among the water molecules, are implicitly accounted for by the adopted water model and the force field.

### 2.3. Simulation strategy and process

All the MD simulations are performed with the LAMMPS package (Plimpton, 1995) and visualized with OVITO software (Stukowski, 2009). In our simulations, the systems are first energy-minimized using the steepest descent method and followed by a 5-ns equilibrium stage in the NVT ensemble at 350 K. The simulation time step is 3 fs. The Nosé–Hoover thermostat with a coupling coefficient of 100 fs is adopted in the simulations (Hoover, 1985). After then, another 60-ns non-equilibrium MD simulation (NEMD) is carried out to simulate the JNP flooding process, with a constant force (0.01 kcal/mol/Å) applied on each of the water molecules along the x-axis of the simulation box. To speed up the simulation of such big systems, rigid JNPs are chosen. As such, any result obtained here in this work applies to relatively rigid nanoparticles used in EOR. At the same time, the rough surface is positionally fixed. Five independent simulations are carried out for the flooding process in each system.

### 3. Results

#### 3.1. Oil displacement dynamics on the rough surface by JNPs

It is known that local wettability alteration is one of the major mechanisms in residual oil displacement by JNPs. Especially, the dynamic ‘adsorption invasion process’ in wettability alteration was identified to be the main motion pattern of the JNPs in the oil displacement (Chang et al., 2022b), as schematically illustrated in Fig. 2. Because of their special surface wettability, JNPs are prone to adsorb at the oil-water interface and onto trapped oil films on rough surfaces. Under the shear flow of the flooding water, JNPs slide on the surface and then linger at the edge of oil trapping grooves because of the pinning effect. Driven by the local water currents, the accumulated JNPs at the edge of the groove are able to invade the entrance of the groove along the sidewall of the groove to displace the trapped oil. The sequential events of JNPs adsorption and invasion result in many JNPs progressing into the deeper position of the groove, forming a JNP adsorption film along the sidewall of the groove and altering the local wettability to be more hydrophilic. The above whole process contributes to the outstanding performance of JNP in displacing residual oil. It is obvious that the important properties of the adsorption JNP film, for instance, the height of the film and the orientation of the adsorbed JNPs, determine the final EOR effect.

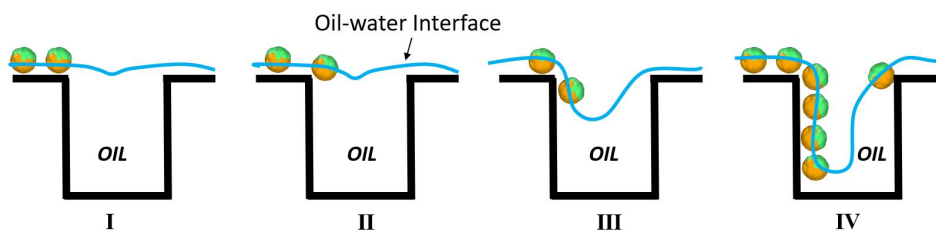


**Fig. 2.** Schematic diagram of the ‘adsorption invasion process’ of JNPs in the flooding. From left to right are I oil-water interface identification and surface adsorption, II edge pinning, III invasion, and IV formation of adsorption film.

The excellent displacement effects on the trapped oil from the rough surface by JNPs thus call for the further unfolding of the influences of the surface morphology parameters. In order to effectively probe the surface wettability and the resulting trapping strength of oil in the grooves of the rough surface, equilibration simulations of oil droplets adsorption on surfaces with varied LJ interaction characteristic energy with water are carried out, as shown in Fig. S1. The surfaces with  $\epsilon_{sw}$  in the range of 0.1 to 0.5 kcal/mol cover the wettability being strongly hydrophobic to weakly hydrophilic.

Within this wettability range, trapped oil displacement from the groove on these surfaces by JNP is then performed, with the resulting system snapshots of each simulation collected in Fig. 3a. Clearly, varied surface wettability ( $\epsilon_{sw}$ ) leads to differences in the amount of retained residual oil and the adsorption JNP film formed on the sidewall of the groove. In order to quantify the oil displacement effect, the percentage of displaced oil molecules (EOR), averaged JNP invasion depth into the groove ( $D$ , that is the averaged absolute coordinate of the adsorbed JNP), and the hydrophilic ratio of adsorbed JNP facing off the sidewall of the groove (as shown in Fig. S2,  $R_{hydrophilic}$  is defined as the ratio of the volume of the hydrophilic beads in the half of NPs away from the surface, representing the degree of surface wettability alteration by individual JNP), are calculated and shown in Fig. 3b. For surfaces  $\epsilon_{sw}$  in the range of 0.25 ~ 0.40 kcal/mol, which approximately corresponds to weak to moderate hydrophobicity, EOR is found to maintain at a higher level. The  $R_{hydrophilic}$  shares a similar trend with that of the EOR effect, which suggests the differences in the orientation of the JNPs in the adsorption film on the sidewall of the groove correlate and underpin the different EOR effects. For both the low- and high-end values of  $\epsilon_{sw}$ , low EOR is associated with high values of  $D$ , meaning JNPs cannot effectively invade the groove. When the surface is strongly hydrophobic (low  $\epsilon_{sw}$ ), oil is firmly trapped in the groove owing to the hydrophobic effect making it difficult for JNPs to adsorb and invade the groove along the surface; when the surface is hydrophilic (high  $\epsilon_{sw}$ ), the adsorption of JNPs at the entrance cannot efficiently form an adsorption film to guide water entering into the groove. Therefore, JNPs are suitable for displacing residual oil on rough surfaces with weak to moderate hydrophobicity. To clarify the rough geometric effects, surfaces with  $\epsilon_{sw}$  of 0.3 kcal/mol (i.e. weak hydrophobic surface) are selected for further simulations.

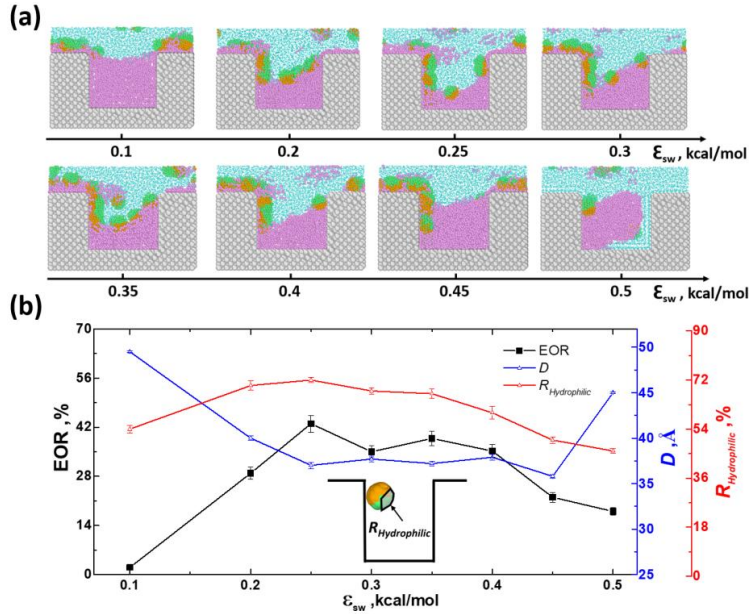


**Fig. 3.** The effect of surface wettability on oil displacement. (a) The final system snapshots after oil displacement on surfaces with varied  $\epsilon_{sw}$ . (b) The resulting EOR,  $D$  and  $R_{hydrophilic}$  obtained after the simulations. The error bar indicates the standard deviation of 5 independent simulations. The inset indicates the definition of the  $R_{hydrophilic}$  of the JNPs on the sidewall of the groove.

### 3.2. Effects of the surface geometric parameters

In the simulation, the rough surface is simplified as a combined unit of the groove and the ridge. The rough surfaces with different geometric characteristics can thus be designed by modifying the four key geometric parameters (tip length of the ridge (**S**), entry angle ( $\alpha$ ), exit angle ( $\beta$ ), and aspect ratio of the groove (**A**)). Based on the oil displacement dynamics by JNPs, it can be expected that varied geometric parameters will affect the specific process of JNP's 'adsorption invasion process'. Therefore, apart from the EOR effect, the quality of the JNP adsorption film on the sidewall (the amount, depth, and orientation of the adsorbed JNPs) should also be the focus of the following study.

#### 3.2.1 Tip length of the ridge (**S**)

In the 'adsorption invasion process', JNPs obtain the initial contact with the surface by identifying the oil film on the plane surface, namely loading on the ridges of the rough surface topography. As such, the larger **S**, the more adsorbed JNPs on the surface. Subsequently, there can be possibly more JNPs entering inside the groove along the

sidewall and a stronger driving force for the deepening of the progressing adsorption film. Indeed, as shown in Fig. 4a, a small value of  $S$  ( $2.5d$ ) leads to the few adsorbed JNPs on the sidewall and low oil displacement performance of the JNPs (the snapshots are shown in Fig. S3). With the tip length slightly increasing from  $2.5d$  to  $3d$ , obvious JNPs adsorption film gradually penetrates downward into the groove with significant oil being displaced outside the groove. However, both EOR and  $D$  confirm that the change in oil displacement effect weakens when  $S$  is over  $3d$ . Such results imply that there is a threshold of  $S$  for the massive adsorption of JNPs onto the rough surface. Once  $S$  reaches this length threshold, the average depth of invading JNPs adsorption film as well as the subsequent EOR effect will reach stable results. In our case, the threshold of  $S$  is three times the diameter of the JNPs ( $3d$ ). The above results suggest that rough surfaces with sharp ridges could be unfriendly for JNPs in EOR in the real reservoir. What's more, the  $S$  also has an obvious influence on the time cost for obtaining the final EOR effect. As exemplified by the systems with the similar EOR effect ( $S$  ranging from  $4d$  to  $10d$ ) shown in Fig. 4b, larger  $S$  generally requires a shorter time of the displacement process. The high value of  $S$ , meaning long plane surface, is a favorite for speeding up the acquisition of the high level of EOR. Of course, if  $S$  is extremely long, the sliding distance of the adsorbed JNPs will increase, which may slow down the EOR process to a certain extent. As such, the system with  $S$  of  $10d$  shows an increase in needed displacement time to its counterpart with  $S$  of  $7.5d$  (Fig. 4b).

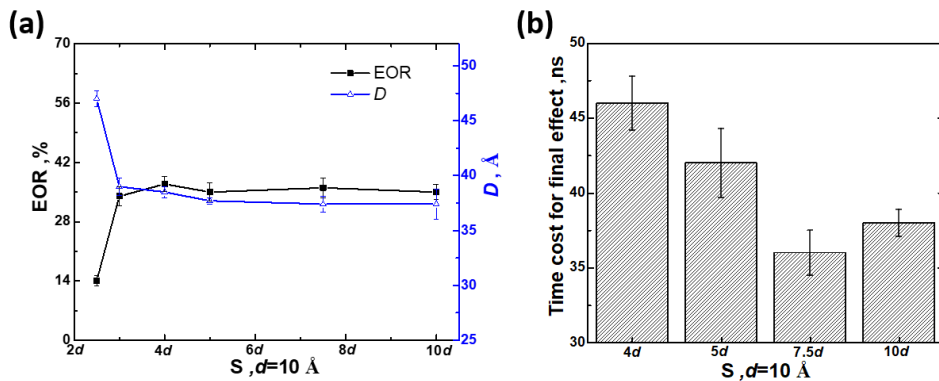


**Fig. 4.** The effect of the tip length of the ridge,  $S$ , on the oil displacement. (a) The EOR and the depth of adsorption film,  $D$ , obtained in systems with varied  $S$ . (b) The time needed for reaching the final stable EOR effect in the system with varied  $S$ . The error bars in the figures are the standard deviation of 5 independent simulations.

### 3.2.2 Entry angle ( $\alpha$ )



The effect of  $\alpha$  on oil displacement is obvious by comparing the final simulation system snapshots, as shown in Fig. 5a. It should be noted here that to ensure the same width of the groove ( $L$ ), the depth of the groove ( $H$ ) reduces if the  $\alpha$  reaches a low value. For example, the  $H$  in the system with  $\alpha$  of  $210^\circ$  is smaller than that in other systems (Fig. 5a). Considering that the sidewall area is no longer the same among the systems, the surface coverage ratio ( $\phi$ ) of adsorbed JNPs on the sidewall (that is, the ratio of the area covered by the adsorbed JNPs) is chosen to characterize the effectiveness of the adsorption film here. As the results of EOR,  $\phi$  and  $R_{hydrophilic}$  shown in Fig. 5b, lowering the  $\alpha$  generally leads to a better oil displacement effect. The resulting  $\phi$  and  $R_{hydrophilic}$  share a highly similar trend at varied  $\alpha$ , suggesting a strong correlation. In conclusion,  $\alpha$  affects the amounts and the orientation of the adsorbed JNPs on the groove sidewall. Favorite properties of the adsorption film, namely high values of  $\phi$  and  $R_{hydrophilic}$ , lead to a preferable oil displacement effect.

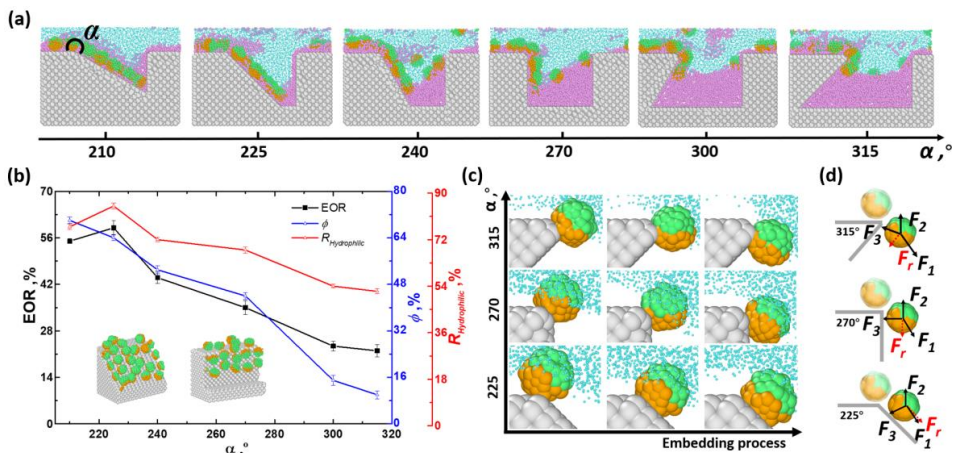


**Fig. 5.** The effect of entry angle on oil displacement. (a) The final system snapshots of oil displacement in grooves with varied entry angles. (b) The EOR, the surface coverage ratio,  $\phi$ , and  $R_{hydrophilic}$  with varied entry angles. Two snapshots of two representatives of adsorption films on the sidewall of the groove are shown as insets. Error bars are standard deviations of 5 independent simulations. (c) Progressing snapshots of JNPs at the entrance of grooves with three different entry angles. (d) The schematic of forces on the JNPs at the entrance of grooves. The black arrows represent component forces while red arrows indicate the resultant forces.  $F_1$  represents the collision force asserted on the JNPs.  $F_2$  is the resisting force of JNPs interacting with the oil molecules.  $F_3$  represents the attraction force from the surface to the JNP.  $F_r$  is the net driving force on the JNP to enter the groove.

The above results obviously indicate that  $\alpha$  affects the dynamics of JNPs pinned at the entrance of the groove and is about to slide onto the groove sidewall. As the

representative JNPs at the entrance of the groove with three different  $\alpha$  monitored and shown in Fig. 5c, the JNPs are similar in orientations but subjected to the different driving forces in collision with other adsorbed JNPs. Because of the different  $\alpha$ , the directions of forces applied to the JNPs at the entrance of the groove are different. As shown in Fig. 5d, the effective force driving JNPs into the groove ( $F_r$ , Fig. 5d) is more in-line with the important collision force ( $F_1$ , Fig. 5d) at lower  $\alpha$ .  $F_r$  increases as  $\alpha$  decreases, which enhances JNPs to enter and invade the groove. This explains the change in the coverage ratio of JNP shown in Fig. 5b. Although the JNPs can adjust the orientation through self-rotation during the simulation under the influence of the interactions between surface, water, and oil, the improvement of the  $R_{hydrophilic}$  is limited in the whole displacement process, giving the same results as previous studies (Chang et al., 2022b). The initial orientation of the pinned JNP at the entrance of the groove largely reflects the final  $R_{hydrophilic}$  of the adsorption film. In summary, smaller  $\alpha$  leads to the favorite initial orientation of the pinned JNPs, and the final larger  $R_{hydrophilic}$ .

### 3.2.3 Exit angle ( $\beta$ )

The exit angle of the groove,  $\beta$ , is also crucially important to the oil displacement results. Compared to the entering sidewall of the groove, the other sidewall facing the flooding direction (the outlet side) has very limited action with the JNPs during the oil displacement process. As the snapshots shown in Fig. S4a, the uncovered trapped oil at the outlet side increases. Specifically, the increase of  $\beta$  leads to a decrease in the recovery efficiency of the oil phase given adsorption JNPs film with similar effectiveness in the groove, as shown in Fig. S4b. In addition, it should be mentioned that the increase of  $\beta$  also eliminates the possibility of JNP adsorption on the sidewall of the groove facing the direction of flooding, which is not conducive to the expansion of the oil-water interface morphology inside the oil-trapping groove.

### 3.2.4 Aspect ratio of the groove ( $A$ )

The aspect ratio of the groove,  $A$ , was found to be an important roughness factor in oil extraction by gas flooding (Fang et al., 2019). Here, the width of the groove changes from 2.5 to 20 times the diameter of JNPs, while the height of the grooves is constant. The corresponding  $A$  of the grooves in the system ranges from 0.625 to 5. The varied

A of grooves leads to significant differences in the final oil displacement results, as the EOR,  $\phi$  and  $R_{hydrophilic}$  shown in Fig. 6a (the snapshots are plotted in Fig. S5). Overall, an increase of  $A$  leads to an increase in EOR in the systems. Although varied  $A$  has a limited effect on the orientation of adsorbed JNPs, it results in the changes in adsorption film coverage,  $\phi$ , showing a pattern of positive correlation (blue curve, Fig. 6a). As verified already by results in former studies (Chen et al., 2017; Fang et al., 2019), the water flow pattern at the oil-water interface can be more concave with the enlargement of the groove width, as shown by the schematics in Fig. 6b. The larger the aspect ratio, the deeper the downward thrust of the water flows over the groove. The curved oil-water interface on the groove with large  $A$  is a favorite for the local fluid flow to exert a driving force on the pinned JNPs at the entrance of the groove, enhancing the invasion of JNPs into the groove along the sidewall and forming the JNPs adsorption film. Nevertheless, the EOR still witnesses significant changes in the periods of stable coverage ratio ( $A = 1.25 \sim 2.5$  or  $A = 3.125 \sim 3.75$ ). This implies that the impact of the aspect ratio of the groove is not only in the coverage area of the adsorption film.

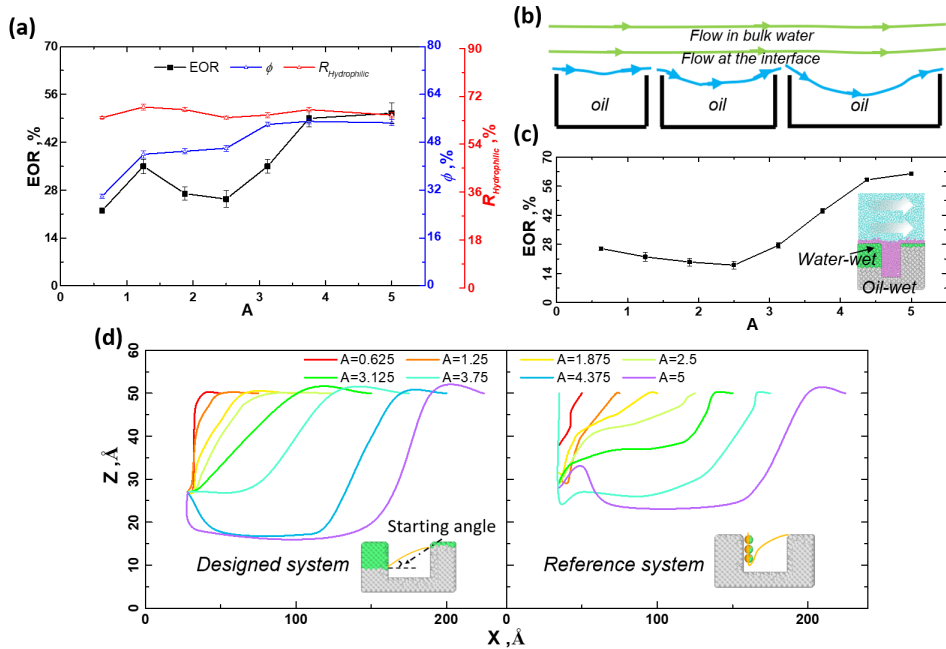


**Fig. 6.** The effect of the aspect ratio of the groove,  $A$ , on oil displacement. (a) The EOR, the surface coverage ratio,  $\phi$ , and the hydrophilic ratio of JNPs adsorption film,  $R_{hydrophilic}$ , with varied aspect ratios. The error bars are the standard deviation of 5 independent simulations (b) The schematics of the influence of aspect ratio on streamlines at the oil-water interface monitored in previous studies. The blue ones are the water streamlines at the interface while the light green ones are that in the bulk water. (c)

The EOR of the designed systems with various aspect ratios. The inset snapshot shows the sketch of the designed system. The green part of the designed surface is hydrophilic while the grey part is hydrophobic. (d) The morphology of the oil-water interface at the end of oil displacement simulations on grooves of different aspect ratios in the designed systems (left) and the reference systems (right). Inset snapshots are the representatives of the morphology of the oil-water interface in the two systems.

It's can be inferred that once the formation of a JNP adsorption film on the sidewall of the groove, namely the local wettability of the sidewall is altered, the influence of  $\mathbf{A}$  on the oil-water interface can be even more complicated. In order to clarify the impact of the wettability alteration of the sidewall, a design system with a hydrophilic sidewall is used to further explore the effect of  $\mathbf{A}$  on oil recovery results and the morphology of the oil-water interface. As the schematic diagram shown in Fig. S6, the sidewall in systems is modified to be partially water wet and share the same properties as the hydrophilic face of the JNPs before the displacement. The hydrophilic parts of the sidewalls in these designed grooves have a fixed height, namely 30 Å on the entering sidewall representing altered wettability and 3 Å on the exiting sidewall also mimicking coverage of JNPs. Meanwhile, the rest of the groove remains hydrophobic, with a  $\varepsilon_{sw}$  of 0.3 kcal/mol. The hydrophilic parts of the grooves in the designed systems are then considered to have been covered by JNP adsorption film. The designed systems are then subjected to a flooding test by pure water to probe the effect of altered wettability in the grooves, with the EOR results shown in Fig. 6c and resulting final system snapshots after oil displacement in Fig. S7. Interestingly, as  $\mathbf{A}$  increases, the EOR slightly decreases first with a minimum near  $\mathbf{A} = 2.5$  and further followed by a significant increase with large  $\mathbf{A}$  values. Such a result is coincident with the EOR results obtained in the reference group (using JNPs) and shown in Fig. 6a. As the morphology of the oil-water interface in the designed systems after oil displacement is shown on the left side of Fig. 6d, obviously, the larger  $\mathbf{A}$ , the more curved the oil-water interface towards the bottom of the groove. Combined with the results shown in Fig. 6c, it can be seen that the dramatic concave of the oil-water interface in grooves with  $\mathbf{A} > 2.5$  underlies the high EOR performance in these systems. The designed system shed light on the understanding of the results obtained using JNPs. As the corresponding morphology of the oil-water interface obtained by JNPs for comparison shown on the right side of Fig. 6d, the general pattern of the oil-water interface in the reference systems is the same as that in the designed systems. The results significantly confirm

the function of surface wettability alteration of JNPs, which is an important contributing factor to consider in EOR materials design.

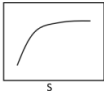
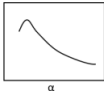
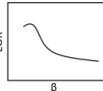
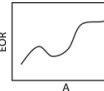
To be concluded, the change of the initial streamline at the oil-water interface caused by varied  $\mathbf{A}$  affects the coverage of the adsorption film on the sidewall of the groove. Also, the formation of the adsorption film transforms the morphology patterns of the oil-water interface in the groove with different  $\mathbf{A}$ . The synergy of the two effects defines the final oil displacement efficiency.

#### 4. Discussion

The above results elaborate on the influence of four important geometric parameters of rough surface on the residual oil displacement by JNPs separately. The resulting EOR and the underlying function of each geometric parameter are summarized in Table 2. Inevitably, there is synergy among the four parameters in their EOR effect. Since  $\mathbf{S}$  characterizes the area size for the adsorption of JNPs on the surface and further determines the formation of the adsorption film inside the groove, the small value of  $\alpha$  (close to  $180^\circ$ ) can contribute to the effect of  $\mathbf{S}$ , given that the entrance of the groove with small  $\alpha$  partially can serve as an extension of the JNPs adsorption area. Namely, the entrance of the grooves with small  $\alpha$  features the flat surface plane of the ridge with a low thickness of the trapped oil, where JNPs can be directly adsorbed at this entrance area of the groove by identifying the oil-water interface. As such, the lower threshold of  $\mathbf{S}$  is needed for the obvious EOR effect by JNPs in grooves with smaller  $\alpha$ . Moreover, there is the interplay of  $\alpha$  and  $\mathbf{A}$  because different properties of the adsorption film on the sidewall of the groove may induce different morphology of the oil-water interface in the groove and further lead to different EOR effects. To gain an overview of oil displacement effects, the EOR,  $\phi$  and  $R_{hydrophilic}$  in grooves with three entry angles of varied aspect ratios are organized in Fig. 7a. Being consistent with the results of single-parameter analysis, the system with smaller  $\alpha$  and larger  $\mathbf{A}$  holds better EOR. For any  $\mathbf{A}$  and  $\alpha$ , the properties of the JNPs adsorption film, namely  $\phi$  and  $R_{hydrophilic}$ , determine the resulting EOR. Interestingly, for the groove with  $\alpha = 300^\circ$  and large aspect ratio  $\mathbf{A}$ , although the  $\phi$  and  $R_{hydrophilic}$  show very low value due to the influence of  $\alpha$ , the corresponding EOR can still achieve a high value. This highlights the dominating effect of the meniscus of the oil-water interface in those grooves with large  $\mathbf{A}$ . As shown in Fig. S8, the oil-water interface in grooves with an extraordinarily

large aspect ratio can even reach the bottom of the groove. The obvious influences in the EOR effects by the exit angle are only observed in grooves with sufficiently small  $A$ . For grooves with a large aspect ratio  $A$ , the effect exit angle can become negligible since the adjacent area to the exit of the groove for trapping oil decreases proportionally. Hence, the outstanding oil displacement effect by JNPs is expected on the rough surface dominated by shallow grooves if only the tip length of the ridge exceeds a size threshold. For highly dense and deep grooves, the smaller  $\alpha$  and  $\beta$  are crucial for high oil recovery efficiency by JNPs. It should be noted that if  $\alpha$  and  $\beta$  are infinitely close to  $180^\circ$  (the surface is close to smooth), the displacement effect of JNP will be poor because of the lack of pinning effect. Once the surface roughness is extremely low, results obtained in smooth channels can be applied (Wang et al., 2019).

**Table 2.** The EOR effects and the underlying functions in oil displacement of the four rough geometric parameters.

Geometric Parameters	Tip Length of the Ridge (S)	Entry Angle ( $\alpha$ )	Exit Angle ( $\beta$ )	Aspect Ratio of the groove (A)
Effect on EOR				
Dominating Factor in Displacement	Number of Adsorbed JNPs on the surface	Area of Adsorption Film & Its Contribution in Wettability Alteration	Uncovered Area of Trapped Oil at Exit Side	Morphology of Oil-water Interface

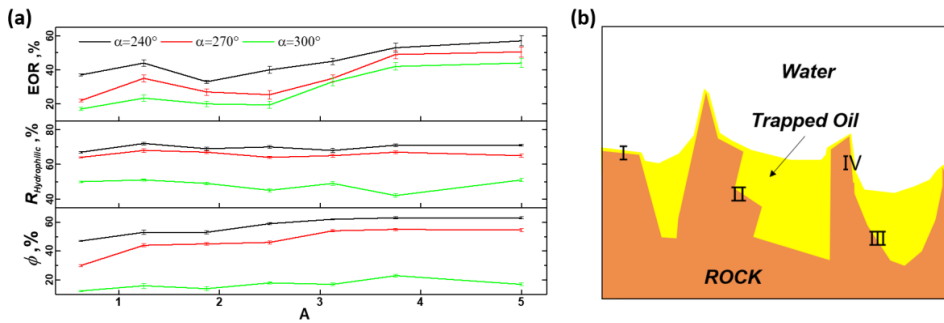


**Fig. 7.** The interplay of the geometric parameters in the EOR effect. (a) The EOR, the hydrophilic ratio,  $R_{hydrophilic}$ , and surface coverage ratio,  $\phi$ , of the JNPs adsorption film in three grooves with different entry angles and varied aspect ratios of the groove. (b) Sketch of the rough surface topography with complex roughness.

It is worth noting that the actual topography of rough surfaces is far more complicated than the modeled groove system in the study. For example, the tip of the ridge can be a slope rather than the plane surface (I or IV, Fig. 7b); the sidewall of the groove can have a rough landscape (II, Fig. 7b); the surface is curved instead of being flat (III, Fig. 7b), and so on. However, the influence of the roughness in EOR can be deciphered using the four geometric parameters discussed above. Taking the tip of the ridge as an example, JNPs are able to land and pin on the top area of the ridge because of the hydrophobic attraction of the top oil film. In this study, the tip of the ridge is a plane surface with an inclination angle of  $0^\circ$ , which yields results indicating the size of the tip of the ridge should exceed the threshold to enable effective adsorption of JNPs for a favorable EOR effect. For ridges with an inclination angle lower than  $0^\circ$  in reality (I, Fig. 7b), the effect of a small groove entry angle can be applied, which also could reduce the size threshold of the ridge for the EOR effect. In contrast, once the inclination angle is greater than  $0^\circ$  (IV, Fig. 7b), the EOR effect monitored in grooves with a large entry angle can be applied, namely difficulty in forming JNP adsorption film and inadequate driving force for the JNP to invade into the groove. In the extreme case where ridges are sharp tips, in other words with zero  $S$ , JNPs can directly adsorb on the sidewall of the groove, which is greatly beneficial to the formation of the JNPs adsorption film and the optimal EOR effect.

It should be emphasized that this work is only the first step in understanding the complex JNPs displacement behavior on the rough surface. In future work, more influencing factors affecting such displacement process should be studied, such as the displacement velocity, surface properties, size, the zeta potential of JNPs, etc. Also, all-atom simulations using real solid surface structures will reveal more detailed mechanisms (Liu et al., 2022). Moreover, machine learning could be an effective tool to clarify the complicated oil displacement effect under the combination of various rough surface parameters. What is even more challenging is to quantitatively link the surface roughness parameters of the actual reservoir with the displacement effect and explore the macro influencing factors in the reservoir like porosity, permeability, and the remaining oil saturation. So that the precise screening can be realized in the application of JNP in EOR.

## **5. Conclusions**

MD simulations are employed to study the effects of surface roughness on oil displacement by JNPs. The results provide an improved understanding of the previously reported ‘adsorption invasion process’ of JNPs in displacing trapped oil. The weakly to moderately hydrophobic surface facilitates the progress of dynamics local wettability alteration and is thus suitable for efficient displacement.

The four geometric factors play specific roles in the oil displacement process and the subsequent EOR results. The tip length of the ridge determines the amount of JNPs accumulated on the surface, and further the formation of the JNPs adsorption film in the groove. As the tip length of the ridge reaches a threshold, the properties of the resulting JNPs adsorption film and the EOR effects stabilize, while the required oil displacement time decreases. Although the EOR effect of entry and exit angle of the groove is found similar (small value is the preference), the underlying mechanisms are different. The entry angle of the groove affects the size of the JNPs adsorption film and thus the wettability alteration on the sidewall of the groove, while the exit angle affects the amount of un-recovered trapped oil at the exit side of the groove.

Lastly, the aspect ratio of the groove exerts a huge impact on the morphology of the oil-water interface in the groove. The oil-water interface can curve to reach the bottom of the groove with a large aspect ratio, which results in an excellent oil displacement effect. High oil displacement performance by JNPs is expected in shallow grooves on rough surfaces. Moreover, compared to the entry and exit angle, the aspect ratio of the groove plays a dominating role in the overall EOR effect as long as the tip length of the rough ridge approaches an effective threshold. Our findings deepen the understanding of the displacement of residual oil on the rough interface by injection of nanofluid with JNPs. This study not only guides the application of JNPs in EOR but also serves as an inspiration to the related research on the two-phase flow phenomena on the rough surface.

#### **Appendix A. Supplementary data:**

Supplementary data to this article can be found online.

#### **Abbreviations**



<b>Term</b>	<b>Meaning</b>
JNPs	Janus nanoparticles
EOR	Enhance oil recovery
DPD	Dissipative particle dynamics
MD	Molecular dynamics
S	Tip length of the ridge
$\alpha$	Entry angle
$\beta$	Exit angle
A	Aspect ratio of the groove
W	Groove width
H	Groove depth
$d$	Diameter of JNPs
mW	Monoatomic water
TraPPE-UA	The Transferable Potentials for Phase Equilibria united-atom
SW	Stillinger–Weber
LJ	Lennard-Jones
NEMD	Non-equilibrium molecular dynamics
$D$	Averaged absolute coordinate of the adsorbed JNP
$R_{hydrophilic}$	Area of surface wettability alteration by individual JNP
$\phi$	Surface coverage ratio

## References

- Ahmadi, M., and Chen, Z., 2021. Comprehensive molecular scale modeling of anionic surfactant-asphaltene interactions. *Fuel* 288, 119729. <https://doi.org/10.1016/j.fuel.2020.119729>
- Chang, Y., Jiang, H., Li, J., et al., 2016. The study on crestal injection for fault block reservoir with high dip and low permeability. *Sci. Technol. Eng.* 16, 179-183. <https://doi.org/10.3969/j.issn.1671-1815.2016.33.032> (in chinese)
- Chang, Y., Xiao, S., Fu, Y., et al., 2021. Nanomechanical characteristics of trapped oil droplets with nanoparticles: a molecular dynamics simulation. *J. Petrol. Sci. Eng.* 203, 108649. <https://doi.org/10.1016/j.petrol.2021.108649>
- Chang, Y., Xiao, S., Ma, R., et al., 2022a. Displacement dynamics of trapped oil in rough channels driven by nanofluids. *Fuel* 314, 122760. <https://doi.org/10.1016/j.fuel.2021.122760>

- Chang, Y., Xiao, S., Ma, R., et al., 2022b. Atomistic insight into oil displacement on rough surface by Janus nanoparticles. *Energy* 245, 123264. <https://doi.org/10.1016/j.energy.2022.123264>
- Chen, Z., Qian, J., Zhan, H., et al., 2017. Effect of roughness on water flow through a synthetic single rough fracture. *Environ. Earth Sci.* 76, 186. <https://doi.org/10.1007/s12665-017-6470-7>
- Durret, J., Szkutnik, P.-D., Frolet, N., et al., 2018. Superhydrophobic polymeric films with hierarchical structures produced by nanoimprint (NIL) and plasma roughening. *Appl. Surf. Sci.* 445, 97-106. <https://doi.org/10.1016/j.apsusc.2018.03.010>
- Fang, T., Zhang, Y., Ma, R., et al., 2019. Oil extraction mechanism in CO<sub>2</sub> flooding from rough surface: Molecular dynamics simulation. *Appl. Surf. Sci.* 494, 80-86. <https://doi.org/10.1016/j.apsusc.2019.07.190>
- Giraldo, L.J., Gallego, J., Villegas, J.P., et al., 2019. Enhanced waterflooding with NiO/SiO<sub>2</sub> 0-D Janus nanoparticles at low concentration. *J. Petrol. Sci. Eng.* 174, 40-48. <https://doi.org/10.1016/j.petrol.2018.11.007>
- Harrison, A., Cracknell, R., Krueger-Venus, J., et al., 2014. Branched versus linear alkane adsorption in carbonaceous slit pores. *Adsorption* 20, 427-437. <https://doi.org/10.1007/s10450-013-9589-1>
- Hoover, W.G., 1985. Canonical dynamics: Equilibrium phase-space distributions. *Phys. Rev. A* 31, 1695. <https://doi.org/10.1103/PhysRevA.31.1695>
- Jia, C., 2020. Development challenges and future scientific and technological researches in China's petroleum industry upstream. *Acta Petrol. Sin.* 41, 1445-1464. <https://doi.org/10.7623/syxb202012001> (in chinese)
- Jia, X., Luo, J., Wang, P., et al., 2021. Synthesis of Dumbbell-like SiO<sub>2</sub> Nanoparticles with Amphiphilic Properties in Aqueous Phase. *Chinese J. Inorg. Chem.* 37, 653-660. <https://doi.org/10.11862/CJIC.2021.061> (in chinese)
- Kang, Y., Tian, J., Luo, P., et al., 2020. Technical bottlenecks and development strategies of enhancing recovery for tight oil reservoirs. *Acta Petrol. Sin.* 41, 467-477. <https://doi.org/10.7623/syxb202004009> (in chinese)
- Kondratyuk, P., Wang, Y., Johnson, J.K., et al., 2005. Observation of a one-dimensional adsorption site on carbon nanotubes: adsorption of alkanes of different molecular lengths. *J. Phys. Chem. B* 109, 20999-21005. <https://doi.org/10.1021/jp0582078>
- Lalegani, F., Saffarian, M.R., Moradi, A., et al., 2018. Effects of different roughness elements on friction and pressure drop of laminar flow in microchannels. *Int. J. Numer. Method H.* 28, 1664-1683. <https://doi.org/10.1108/hff-04-2017-0140>
- Li, S., Guo, P., Dai, L., et al., 2000. Strengthen gas injection for enhanced oil recovery. *J. Southwest Petrol. Univ. (Science & Technology Edition)* 22, 41. <https://doi.org/10.3863/j.issn.1000-2634.2000.03.011> (in chinese)
- Li, W., Nan, Y., You, Q., et al., 2020. Effects of salts and silica nanoparticles on oil-brine interfacial properties under hydrocarbon reservoir conditions: A molecular dynamics simulation study. *J. Mol. Liq.* 305, 112860. <https://doi.org/10.1016/j.molliq.2020.112860>
- Liang, F., Liu, B., Cao, Z., et al., 2017. Janus colloids toward interfacial engineering. *Langmuir* 34, 4123-4131. <https://doi.org/10.1021/acs.langmuir.7b02308>
- Liang, T., Hou, J.-R., Qu, M., et al., 2021. Application of nanomaterial for enhanced oil recovery. *Petrol. Sci.* <https://doi.org/10.1016/j.petsci.2021.11.011>

- Liu, J., Yang, Y., Sun, S., et al., 2022. Flow behaviors of shale oil in kerogen slit by molecular dynamics simulation. *Chem. Eng. J.* 434, 134682. <https://doi.org/10.1016/j.ccej.2022.134682>
- Liu, P., Li, X., Yu, H., et al., 2020. Functional Janus-SiO<sub>2</sub> Nanoparticles Prepared by a Novel “Cut the Gordian Knot” Method and Their Potential Application for Enhanced Oil Recovery. *ACS Appl. Mater. Interfaces* 12, 24201-24208. <https://doi.org/10.1021/acsami.0c01593>
- Luo, D., Wang, F., Zhu, J., et al., 2016. Nanofluid of graphene-based amphiphilic Janus nanosheets for tertiary or enhanced oil recovery: High performance at low concentration. *Proc. Natl. Acad. Sci.* 113, 7711-7716. <https://doi.org/10.1073/pnas.160813511>
- Luu, X.C., and Striolo, A., 2014. Ellipsoidal Janus nanoparticles assembled at spherical oil/water interfaces. *J. Phys. Chem. B* 118, 13737-13743. <https://doi.org/10.1021/jp508542z>
- Martin, M.G., and Siepmann, J.I., 1998. Transferable potentials for phase equilibria. 1. United-atom description of n-alkanes. *J. Phys. Chem. B* 102, 2569-2577. <https://doi.org/10.1021/jp972543+>
- Molinero, V., and Moore, E.B., 2009. Water modeled as an intermediate element between carbon and silicon. *J. Phys. Chem. B* 113, 4008-4016. <https://doi.org/10.1021/jp805227c>
- Niu, D., and Tang, G., 2014. Static and dynamic behavior of water droplet on solid surfaces with pillar-type nanostructures from molecular dynamics simulation. *Int. J. Heat Mass Transfer* 79, 647-654. <https://doi.org/10.1016/j.ijheatmasstransfer.2014.08.047>
- Plimpton, S., 1995. Fast parallel algorithms for short-range molecular dynamics. *J. Comput. Phys.* 117, 1-19. <https://doi.org/10.1006/jcph.1995.1039>
- Qian, B., and Li, M., 2018. The energy structure continues to diversify with the growth of energy demand—Interpretation of the 2018 World Energy Statistical Yearbook. *Econ. Anal. China's Petrol. Chem. Indus.* 8, 51-54. <https://doi.org/CNKI:SUN:SYFX.0.2018-08-023> (in chinese)
- Savoy, E.S., and Escobedo, F.A., 2012. Molecular simulations of wetting of a rough surface by an oily fluid: Effect of topology, chemistry, and droplet size on wetting transition rates. *Langmuir* 28, 3412-3419. <https://doi.org/10.1021/la203921h>
- Shi, F., Wu, J., Zhao, B., et al., 2019. Structural characterization and oil displacement performance of Janus micro-nanocapsules. *J. Silicate* 11, 1677-1682. <https://doi.org/10.14062/j.issn.0454-5648.2019.11.20> (in chinese)
- Song, F., Ma, L., Fan, J., et al., 2018. Wetting behaviors of a nano-droplet on a rough solid substrate under perpendicular electric field. *Nanomaterials* 8, 340. <https://doi.org/10.3390/nano8050340>
- Stukowski, A., 2009. Visualization and analysis of atomistic simulation data with OVITO—the Open Visualization Tool. *Modell. Simul. Mater. Sci. Eng.* 18, 015012. <https://doi.org/10.1088/0965-0393/18/1/015012>
- Sun, D., Ye, Y., Liang, F., et al., 2021. Some recent advances in Janus particulate emulsifiers. *CIESC Journal* 72, 6203-6215. <https://doi.org/10.11949/0438-1157.20211277> (in chinese)
- Sun, X., Dong, M., Zhang, Y., et al., 2015. Enhanced heavy oil recovery in thin reservoirs using foamy oil-assisted methane huff-n-puff method. *Fuel* 159, 962-973. <https://doi.org/10.1016/j.fuel.2015.07.056>

- Wang, G., Wang, Y., Wang, J., et al., 2017. Kinetic Monte Carlo study on the evolution of silicon surface roughness under hydrogen thermal treatment. *Appl. Surf. Sci.* 414, 361-364. <https://doi.org/10.1016/j.apsusc.2017.04.002>
- Wang, X., Xiao, S., Zhang, Z., et al., 2019. Transportation of Janus nanoparticles in confined nanochannels: a molecular dynamics simulation. *Environ. Sci.: Nano* 6, 2810-2819. <https://doi.org/10.1039/C9EN00314B>
- Wu, H., Gao, K., Lu, Y., et al., 2020a. Silica-based amphiphilic Janus nanofluid with improved interfacial properties for enhanced oil recovery. *Colloids Surf. Physicochem Eng. Aspects* 586, 124162. <https://doi.org/10.1016/j.colsurfa.2019.124162>
- Wu, J., Shi, F., Zhao, Y., et al., 2020b. Research progress of functional nano oil displacement agents. *J. Northeast Petrol. Univ.* 44, 70-75. <https://doi.org/10.3969/j.issn.2095-4107.2020.05.001> (in chinese)
- Xiang, W., Zhao, S., Song, X., et al., 2017. Amphiphilic nanosheet self-assembly at the water/oil interface: computer simulations. *Phys. Chem. Chem. Phys.* 19, 7576-7586. <https://doi.org/10.1039/C6CP08654C>
- Xie, J.-F., and Cao, B.-Y., 2016. Nanochannel flow past permeable walls via molecular dynamics. *AIP Advances* 6, 075307. <https://doi.org/10.1063/1.4959022>
- Yaghoubi, H., and Foroutan, M., 2018. Molecular investigation of the wettability of rough surfaces using molecular dynamics simulation. *Phys. Chem. Chem. Phys.* 20, 22308-22319. <https://doi.org/10.1039/C8CP03762K>
- Yin, T., Yang, Z., Dong, Z., et al., 2019. Physicochemical properties and potential applications of silica-based amphiphilic Janus nanosheets for enhanced oil recovery. *Fuel* 237, 344-351. <https://doi.org/10.1016/j.fuel.2018.10.028>
- Yin, T., Yang, Z., Zhang, F., et al., 2021. Assembly and mechanical response of amphiphilic Janus nanosheets at oil-water interfaces. *J. Colloid Interface Sci.* 583, 214-221. <https://doi.org/10.1016/j.jcis.2020.09.026>
- Zhang, X., Guo, J., Gao, C., et al., 2022. Application Progress of Nanoparticle Enhancement for Enhanced Oil Recovery. *Oilfield Chemistry*. <https://doi.org/10.19346/j.cnki.1000-4092.2022.01.031> (in chinese)
- Zhang, Y., 2016. Effect of wall surface roughness on mass transfer in a nano channel. *Int. J. Heat Mass Transfer* 100, 295-302. <https://doi.org/10.1016/j.ijheatmasstransfer.2016.04.097>
- Zhao, J., Yao, G., Ramisetty, S.B., et al., 2019. Molecular dynamics investigation of substrate wettability alteration and oil transport in a calcite nanopore. *Fuel* 239, 1149-1161. <https://doi.org/10.1016/j.fuel.2018.11.089>

## Supporting Information

## Unraveling the Influence of Surface Roughness on Oil Displacement by Janus Nanoparticles

Yuanhao Chang <sup>a</sup>, Senbo Xiao <sup>a,1</sup>, Rui Ma <sup>a</sup>, Zhiliang Zhang <sup>a</sup>, Jianying He <sup>a,2</sup>

<sup>a</sup> Department of Structural Engineering, Norwegian University of Science and Technology (NTNU), 7491 Trondheim, Norway

**Table S1.** Energy well depth (characteristic energy, kcal/mol) of interaction Lennard-Jones (LJ) potential between the hydrophilic/hydrophobic parts of the Janus NPs with the other components in the simulation systems.

Characteristic energy (kcal/mol)	Water	Oil	Surface
Hydrophilic part of NPs	0.4	0.01	0.7
Hydrophobic part of NPs	0.01	0.2	

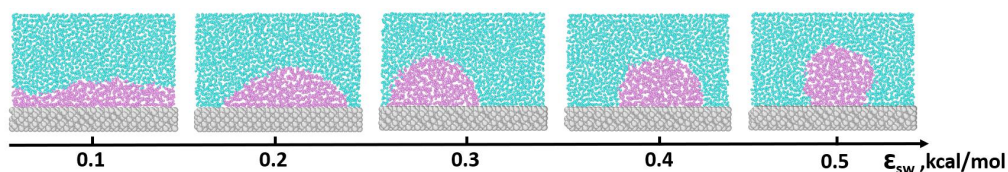


**Fig. S1.** Oil droplet morphologies after 20-ns equilibration on the surfaces with varied characteristic energy  $\epsilon_{sw}$  (kcal/mol) of LJ potential between surface and water.

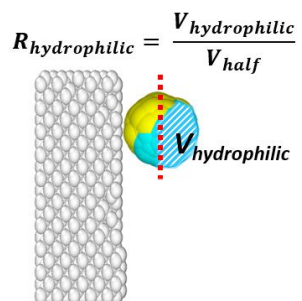


Fig. S2. The sketch of the  $R_{hydrophobic}$  definition.

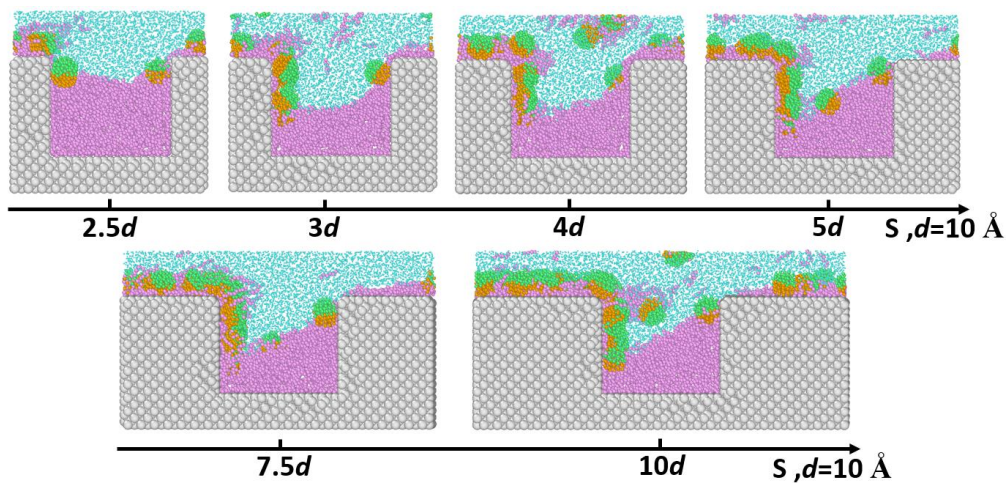
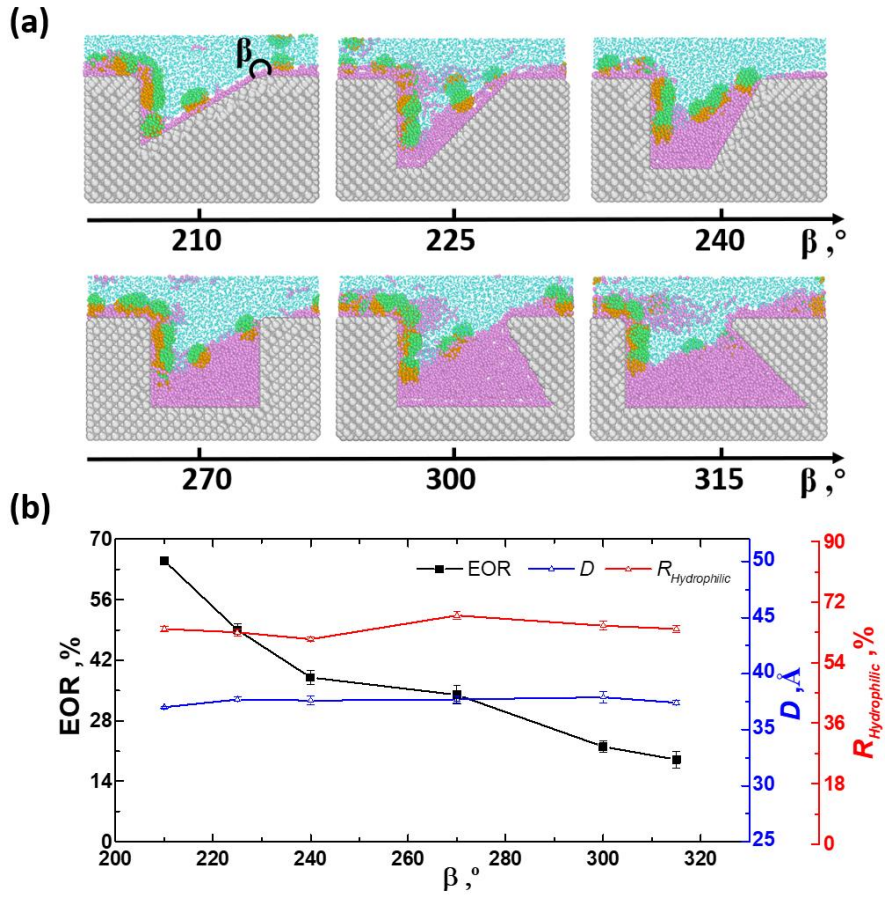
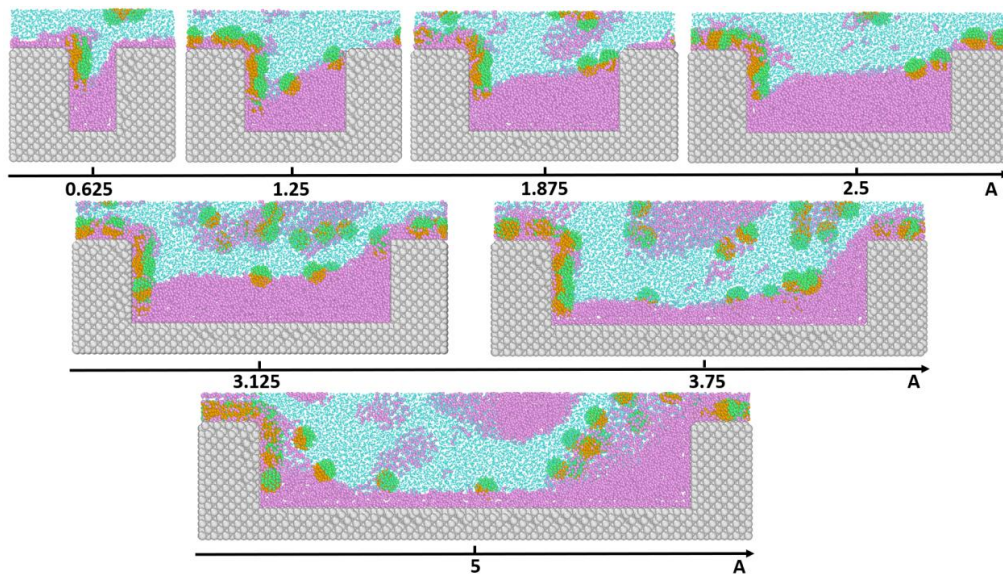


Fig. S3. The final snapshots system with varied  $S$  after displacement simulations.



**Fig. S4.** The effect of exit angle,  $\beta$ , on oil displacement. (a) The final snapshots after oil displacement of system with varied  $\beta$ . (b) The EOR,  $D$  and  $R_{\text{hydrophilic}}$  of the adsorption JNP film with varied  $\beta$ .



**Fig. S5.** The final snapshots after oil displacement on grooves with varied aspect ratios.

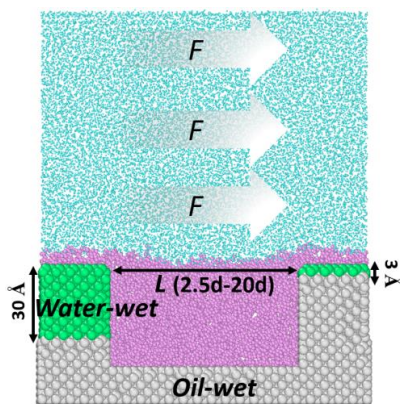


**Fig. S6.** Representative structure of the designed system. The white arrows indicate the flooding direction in the periodic simulation box. The colors for different components in the system: water (light blue), oil (pink), hydrophobic part of the surface (grey) and hydrophilic part of the surface (green).



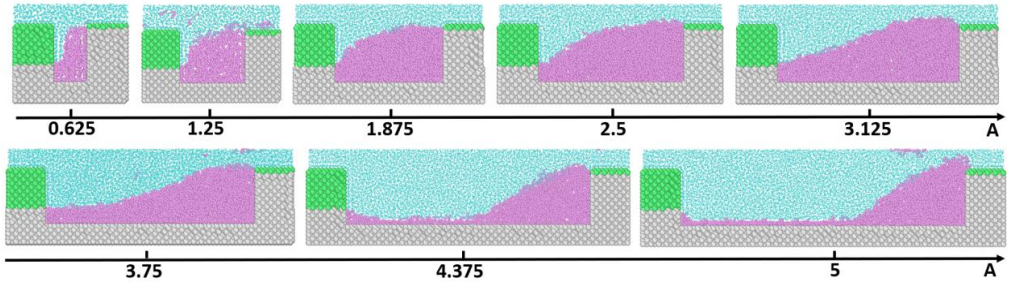


Fig. S7. The final system snapshots of the designed systems with varied groove aspect ratios after flooding by water.

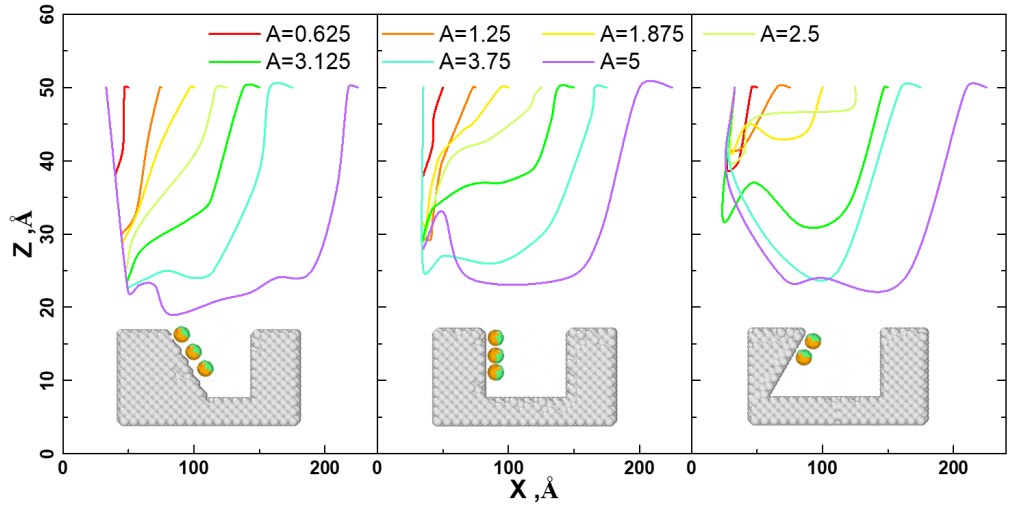


Fig. S8. The morphology of the oil-water interface after oil displacement in grooves with varied aspect ratios and three entry angles of  $240^\circ$ ,  $270^\circ$ , and  $300^\circ$ . The representative snapshots of each system are shown as insets.

#### **A.4 Paper IV**

---

### **Deformation and rupture of Janus nanoparticle stabilized Pickering emulsion on the solid surface**

Authors: Yuanhao Chang, Senbo Xiao, Rui Ma, Yuequn Fu, Zhiliang Zhang, and Jianying He

To be submitted.

This paper is awaiting publication and is not included in NTNU Open



## **A.5 Paper V**

---

### **Transport of Pickering emulsion across nanopore throat**

Authors: Yuanhao Chang, Senbo Xiao, Rui Ma, Yuequn Fu, Zhiliang Zhang and Jianying He

To be submitted.

This paper is awaiting publication and is not included in NTNU Open

## **Appendix B**

List of previous PhD theses at Department of Structural Engineering

**Appendix B**

---

**DEPARTMENT OF STRUCTURAL ENGINEERING  
NORWEGIAN UNIVERSITY OF SCIENCE AND TECHNOLOGY**

N-7491 TRONDHEIM, NORWAY  
Telephone: +47 73 59 47 00

"Reliability Analysis of Structural Systems using Nonlinear Finite Element Methods",  
C. A. Holm, 1990:23, ISBN 82-7119-178-0.

"Uniform Stratified Flow Interaction with a Submerged Horizontal Cylinder",  
Ø. Arntsen, 1990:32, ISBN 82-7119-188-8.

"Large Displacement Analysis of Flexible and Rigid Systems Considering  
Displacement-Dependent Loads and Nonlinear Constraints",  
K. M. Mathisen, 1990:33, ISBN 82-7119-189-6.

"Solid Mechanics and Material Models including Large Deformations",  
E. Levold, 1990:56, ISBN 82-7119-214-0, ISSN 0802-3271.

"Inelastic Deformation Capacity of Flexurally-Loaded Aluminium Alloy Structures",  
T. Welo, 1990:62, ISBN 82-7119-220-5, ISSN 0802-3271.

"Visualization of Results from Mechanical Engineering Analysis",  
K. Aamnes, 1990:63, ISBN 82-7119-221-3, ISSN 0802-3271.

"Object-Oriented Product Modeling for Structural Design",  
S. I. Dale, 1991:6, ISBN 82-7119-258-2, ISSN 0802-3271.

"Parallel Techniques for Solving Finite Element Problems on Transputer Networks",  
T. H. Hansen, 1991:19, ISBN 82-7119-273-6, ISSN 0802-3271.

"Statistical Description and Estimation of Ocean Drift Ice Environments",  
R. Korsnes, 1991:24, ISBN 82-7119-278-7, ISSN 0802-3271.

"Properties of concrete related to fatigue damage: with emphasis on high strength  
concrete",  
G. Petkovic, 1991:35, ISBN 82-7119-290-6, ISSN 0802-3271.

"Turbidity Current Modelling",  
B. Brørs, 1991:38, ISBN 82-7119-293-0, ISSN 0802-3271.

"Zero-Slump Concrete: Rheology, Degree of Compaction and Strength. Effects of  
Fillers as Part Cement-Replacement",  
C. Sørensen, 1992:8, ISBN 82-7119-357-0, ISSN 0802-3271.

"Nonlinear Analysis of Reinforced Concrete Structures Exposed to Transient  
Loading",  
K. V. Høiseith, 1992:15, ISBN 82-7119-364-3, ISSN 0802-3271.

- "Finite Element Formulations and Solution Algorithms for Buckling and Collapse Analysis of Thin Shells",  
R. O. Bjærum, 1992:30, ISBN 82-7119-380-5, ISSN 0802-3271.
- "Response Statistics of Nonlinear Dynamic Systems",  
J. M. Johnsen, 1992:42, ISBN 82-7119-393-7, ISSN 0802-3271.
- "Digital Models in Engineering. A Study on why and how engineers build and operate digital models for decision support",  
J. Høyte, 1992:75, ISBN 82-7119-429-1, ISSN 0802-3271.
- "Sparse Solution of Finite Element Equations",  
A. C. Damhaug, 1992:76, ISBN 82-7119-430-5, ISSN 0802-3271.
- "Some Aspects of Floating Ice Related to Sea Surface Operations in the Barents Sea",  
S. Løset, 1992:95, ISBN 82-7119-452-6, ISSN 0802-3271.
- "Modelling of Cyclic Plasticity with Application to Steel and Aluminium Structures",  
O. S. Hopperstad, 1993:7, ISBN 82-7119-461-5, ISSN 0802-3271.
- "The Free Formulation: Linear Theory and Extensions with Applications to Tetrahedral Elements with Rotational Freedoms",  
G. Skeie, 1993:17, ISBN 82-7119-472-0, ISSN 0802-3271.
- "Høyfast betongs motstand mot piggdekkslitasje. Analyse av resultater fra prøving i Veisliter'n",  
T. Tveter, 1993:62, ISBN 82-7119-522-0, ISSN 0802-3271.
- "A Nonlinear Finite Element Based on Free Formulation Theory for Analysis of Sandwich Structures",  
O. Aamlid, 1993:72, ISBN 82-7119-534-4, ISSN 0802-3271.
- "The Effect of Curing Temperature and Silica Fume on Chloride Migration and Pore Structure of High Strength Concrete",  
C. J. Hauck, 1993:90, ISBN 82-7119-553-0, ISSN 0802-3271.
- "Failure of Concrete under Compressive Strain Gradients",  
G. Markeset, 1993:110, ISBN 82-7119-575-1, ISSN 0802-3271.
- "An experimental study of internal tidal amphidromes in Vestfjorden",  
J. H. Nilsen, 1994:39, ISBN 82-7119-640-5, ISSN 0802-3271.
- "Structural analysis of oil wells with emphasis on conductor design",  
H. Larsen, 1994:46, ISBN 82-7119-648-0, ISSN 0802-3271.
- "Adaptive methods for non-linear finite element analysis of shell structures",  
K. M. Okstad, 1994:66, ISBN 82-7119-670-7, ISSN 0802-3271.

- "On constitutive modelling in nonlinear analysis of concrete structures",  
O. Fyrtlev, 1994:115, ISBN 82-7119-725-8, ISSN 0802-3271.
- "Fluctuating wind load and response of a line-like engineering structure with emphasis on motion-induced wind forces",  
J. Bogunovic Jakobsen, 1995:62, ISBN 82-7119-809-2, ISSN 0802-3271.
- "An experimental study of beam-columns subjected to combined torsion, bending and axial actions",  
A. Aalberg, 1995:66, ISBN 82-7119-813-0, ISSN 0802-3271.
- "Scaling and cracking in unsealed freeze/thaw testing of Portland cement and silica fume concretes",  
S. Jacobsen, 1995:101, ISBN 82-7119-851-3, ISSN 0802-3271.
- "Damping of water waves by submerged vegetation. A case study of laminaria hyperborea",  
A. M. Dubi, 1995:108, ISBN 82-7119-859-9, ISSN 0802-3271.
- "The dynamics of a slope current in the Barents Sea",  
Sheng Li, 1995:109, ISBN 82-7119-860-2, ISSN 0802-3271.
- "Modellering av delmaterialenes betydning for betongens konsistens",  
Ernst Mørtzell, 1996:12, ISBN 82-7119-894-7, ISSN 0802-3271.
- "Bending of thin-walled aluminium extrusions",  
Birgit Søvik Opheim, 1996:60, ISBN 82-7119-947-1, ISSN 0802-3271.
- "Material modelling of aluminium for crashworthiness analysis",  
Torodd Berstad, 1996:89, ISBN 82-7119-980-3, ISSN 0802-3271.
- "Estimation of structural parameters from response measurements on submerged floating tunnels",  
Rolf Magne Larssen, 1996:119, ISBN 82-471-0014-2, ISSN 0802-3271.
- "Numerical modelling of plain and reinforced concrete by damage mechanics",  
Mario A. Polanco-Loria, 1997:20, ISBN 82-471-0049-5, ISSN 0802-3271.
- "Nonlinear random vibrations - numerical analysis by path integration methods",  
Vibeke Moe, 1997:26, ISBN 82-471-0056-8, ISSN 0802-3271.
- "Numerical prediction of vortex-induced vibration by the finite element method",  
Joar Martin Dalheim, 1997:63, ISBN 82-471-0096-7, ISSN 0802-3271.
- "Time domain calculations of buffeting response for wind sensitive structures",  
Ketil Aas-Jakobsen, 1997:148, ISBN 82-471-0189-0, ISSN 0802-3271.
- "A numerical study of flow about fixed and flexibly mounted circular cylinders",  
Trond Stokka Meling, 1998:48, ISBN 82-471-0244-7, ISSN 0802-3271.



- “Estimation of chloride penetration into concrete bridges in coastal areas”,  
Per Egil Steen, 1998:89, ISBN 82-471-0290-0, ISSN 0802-3271.
- “Stress-resultant material models for reinforced concrete plates and shells”,  
Jan Arve Øverli, 1998:95, ISBN 82-471-0297-8, ISSN 0802-3271.
- “Chloride binding in concrete. Effect of surrounding environment and concrete composition”,  
Claus Kenneth Larsen, 1998:101, ISBN 82-471-0337-0, ISSN 0802-3271.
- “Rotational capacity of aluminium alloy beams”,  
Lars A. Moen, 1999:1, ISBN 82-471-0365-6, ISSN 0802-3271.
- “Stretch Bending of Aluminium Extrusions”,  
Arild H. Clausen, 1999:29, ISBN 82-471-0396-6, ISSN 0802-3271.
- “Aluminium and Steel Beams under Concentrated Loading”,  
Tore Tryland, 1999:30, ISBN 82-471-0397-4, ISSN 0802-3271.
- "Engineering Models of Elastoplasticity and Fracture for Aluminium Alloys",  
Odd-Geir Lademo, 1999:39, ISBN 82-471-0406-7, ISSN 0802-3271.
- "Kapasitet og duktilitet av dybelforbindelser i trekonstruksjoner",  
Jan Siem, 1999:46, ISBN 82-471-0414-8, ISSN 0802-3271.
- “Etablering av distribuert ingeniørarbeid; Teknologiske og organisatoriske erfaringer fra en norsk ingeniørbedrift”,  
Lars Line, 1999:52, ISBN 82-471-0420-2, ISSN 0802-3271.
- “Estimation of Earthquake-Induced Response”,  
Símon Ólafsson, 1999:73, ISBN 82-471-0443-1, ISSN 0802-3271.
- “Coastal Concrete Bridges: Moisture State, Chloride Permeability and Aging Effects”  
Ragnhild Holen Relling, 1999:74, ISBN 82-471-0445-8, ISSN 0802-3271.
- ”Capacity Assessment of Titanium Pipes Subjected to Bending and External Pressure”,  
Arve Bjørset, 1999:100, ISBN 82-471-0473-3, ISSN 0802-3271.
- “Validation of Numerical Collapse Behaviour of Thin-Walled Corrugated Panels”,  
Håvar Ilstad, 1999:101, ISBN 82-471-0474-1, ISSN 0802-3271.
- “Strength and Ductility of Welded Structures in Aluminium Alloys”,  
Miroslaw Matusiak, 1999:113, ISBN 82-471-0487-3, ISSN 0802-3271.
- “Thermal Dilation and Autogenous Deformation as Driving Forces to Self-Induced Stresses in High Performance Concrete”,  
Øyvind Bjøntegaard, 1999:121, ISBN 82-7984-002-8, ISSN 0802-3271.

- “Some Aspects of Ski Base Sliding Friction and Ski Base Structure”,  
Dag Anders Moldestad, 1999:137, ISBN 82-7984-019-2, ISSN 0802-3271.
- "Electrode reactions and corrosion resistance for steel in mortar and concrete",  
Roy Antonsen, 2000:10, ISBN 82-7984-030-3, ISSN 0802-3271.
- "Hydro-Physical Conditions in Kelp Forests and the Effect on Wave Damping and Dune Erosion. A case study on Laminaria Hyperborea",  
Stig Magnar Løvås, 2000:28, ISBN 82-7984-050-8, ISSN 0802-3271.
- "Random Vibration and the Path Integral Method",  
Christian Skaug, 2000:39, ISBN 82-7984-061-3, ISSN 0802-3271.
- "Buckling and geometrical nonlinear beam-type analyses of timber structures",  
Trond Even Eggen, 2000:56, ISBN 82-7984-081-8, ISSN 0802-3271.
- ”Structural Crashworthiness of Aluminium Foam-Based Components”,  
Arve Grønsund Hanssen, 2000:76, ISBN 82-7984-102-4, ISSN 0809-103X.
- “Measurements and simulations of the consolidation in first-year sea ice ridges, and some aspects of mechanical behaviour”,  
Knut V. Høyland, 2000:94, ISBN 82-7984-121-0, ISSN 0809-103X.
- ”Kinematics in Regular and Irregular Waves based on a Lagrangian Formulation”,  
Svein Helge Gjørund, 2000-86, ISBN 82-7984-112-1, ISSN 0809-103X.
- ”Self-Induced Cracking Problems in Hardening Concrete Structures”,  
Daniela Bosnjak, 2000-121, ISBN 82-7984-151-2, ISSN 0809-103X.
- "Ballistic Penetration and Perforation of Steel Plates",  
Tore Børvik, 2000:124, ISBN 82-7984-154-7, ISSN 0809-103X.
- "Freeze-Thaw resistance of Concrete. Effect of: Curing Conditions, Moisture Exchange and Materials",  
Terje Finnerup Rønning, 2001:14, ISBN 82-7984-165-2, ISSN 0809-103X
- "Structural behaviour of post tensioned concrete structures. Flat slab. Slabs on ground",  
Steinar Trygstad, 2001:52, ISBN 82-471-5314-9, ISSN 0809-103X.
- "Slipforming of Vertical Concrete Structures. Friction between concrete and slipform panel",  
Kjell Tore Fosså, 2001:61, ISBN 82-471-5325-4, ISSN 0809-103X.
- "Some numerical methods for the simulation of laminar and turbulent incompressible flows",  
Jens Holmen, 2002:6, ISBN 82-471-5396-3, ISSN 0809-103X.
- “Improved Fatigue Performance of Threaded Drillstring Connections by Cold Rolling”,

- Steinar Kristoffersen, 2002:11, ISBN: 82-421-5402-1, ISSN 0809-103X.
- "Deformations in Concrete Cantilever Bridges: Observations and Theoretical Modelling",  
Peter F. Takács, 2002:23, ISBN 82-471-5415-3, ISSN 0809-103X.
- "Stiffened aluminium plates subjected to impact loading",  
Hilde Giæver Hildrum, 2002:69, ISBN 82-471-5467-6, ISSN 0809-103X.
- "Full- and model scale study of wind effects on a medium-rise building in a built up area",  
Jónas Thór Snæbjörnsson, 2002:95, ISBN82-471-5495-1, ISSN 0809-103X.
- "Evaluation of Concepts for Loading of Hydrocarbons in Ice-infested water",  
Arnor Jensen, 2002:114, ISBN 82-417-5506-0, ISSN 0809-103X.
- "Numerical and Physical Modelling of Oil Spreading in Broken Ice",  
Janne K. Økland Gjølsteen, 2002:130, ISBN 82-471-5523-0, ISSN 0809-103X.
- "Diagnosis and protection of corroding steel in concrete",  
Franz Pruckner, 20002:140, ISBN 82-471-5555-4, ISSN 0809-103X.
- "Tensile and Compressive Creep of Young Concrete: Testing and Modelling",  
Dawood Atrushi, 2003:17, ISBN 82-471-5565-6, ISSN 0809-103X.
- "Rheology of Particle Suspensions. Fresh Concrete, Mortar and Cement Paste with Various Types of Lignosulfonates",  
Jon Elvar Wallevik, 2003:18, ISBN 82-471-5566-4, ISSN 0809-103X.
- "Oblique Loading of Aluminium Crash Components",  
Aase Reyes, 2003:15, ISBN 82-471-5562-1, ISSN 0809-103X.
- "Utilization of Ethiopian Natural Pozzolans",  
Surafel Ketema Desta, 2003:26, ISSN 82-471-5574-5, ISSN:0809-103X.
- "Behaviour and strength prediction of reinforced concrete structures with discontinuity regions", Helge Brå, 2004:11, ISBN 82-471-6222-9, ISSN 1503-8181.
- "High-strength steel plates subjected to projectile impact. An experimental and numerical study", Sumita Dey, 2004:38, ISBN 82-471-6282-2 (printed version), ISBN 82-471-6281-4 (electronic version), ISSN 1503-8181.
- "Alkali-reactive and inert fillers in concrete. Rheology of fresh mixtures and expansive reactions."  
Bård M. Pedersen, 2004:92, ISBN 82-471-6401-9 (printed version), ISBN 82-471-6400-0 (electronic version), ISSN 1503-8181.
- "On the Shear Capacity of Steel Girders with Large Web Openings".  
Nils Christian Hagen, 2005:9 ISBN 82-471-6878-2 (printed version), ISBN 82-471-6877-4 (electronic version), ISSN 1503-8181.

- ”Behaviour of aluminium extrusions subjected to axial loading”.  
Østen Jensen, 2005:7, ISBN 82-471-6873-1 (printed version), ISBN 82-471-6872-3 (electronic version), ISSN 1503-8181.
- ”Thermal Aspects of corrosion of Steel in Concrete”.  
Jan-Magnus Østvik, 2005:5, ISBN 82-471-6869-3 (printed version), ISBN 82-471-6868 (electronic version), ISSN 1503-8181.
- ”Mechanical and adaptive behaviour of bone in relation to hip replacement.” A study of bone remodelling and bone grafting.  
Sébastien Muller, 2005:34, ISBN 82-471-6933-9 (printed version), ISBN 82-471-6932-0 (electronic version), ISSN 1503-8181.
- “Analysis of geometrical nonlinearities with applications to timber structures”.  
Lars Wollebæk, 2005:74, ISBN 82-471-7050-5 (printed version), ISBN 82-471-7019-1 (electronic version), ISSN 1503-8181.
- “Pedestrian induced lateral vibrations of slender footbridges”,  
Anders Rönnquist, 2005:102, ISBN 82-471-7082-5 (printed version), ISBN 82-471-7081-7 (electronic version), ISSN 1503-8181.
- “Initial Strength Development of Fly Ash and Limestone Blended Cements at Various Temperatures Predicted by Ultrasonic Pulse Velocity”,  
Tom Ivar Fredvik, 2005:112, ISBN 82-471-7105-8 (printed version), ISBN 82-471-7103-1 (electronic version), ISSN 1503-8181.
- “Behaviour and modelling of thin-walled cast components”,  
Cato Dørum, 2005:128, ISBN 82-471-7140-6 (printed version), ISBN 82-471-7139-2 (electronic version), ISSN 1503-8181.
- “Behaviour and modelling of selfpiercing riveted connections”,  
Raffaele Porcaro, 2005:165, ISBN 82-471-7219-4 (printed version), ISBN 82-471-7218-6 (electronic version), ISSN 1503-8181.
- ”Behaviour and Modelling of Aluminium Plates subjected to Compressive Load”,  
Lars Rønning, 2005:154, ISBN 82-471-7169-1 (printed version), ISBN 82-471-7195-3 (electronic version), ISSN 1503-8181.
- ”Bumper beam-longitudinal system subjected to offset impact loading”,  
Satyanarayana Kokkula, 2005:193, ISBN 82-471-7280-1 (printed version), ISBN 82-471-7279-8 (electronic version), ISSN 1503-8181.
- “Control of Chloride Penetration into Concrete Structures at Early Age”,  
Guofei Liu, 2006:46, ISBN 82-471-7838-9 (printed version), ISBN 82-471-7837-0 (electronic version), ISSN 1503-8181.
- “Modelling of Welded Thin-Walled Aluminium Structures”,

Ting Wang, 2006:78, ISBN 82-471-7907-5 (printed version), ISBN 82-471-7906-7 (electronic version), ISSN 1503-8181.

”Time-variant reliability of dynamic systems by importance sampling and probabilistic analysis of ice loads”,

Anna Ivanova Olsen, 2006:139, ISBN 82-471-8041-3 (printed version), ISBN 82-471-8040-5 (electronic version), ISSN 1503-8181.

“Fatigue life prediction of an aluminium alloy automotive component using finite element analysis of surface topography”.

Sigmund Kyrre Ås, 2006:25, ISBN 82-471-7791-9 (printed version), ISBN 82-471-7791-9 (electronic version), ISSN 1503-8181.

”Constitutive models of elastoplasticity and fracture for aluminium alloys under strain path change”.

Dasharatha Achani, 2006:76, ISBN 82-471-7903-2 (printed version), ISBN 82-471-7902-4 (electronic version), ISSN 1503-8181.

“Simulations of 2D dynamic brittle fracture by the Element-free Galerkin method and linear fracture mechanics”.

Tommy Karlsson, 2006:125, ISBN 82-471-8011-1 (printed version), ISBN 82-471-8010-3 (electronic version), ISSN 1503-8181.

“Penetration and Perforation of Granite Targets by Hard Projectiles”.

Chong Chiang Seah, 2006:188, ISBN 82-471-8150-9 (printed version), ISBN 82-471-8149-5 (electronic version), ISSN 1503-8181.

“Deformations, strain capacity and cracking of concrete in plastic and early hardening phases”.

Tor Arne Hammer, 2007:234, ISBN 978-82-471-5191-4 (printed version), ISBN 978-82-471-5207-2 (electronic version), ISSN 1503-8181.

“Crashworthiness of dual-phase high-strength steel: Material and Component behaviour”, Venkatapathi Tarigopula, 2007:230, ISBN 82-471-5076-4 (printed version), ISBN 82-471-5093-1 (electronic version), ISSN 1503-8181.

“Fibre reinforcement in load carrying concrete structures”.

Åse Lyslo Døssland, 2008:50, ISBN 978-82-471-6910-0 (printed version), ISBN 978-82-471-6924-7 (electronic version), ISSN 1503-8181.

“Low-velocity penetration of aluminium plates”.

Frode Grytten, 2008:46, ISBN 978-82-471-6826-4 (printed version), ISBN 978-82-471-6843-1 (electronic version), ISSN 1503-8181.

“Robustness studies of structures subjected to large deformations”.

Ørjan Fyllingen, 2008:24, ISBN 978-82-471-6339-9 (printed version), ISBN 978-82-471-6342-9 (electronic version), ISSN 1503-8181.

- “Constitutive modelling of morsellised bone”,  
Knut Birger Lunde, 2008:92, ISBN 978-82-471-7829-4 (printed version), ISBN 978-82-471-7832-4 (electronic version), ISSN 1503-8181.
- “Experimental Investigations of Wind Loading on a Suspension Bridge Girder”,  
Bjørn Isaksen, 2008:131, ISBN 978-82-471-8656-5 (printed version), ISBN 978-82-471-8673-2 (electronic version), ISSN 1503-8181.
- “Cracking Risk of Concrete Structures in The Hardening Phase”,  
Guomin Ji, 2008:198, ISBN 978-82-471-1079-9 (printed version), ISBN 978-82-471-1080-5 (electronic version), ISSN 1503-8181.
- “Modelling and numerical analysis of the porcine and human mitral apparatus”,  
Victorien Emile Prot, 2008:249, ISBN 978-82-471-1192-5 (printed version), ISBN 978-82-471-1193-2 (electronic version), ISSN 1503-8181.
- “Strength analysis of net structures”,  
Heidi Moe, 2009:48, ISBN 978-82-471-1468-1 (printed version), ISBN 978-82-471-1469-8 (electronic version), ISSN 1503-8181.
- “Numerical analysis of ductile fracture in surface cracked shells”,  
Espen Berg, 2009:80, ISBN 978-82-471-1537-4 (printed version), ISBN 978-82-471-1538-1 (electronic version), ISSN 1503-8181.
- “Subject specific finite element analysis of bone – for evaluation of the healing of a leg lengthening and evaluation of femoral stem design”,  
Sune Hansborg Pettersen, 2009:99, ISBN 978-82-471-1579-4 (printed version), ISBN 978-82-471-1580-0 (electronic version), ISSN 1503-8181.
- “Evaluation of fracture parameters for notched multi-layered structures”,  
Lingyun Shang, 2009:137, ISBN 978-82-471-1662-3 (printed version), ISBN 978-82-471-1663-0 (electronic version), ISSN 1503-8181.
- “Modelling of Dynamic Material Behaviour and Fracture of Aluminium Alloys for Structural Applications”  
Yan Chen, 2009:69, ISBN 978-82-471-1515-2 (printed version), ISBN 978-82-471-1516-9 (electronic version), ISSN 1503-8181.
- “Nanomechanics of polymer and composite particles”  
Jianying He 2009:213, ISBN 978-82-471-1828-3 (printed version), ISBN 978-82-471-1829-0 (electronic version), ISSN 1503-8181.
- “Mechanical properties of clear wood from Norway spruce”  
Kristian Berbohm Dahl 2009:250, ISBN 978-82-471-1911-2 (printed version) ISBN 978-82-471-1912-9 (electronic version), ISSN 1503-8181.
- “Modeling of the degradation of TiB<sub>2</sub> mechanical properties by residual stresses and liquid Al penetration along grain boundaries”

Micol Pezzotta 2009:254, ISBN 978-82-471-1923-5 (printed version) ISBN 978-82-471-1924-2 (electronic version) ISSN 1503-8181.

“Effect of welding residual stress on fracture”

Xiabo Ren 2010:77, ISBN 978-82-471-2115-3 (printed version) ISBN 978-82-471-2116-0 (electronic version), ISSN 1503-8181.

“Pan-based carbon fiber as anode material in cathodic protection system for concrete structures”

Mahdi Chini 2010:122, ISBN 978-82-471-2210-5 (printed version) ISBN 978-82-471-2213-6 (electronic version), ISSN 1503-8181.

“Structural Behaviour of deteriorated and retrofitted concrete structures”

Irina Vasililjeva Sæther 2010:171, ISBN 978-82-471-2315-7 (printed version) ISBN 978-82-471-2316-4 (electronic version) ISSN 1503-8181.

“Prediction of local snow loads on roofs”

Vivian Meløysund 2010:247, ISBN 978-82-471-2490-1 (printed version) ISBN 978-82-471-2491-8 (electronic version) ISSN 1503-8181.

“Behaviour and modelling of polymers for crash applications”

Virgile Delhaye 2010:251, ISBN 978-82-471-2501-4 (printed version) ISBN 978-82-471-2502-1 (electronic version) ISSN 1503-8181.

“Blended cement with reduced CO<sub>2</sub> emission – Utilizing the Fly Ash-Limestone Synergy”,

Klaartje De Weerd 2011:32, ISBN 978-82-471-2584-7 (printed version) ISBN 978-82-471-2584-4 (electronic version) ISSN 1503-8181.

“Chloride induced reinforcement corrosion in concrete” Concept of critical chloride content – methods and mechanisms.

Ueli Angst 2011:113, ISBN 978-82-471-2769-9 (printed version) ISBN 978-82-471-2763-6 (electronic version) ISSN 1503-8181.

“A thermo-electric-Mechanical study of the carbon anode and contact interface for Energy savings in the production of aluminium”.

Dag Herman Andersen 2011:157, ISBN 978-82-471-2859-6 (printed version) ISBN 978-82-471-2860-2 (electronic version) ISSN 1503-8181.

“Structural Capacity of Anchorage Ties in Masonry Veneer Walls Subjected to Earthquake”. The implications of Eurocode 8 and Eurocode 6 on a typical Norwegian veneer wall.

Ahmed Mohamed Yousry Hamed 2011:181, ISBN 978-82-471-2911-1 (printed version) ISBN 978-82-471-2912-8 (electronic ver.) ISSN 1503-8181.

“Work-hardening behaviour in age-hardenable Al-Zn-Mg(-Cu) alloys”.

Ida Westermann, 2011:247, ISBN 978-82-471-3056-8 (printed ver.) ISBN 978-82-471-3057-5 (electronic ver.) ISSN 1503-8181.

- “Behaviour and modelling of selfpiercing riveted connections using aluminium rivets”. Nguyen-Hieu Hoang, 2011:266, ISBN 978-82-471-3097-1 (printed ver.) ISBN 978-82-471-3099-5 (electronic ver.) ISSN 1503-8181.
- “Fibre reinforced concrete”.  
Sindre Sandbakk, 2011:297, ISBN 978-82-471-3167-1 (printed ver.) ISBN 978-82-471-3168-8 (electronic ver.) ISSN 1503-8181.
- “Dynamic behaviour of cablesupported bridges subjected to strong natural wind”.  
Ole Andre Øiseth, 2011:315, ISBN 978-82-471-3209-8 (printed ver.) ISBN 978-82-471-3210-4 (electronic ver.) ISSN 1503-8181.
- “Constitutive modeling of solargrade silicon materials”  
Julien Cochard, 2011:307, ISBN 978-82-471-3189-3 (printed ver.) ISBN 978-82-471-3190-9 (electronic ver.) ISSN 1503-8181.
- “Constitutive behavior and fracture of shape memory alloys”  
Jim Stian Olsen, 2012:57, ISBN 978-82-471-3382-8 (printed ver.) ISBN 978-82-471-3383-5 (electronic ver.) ISSN 1503-8181.
- “Field measurements in mechanical testing using close-range photogrammetry and digital image analysis”  
Egil Fagerholt, 2012:95, ISBN 978-82-471-3466-5 (printed ver.) ISBN 978-82-471-3467-2 (electronic ver.) ISSN 1503-8181.
- “Towards a better understanding of the ultimate behaviour of lightweight aggregate concrete in compression and bending”,  
Håvard Nedrelid, 2012:123, ISBN 978-82-471-3527-3 (printed ver.) ISBN 978-82-471-3528-0 (electronic ver.) ISSN 1503-8181.
- “Numerical simulations of blood flow in the left side of the heart”  
Sigrid Kaarstad Dahl, 2012:135, ISBN 978-82-471-3553-2 (printed ver.) ISBN 978-82-471-3555-6 (electronic ver.) ISSN 1503-8181.
- “Moisture induced stresses in glulam”  
Vanessa Angst-Nicollier, 2012:139, ISBN 978-82-471-3562-4 (printed ver.) ISBN 978-82-471-3563-1 (electronic ver.) ISSN 1503-8181.
- “Biomechanical aspects of distraction osteogenesis”  
Valentina La Russa, 2012:250, ISBN 978-82-471-3807-6 (printed ver.) ISBN 978-82-471-3808-3 (electronic ver.) ISSN 1503-8181.
- “Ductile fracture in dual-phase steel. Theoretical, experimental and numerical study”  
Gaute Gruben, 2012:257, ISBN 978-82-471-3822-9 (printed ver.) ISBN 978-82-471-3823-6 (electronic ver.) ISSN 1503-8181.
- “Damping in Timber Structures”  
Nathalie Labonnote, 2012:263, ISBN 978-82-471-3836-6 (printed ver.) ISBN 978-82-471-3837-3 (electronic ver.) ISSN 1503-8181.



- “Biomechanical modeling of fetal veins: The umbilical vein and ductus venosus bifurcation”  
Paul Roger Leinan, 2012:299, ISBN 978-82-471-3915-8 (printed ver.) ISBN 978-82-471-3916-5 (electronic ver.) ISSN 1503-8181.
- “Large-Deformation behaviour of thermoplastics at various stress states”  
Anne Serine Ognedal, 2012:298, ISBN 978-82-471-3913-4 (printed ver.) ISBN 978-82-471-3914-1 (electronic ver.) ISSN 1503-8181.
- “Hardening accelerator for fly ash blended cement”  
Kien Dinh Hoang, 2012:366, ISBN 978-82-471-4063-5 (printed ver.) ISBN 978-82-471-4064-2 (electronic ver.) ISSN 1503-8181.
- “From molecular structure to mechanical properties”  
Jianyang Wu, 2013:186, ISBN 978-82-471-4485-5 (printed ver.) ISBN 978-82-471-4486-2 (electronic ver.) ISSN 1503-8181.
- “Experimental and numerical study of hybrid concrete structures”  
Linn Grepstad Nes, 2013:259, ISBN 978-82-471-4644-6 (printed ver.) ISBN 978-82-471-4645-3 (electronic ver.) ISSN 1503-8181.
- “Mechanics of ultra-thin multi crystalline silicon wafers”  
Saber Saffar, 2013:199, ISBN 978-82-471-4511-1 (printed ver.) ISBN 978-82-471-4513-5 (electronic ver.) ISSN 1503-8181.
- “Through process modelling of welded aluminium structures”  
Anizahyati Alisibramulisi, 2013:325, ISBN 978-82-471-4788-7 (printed ver.) ISBN 978-82-471-4789-4 (electronic ver.) ISSN 1503-8181.
- “Combined blast and fragment loading on steel plates”  
Knut Gaarder Rakvåg, 2013:361, ISBN 978-82-471-4872-3 (printed ver.) ISBN 978-82-4873-0 (electronic ver.) ISSN 1503-8181.
- “Characterization and modelling of the anisotropic behaviour of high-strength aluminium alloy”  
Marion Fourmeau, 2014:37, ISBN 978-82-326-0008-3 (printed ver.) ISBN 978-82-326-0009-0 (electronic ver.) ISSN 1503-8181.
- “Behaviour of threaded steel fasteners at elevated deformation rates”  
Henning Fransplass, 2014:65, ISBN 978-82-326-0054-0 (printed ver.) ISBN 978-82-326-0055-7 (electronic ver.) ISSN 1503-8181.
- “Sedimentation and Bleeding”  
Ya Peng, 2014:89, ISBN 978-82-326-0102-8 (printed ver.) ISBN 978-82-326-0103-5 (electric ver.) ISSN 1503-8181.
- “Impact against X65 offshore pipelines”  
Martin Kristoffersen, 2014:362, ISBN 978-82-326-0636-8 (printed ver.) ISBN 978-82-326-0637-5 (electronic ver.) ISSN 1503-8181.

- “Formability of aluminium alloy subjected to prestrain by rolling”  
Dmitry Vysochinskiy, 2014:363,, ISBN 978-82-326-0638-2 (printed ver.) ISBN 978-82-326-0639-9 (electronic ver.) ISSN 1503-8181.
- “Experimental and numerical study of Yielding, Work-Hardening and anisotropy in textured AA6xxx alloys using crystal plasticity models”  
Mikhail Khadyko, 2015:28, ISBN 978-82-326-0724-2 (printed ver.) ISBN 978-82-326-0725-9 (electronic ver.) ISSN 1503-8181.
- “Behaviour and Modelling of AA6xxx Aluminium Alloys Under a Wide Range of Temperatures and Strain Rates”  
Vincent Vilamosa, 2015:63, ISBN 978-82-326-0786-0 (printed ver.) ISBN 978-82-326-0787-7 (electronic ver.) ISSN 1503-8181.
- “A Probabilistic Approach in Failure Modelling of Aluminium High Pressure Die-Castings”  
Octavian Knoll, 2015:137, ISBN 978-82-326-0930-7 (printed ver.) ISBN 978-82-326-0931-4 (electronic ver.) ISSN 1503-8181.
- “Ice Abrasion on Marine Concrete Structures”  
Egil Møen, 2015:189, ISBN 978-82-326-1034-1 (printed ver.) ISBN 978-82-326-1035-8 (electronic ver.) ISSN 1503-8181.
- “Fibre Orientation in Steel-Fibre-Reinforced Concrete”  
Giedrius Zirgulis, 2015:229, ISBN 978-82-326-1114-0 (printed ver.) ISBN 978-82-326-1115-7 (electronic ver.) ISSN 1503-8181.
- “Effect of spatial variation and possible interference of localised corrosion on the residual capacity of a reinforced concrete beam”  
Mohammad Mahdi Kioumarsi, 2015:282, ISBN 978-82-326-1220-8 (printed ver.) ISBN 978-82-1221-5 (electronic ver.) ISSN 1503-8181.
- “The role of concrete resistivity in chloride-induced macro-cell corrosion”  
Karla Horbostel, 2015:324, ISBN 978-82-326-1304-5 (printed ver.) ISBN 978-82-326-1305-2 (electronic ver.) ISSN 1503-8181.
- “Flowable fibre-reinforced concrete for structural applications”  
Elena Vidal Sarmiento, 2015-335, ISBN 978-82-326-1324-3 (printed ver.) ISBN 978-82-326-1325-0 (electronic ver.) ISSN 1503-8181.
- “Development of chushed sand for concrete production with microproportioning”  
Rolands Cepuritis, 2016:19, ISBN 978-82-326-1382-3 (printed ver.) ISBN 978-82-326-1383-0 (electronic ver.) ISSN 1503-8181.
- “Withdrawal properties of threaded rods embedded in glued-laminated timber elements”  
Haris Stamatopoulos, 2016:48, ISBN 978-82-326-1436-3 (printed ver.) ISBN 978-82-326-1437-0 (electronic ver.) ISSN 1503-8181.

- “An Experimental and numerical study of thermoplastics at large deformation”  
Marius Andersen, 2016:191, ISBN 978-82-326-1720-3 (printed ver.) ISBN 978-82-326-1721-0 (electronic ver.) ISSN 1503-8181.
- “Modeling and Simulation of Ballistic Impact”  
Jens Kristian Holmen, 2016:240, ISBN 978-82-326-1818-7 (printed ver.) ISBN 978-82-326-1819-4 (electronic ver.) ISSN 1503-8181.
- “Early age crack assessment of concrete structures”  
Anja B. Estensen Klausen, 2016:256, ISBN 978-82-326-1850-7 (printed ver.) ISBN 978-82-326-1851-4 (electronic ver.) ISSN 1503-8181.
- “Uncertainty quantification and sensitivity analysis for cardiovascular models”  
Vinzenc Gregor Eck, 2016:234, ISBN 978-82-326-1806-4 (printed ver.) ISBN 978-82-326-1807-1 (electronic ver.) ISSN 1503-8181.
- “Dynamic behaviour of existing and new railway catenary systems under Norwegian conditions”  
Petter Røe Nåvik, 2016:298, ISBN 978-82-326-1935-1 (printed ver.) ISBN 978-82-326-1934-4 (electronic ver.) ISSN 1503-8181.
- “Mechanical behaviour of particle-filled elastomers at various temperatures”  
Arne IIseng, 2016:295, ISBN 978-82-326-1928-3 (printed ver.) ISBN 978-82-326-1929-0 (electronic ver.) ISSN 1503-8181.
- “Nanotechnology for Anti-Icing Application”  
Zhiwei He, 2016:348, ISBN 978-82-326-2038-8 (printed ver.) ISBN 978-82-326-2019-5 (electronic ver.) ISSN 1503-8181.
- “Conduction Mechanisms in Conductive Adhesives with Metal-Coated Polymer Spheres”  
Sigurd Rolland Pettersen, 2016:349, ISBN 978-82-326-2040-1 (printed ver.) ISBN 978-82-326-2041-8 (electronic ver.) ISSN 1503-8181.
- “The interaction between calcium lignosulfonate and cement”  
Alessia Colombo, 2017:20, ISBN 978-82-326-2122-4 (printed ver.) ISBN 978-82-326-2123-1 (electronic ver.) ISSN 1503-8181.
- “Behaviour and Modelling of Flexible Structures Subjected to Blast Loading”  
Vegard Aune, 2017:101, ISBN 978-82-326-2274-0 (printed ver.) ISBN 978-82-326-2275-7 (electronic ver.) ISSN 1503-8181.
- “Behaviour of steel connections under quasi-static and impact loading”  
Erik Løhre Grimsmo, 2017:159, ISBN 978-82-326-2390-7 (printed ver.) ISBN 978-82-326-2391-4 (electronic ver.) ISSN 1503-8181.
- “An experimental and numerical study of cortical bone at the macro and Nano-scale”  
Masoud Ramenzanzadehkoldeh, 2017:208, ISBN 978-82-326-2488-1 (printed ver.) ISBN 978-82-326-2489-8 (electronic ver.) ISSN 1503-8181.

- “Optoelectrical Properties of a Novel Organic Semiconductor: 6,13-Dichloropentacene” Mao Wang, 2017:130, ISBN 978-82-326-2332-7 (printed ver.) ISBN 978-82-326-2333-4 (electronic ver.) ISSN 1503-8181.
- “Core-shell structured microgels and their behavior at oil and water interface” Yi Gong, 2017:182, ISBN 978-82-326-2436-2 (printed. ver.) ISBN 978-82-326-2437-9 (electronic ver.) ISSN 1503-8181.
- “Aspects of design of reinforced concrete structures using nonlinear finite element analyses” Morten Engen, 2017:149, ISBN 978-82-326-2370-9 (printed ver.) ISBN 978-82-326-2371-6 (electronic ver.) ISSN 1503-8181.
- “Numerical studies on ductile failure of aluminium alloys” Lars Edvard Dæhli, 2017:284, ISBN 978-82-326-2636-6 (printed ver.) ISBN 978-82-326-2637-3 (electronic ver.) ISSN 1503-8181.
- “Modelling and Assessment of Hydrogen Embrittlement in Steels and Nickel Alloys” Haiyang Yu, 2017:278, ISBN 978-82-326-2624-3 (printed. ver.) ISBN 978-82-326-2625-0 (electronic ver.) ISSN 1503-8181.
- “Network arch timber bridges with light timber deck on transverse crossbeams” Anna Weronika Ostrycharczyk, 2017:318, ISBN 978-82-326-2704-2 (printed ver.) ISBN 978-82-326-2705-9 (electronic ver.) ISSN 1503-8181.
- “Splicing of Large Glued Laminated Timber Elements by Use of Long Threaded Rods” Martin Cepelka, 2017:320, ISBN 978-82-326-2708-0 (printed ver.) ISBN 978-82-326-2709-7 (electronic ver.) ISSN 1503-8181.
- “Thermomechanical behaviour of semi-crystalline polymers: experiments, modelling and simulation” Joakim Johnsen, 2017:317, ISBN 978-82-326-2702-8 (printed ver.) ISBN 978-82-326-2703-5 (electronic ver.) ISSN 1503-8181.
- “Small-Scale Plasticity under Hydrogen Environment” Kai Zhao, 2017:356, ISBN 978-82-326-2782-0 (printed ver.) ISBN 978-82-326-2783-7 (electronic er.) ISSN 1503-8181.
- “Risk and Reliability Based Calibration of Structural Design Codes” Michele Baravalle, 2017:342, ISBN 978-82-326-2752-3 (printed ver.) ISBN 978-82-326-2753-0 (electronic ver.) ISSN 1503-8181.
- “Dynamic behaviour of floating bridges exposed to wave excitation” Knut Andreas Kvåle, 2017:365, ISBN 978-82-326-2800-1 (printed ver.) ISBN 978-82-326-2801-8 (electronic ver.) ISSN 1503-8181.
- “Dolomite calcined clay composite cement – hydration and durability”

Alisa Lydia Machner, 2018:39, ISBN 978-82-326-2872-8 (printed ver.). ISBN 978-82-326-2873-5 (electronic ver.) ISSN 1503-8181.

“Modelling of the self-excited forces for bridge decks subjected to random motions: an experimental study”

Bartosz Siedziako, 2018:52, ISBN 978-82-326-2896-4 (printed ver.). ISBN 978-82-326-2897-1 (electronic ver.) ISSN 1503-8181.

“A probabilistic-based methodology for evaluation of timber facade constructions”

Klodian Gradeci, 2018:69, ISBN 978-82-326-2928-2 (printed ver.) ISBN 978-82-326-2929-9 (electronic ver.) ISSN 1503-8181.

“Behaviour and modelling of flow-drill screw connections”

Johan Kolstø Sønstabø, 2018:73, ISBN 978-82-326-2936-7 (printed ver.) ISBN 978-82-326-2937-4 (electronic ver.) ISSN 1503-8181.

“Full-scale investigation of the effects of wind turbulence characteristics on dynamic behavior of long-span cable-supported bridges in complex terrain”

Aksel Fenerci, 2018 100, ISBN 9978-82-326-2990-9 (printed ver.) ISBN 978-82-326-2991-6 (electronic ver.) ISSN 1503-8181.

“Modeling and simulation of the soft palate for improved understanding of the obstructive sleep apnea syndrome”

Hongliang Liu, 2018:101, ISBN 978-82-326-2992-3 (printed ver.) ISBN 978-82-326-2993-0 (electronic ver.) ISSN 1503-8181.

“Long-term extreme response analysis of cable-supported bridges with floating pylons subjected to wind and wave loads”.

Yuwang Xu, 2018:229, ISBN 978-82-326-3248-0 (printed ver.) ISBN 978-82-326-3249-7 (electronic ver.) ISSN 1503-8181.

“Reinforcement corrosion in carbonated fly ash concrete”

Andres Belda Revert, 2018:230, ISBN 978-82-326-3250-3 (printed ver.) ISBN 978-82-326-3251-0 (electronic ver.) ISSN 1503-8181.

“Direct finite element method for nonlinear earthquake analysis of concrete dams including dam-water-foundation rock interaction”

Arnkjell Løkke, 2018:252, ISBN 978-82-326-3294-7 (printed ver.) ISBN 978-82-326-3295-4 (electronic ver.) ISSN 1503-8181.

“Electromechanical characterization of metal-coated polymer spheres for conductive adhesives”

Molly Strimbeck Bazilchuk, 2018:295, ISBN 978-82-326-3380-7 (printed. ver.) ISBN 978-82-326-3381-4 (electrical ver.) ISSN 1503-8181.

“Determining the tensile properties of Arctic materials and modelling their effects on fracture”

Shengwen Tu, 2018:269, ISBN 978-82-326-3328-9 (printed ver.) ISBN 978-82-326-3329-6 (electronic ver.) ISSN 1503-8181.

- “Atomistic Insight into Transportation of Nanofluid in Ultra-confined Channel”  
Xiao Wang, 2018:334, ISBN 978-82-326-3456-9 (printed ver.) ISBN 978-82-326-3457-6 (electronic ver.) ISSN 1503-8181.
- “An experimental and numerical study of the mechanical behaviour of short glass-fibre reinforced thermoplastics”  
Jens Petter Henrik Holmstrøm, 2019:79, ISBN 978-82-326-3760-7 (printed ver.) ISBN 978-82-326-3761-4 (electronic ver.) ISSN 1503-8181.
- “Uncertainty quantification and sensitivity analysis informed modeling of physical systems”  
Jacob Sturdy, 2019:115, ISBN 978-82-326-3828-4 (printed ver.) ISBN 978-82-326-3829-1 (electronic ver.) ISSN 1503-8181.
- “Load model of historic traffic for fatigue life estimation of Norwegian railway bridges”  
Gunnstein T. Frøseth, 2019:73, ISBN 978-82-326-3748-5 (printed ver.) ISBN 978-82-326-3749-2 (electronic ver.) ISSN 1503-8181.
- “Force identification and response estimation in floating and suspension bridges using measured dynamic response”  
Øyvind Wiig Petersen, 2019:88, ISBN 978-82-326-3778-2 (printed ver.) ISBN 978-82-326-3779-9 (electronic ver.) ISSN 1503-8181.
- “Consistent crack width calculation methods for reinforced concrete elements subjected to 1D and 2D stress states”  
Reignard Tan, 2019:147, ISBN 978-82-326-3892-5 (printed ver.) ISBN 978-82-326-3893-2 (electronic ver.) ISSN 1503-8181.
- “Nonlinear static and dynamic isogeometric analysis of slender spatial and beam type structures”  
Siv Bente Raknes, 2019:181, ISBN 978-82-326-3958-8 (printed ver.) ISBN 978-82-326-3959-5 (electronic ver.) ISSN 1503-8181.
- “Experimental study of concrete-ice abrasion and concrete surface topography modification”  
Guzel Shamsutdinova, 2019:182, ISBN 978-82-326-3960-1 (printed ver.) ISBN 978-82-326-3961-8 (electronic ver.) ISSN 1503-8181.
- “Wind forces on bridge decks using state-of-the art FSI methods”  
Tore Andreas Helgedagsrud, 2019:180, ISBN 978-82-326-3956-4 (printed ver.) ISBN 978-82-326-3957-1 (electronic ver.) ISSN 1503-8181.
- “Numerical Study on Ductile-to-Brittle Transition of Steel and its Behavior under Residual Stresses”  
Yang Li, 2019:227, ISBN 978-82-326-4050-8 (printed ver.) ISBN 978-82-326-4015-5 (electronic ver.) ISSN 1503-8181.
- “Micromechanical modelling of ductile fracture in aluminium alloys”

Bjørn Håkon Frodal, 2019:253, ISBN 978-82-326-4102-4 (printed ver.) ISBN 978-82-326-4103-1 (electronic ver.) ISSN 1503-8181.

“Monolithic and laminated glass under extreme loading: Experiments, modelling and simulations”

Karoline Osnes, 2019:304, ISBN 978-82-326-4204-5 (printed ver.) ISBN 978-82-326-4205-2 (electronic ver.) ISSN 1503-8181.

“Plastic flow and fracture of isotropic and anisotropic 6000-series aluminium alloys: Experiments and numerical simulations “

Susanne Thomesen, 2019:312, ISBN 978-82-326-4220-5 (printed ver.), ISBN 978-82-326-4221-2 (electronic ver.) ISSN 1503-8181

“Stress-laminated timber decks in bridges”

Francesco Mirko Massaro, 2019:346, ISBN 978-82-326-4288-5 (printed ver.), ISBN 978-82-326-4289-2 (electronic ver.) ISSN 1503-8181

“Connections between steel and aluminium using adhesive bonding combined with self-piercing riveting: Testing, modelling and analysis”

Matthias Reil, 2019:319, ISBN 978-82-326-4234-2 (printed ver.), ISBN 978-82-326-4235-9 (electronic ver.) ISSN 1503-8181

“Designing Polymeric Icephobic Materials”

Yizhi Zhuo, 2019:345, ISBN 978-82-326-4286-1 (printed ver.), ISBN 978-82-326-4287-8 (electronic ver.) ISSN 1503-8181

“Fundamental Mechanisms of Ice Adhesion”

Rønneberg, Sigrid 2020:87, ISBN 978-82-326-4527-8 (printed version) ISBN 978-82-326-4524-5 (electronic version) ISSN 1503-8181

“Mechanical modeling of the polymeric coating on a subsea pipeline” Vestrum, Ole 2020:105, ISBN 978-82-326-4562-6 (printed version) ISBN 978-82-4563-3 (electronic version) ISSN 1503-8181

“Conceptual form-finding in structural engineering” Marcin Luczkowski 2020: “Self-assembled superstructures of magnetic nanoparticles: advanced nanofabrication and enhanced mechanical properties”

“Self-assembled superstructures of magnetic nanoparticles: advanced nanofabrication and enhanced mechanical properties” Verner Håkonsen 2020:271, ISBN 978-82-326-4890-0 (printed version) ISBN 978-82-326-4891-7 (electronic version) ISSN 1503-8181

“Micromechanical modelling of fracture in ductile alloys with applications to high-strength steel”

Sondre Bergh 2020:313, ISBN 978-82-326-4974-7 (printed version) ISBN 978-82-326-4975-4 (electronic version) ISSN 1503-8181

- “Fracture in wood of Norway spruce - Experimental and numerical study” Katarzyna Ostapska 2020:314, ISBN 978-82-326-4976-1 (printed version) ISBN 978-82-326-4977-8 (electronic version) ISSN 1503-8181
- “Dynamic anti-icing surfaces (DAIS)” Feng Wang 2020:330 ISBN 978-82-326-5006-4 (printed version) ISBN 978-82-326-5007-1 (electronic version) ISSN 1503-8181
- “«Multiaxial Fatigue analysis of offshore mooring chains, considering the effects of residual stresses and corrosion pits» Ershad P. Zarandi 2020:337 ISBN 978-82-326-5020-0 (printed version) ISBN 978-82-326-5021-7 (electronic version) ISSN 1503-8181
- “Production and documentation of frost durable high-volume fly ash concrete: air entrainment, cracking and scaling in performance testing” Andrei Shpak 2020:366 ISBN 978-82-326-5078-1 (printed version) ISBN 978-82-326-5079-8 (electronic version) ISSN 1503-8181
- “Physics-based and data-driven reduced-order blood flow models: Applications to coronary artery disease diagnostics” Fredrik Eikeland Fossan 2020:362 ISBN 978-82-326-5070-5 (printed version) ISBN 978-82-326-5071-2 (electronic version) ISSN 1503-8181
- “Multi-scale modelling and simulation of ductile failure in aluminium structures” Henrik Granum 2020:374 ISBN 978-82-326-5094-1 (printed version) ISBN 978-82-326-5095-8 (electronic version) ISSN 1503-8181
- “Testing and modelling of multi-material joints” Jon Fredrick Berntsen 2020:368 ISBN 978-82-326-5082-8 (printed version) ISBN 978-82-326-5083-5 ISSN 1503-8181
- “Heuristic models for wear prediction and dynamic-based condition monitoring techniques in pantograph-catenary interaction” Stefano Derosa 2020:381 ISBN 978-82-326-5108-5 (printed version) ISBN 978-82-326-5109-2 (electronic version) ISSN 1503-8181
- “Experimental and numerical study of dilation in mineral filled PVC” Sindre Nordmark Olufsen 2020:388 ISBN 978-82-326-5122-1 (printed version) ISBN 978-82-326-5123-8 (electronic version) ISSN 1503-8181
- “Residual stresses and dimensional deviation in metal additive manufacturing: prediction and mitigation methods” Li Sun 2020:411 ISBN 978-82-471-9600-7 (printed version) ISBN 978-82-471-9581-9 (electronic version) ISSN 1503-8181 (printed version) ISSN 2703-8084 (online version)
- “Moment-resisting timber frames with semi-rigid connections” Aivars Vilguts 2021:88 ISBN 978-82-326-6987 (printed version) ISBN 978-82-326-5737-7 (electronic version) ISSN 2703-8084 (online version)
- “Thermal transport in metal-polymer systems” Susanne Sandell 2021:63 ISBN 978-82-326-5304-1 (printed version) ISBN 978-82-326-6278-4 (electronic version) ISSN 2703-8084 (online version)



- “Competitive timber floors” Sveinung Ørjan Nesheim 2021:134 ISBN 978-82-326-6481-8 (printed version) ISBN 978-82-326-5399-7 (electronic version) ISSN 2703-8084
- “Thermodynamics of Nanoscale Films and Fluid Volumes” Bjørn Andre Strøm 2021:166 ISBN 978-82-326-6778-9 (printed version) ISBN 978-82-326-5900-5 (electronic version) ISSN 2703-8084 (online version)
- “Characterization and modeling of the mechanical behavior of polymer foam” Daniel Thor Morton 2021:173 ISBN 978-82-326-6245-6 (printed version) ISBN 978-82-326-5699-8 (electronic version) ISSN 2703-8084 (online version)
- “Atomistic Insights to Interfacial Dynamics” Yuequn Fu 2021:233 ISBN 978-82-326-5530-4 (printed version) ISBN 978-82-326-6894-6 (electronic version) ISSN 2703-8084 (online version)
- “Mechanisms and enhancement of CO<sub>2</sub> condensation heat transfer” Ingrid Snustad 2021:236 ISBN 978-82-326-5606-6 ISBN 978-82-236-6715-4 (electronic version) ISSN 2703-8084
- “Experimental study of reinforced concrete slabs subjected to fire exposure and blast loading” Assis Arano Barenys 2021:239 ISBN 978-82-326-5289-1 ISBN 978-82-326-5876-3 (electronic version) ISSN 2703-8084 (online version)
- “Long-term extreme buffeting response investigations for long-span bridges considering uncertain turbulence parameters based on field measurements” Tor Martin Lystad 2021:216 ISBN 978-82-326-5797-1 (printed version) ISBN 978-82-326-6154-1 (electronic version) ISSN 2703-8084 (online version)
- “Development and Application of a Vision-Based System for Structural Monitoring of Railway Catenary System” Tengjiao Jiang 2021:280 ISBN 978-82-326-6866-3 (printed ver.) ISBN 978-82-326-5778-0 (electronic ver.) ISSN 1503-8181 (online ver.)
- “Integrated design and maintenance of deteriorating structural systems” Jorge Mendoza Espinosa 2021:351 ISBN 978-82-326-6608-9 (printed ver.) ISBN 978-82-326-6954-7 (electronic ver.) ISSN 2703-8084 (online ver.)
- “Numerical and experimental studies for damage detection and structural health monitoring of steel bridges” Bjørn T. Svendsen 2021:382 ISBN 978-82-326-6327-9 (printed ver.) ISBN 978-82-326-5895-4 (electronic ver.) ISSN 2703-8084 (online ver.)
- “Uncertainty quantification for multiphase flow” Andreas Strand 2021:410 ISBN 978-82-326-6519-8 (printed ver.) ISBN 978-82-326-6928-8 (electronic ver.) ISSN 2703-8084 (online ver.)
- “Prediction of rheological properties of filler modified cement paste from constituent properties, flow measurements and modelling” Elisabeth Leite Skare 2022:38 ISBN

978-82-326-5753-7 (printed ver.) ISBN 978-82-326-6958-5 (electronic ver.) ISSN 2703-8084 (online ver.)

“Nanomechanical characterization of additively manufactured metallic alloys” Siqi Liu 2022:96 ISBN 978-82-326-5457-4 (printed ver.) ISBN 978-82-326-5481-9 (electronic ver.) ISSN 2703-8084 (online ver.)

“Modeling and experiments in transient potential drop measurements for nondestructive evaluation” Øyvind Othar Aunet Persvik 2022:146 ISBN 978-82326-5682-0 (printed ver.) ISBN 978-82-326-5365-2 (electronic ver.) ISSN 2703-8084 (online ver.)

“Ductile fracture of aluminium alloys in the low to moderate stress triaxiality range” Asle Joachim Tomstad 2022:150 ISBN 978-82-326-6681-2 (printed ver.) ISBN 978-82-326-5506-9 (electronic ver.) ISSN 2703-8084 (online ver.)

“Application of marine field data for prediction of chloride ingress in concrete” Simon Fjendbo 2022:173 ISBN 978-82-326-6071-1 (printed ver.) ISBN 978-82-326-6659-1 (electronic ver.) ISSN 1503-8181 (online ver.)

“On the use of a virtual laboratory for aluminum alloys: application to large-scale analyses of extruded profiles” Marcos Fernandez Garcia 2022:199 ISBN 978-82-326-5527-4 (printed ver.) ISBN 978-82-326-6036-0 (electronic ver.) ISSN 2703-8084 (online ver.)

“Energy absorption and failure in aluminum alloys: An experimental and numerical study” Kristin Qvale 2022:213 ISBN 978-82-326-5172-6 (printed ver.) ISBN 978-82-326-5208-2 (electronic ver.) ISSN 2703-8084 (online ver.)

“Probabilistic modelling of wind induced load effects for suspension bridges with emphasis on long-term extreme value analysis” Dario Rafael Fernandez Castellon 2022:218 ISBN 978-82-326-5343-0 (printed ver.) ISBN 978-82-326-5401-7 (electronic ver.) ISSN 2703-8084 (online ver.)

“Fatigue crack initiation in corroded offshore mooring chains” Paul Qvale 2022:296 ISBN 978-82-326-5720-9 (printed er.) ISBN 978-82-326-5943-2 (electronic ver.) ISSN 2703-8084 (online ver.)

“Durability and structural performance of pretensioned concrete girders in coastal climate bridges” Magdalena Jadwiga Osmolska 2022:372 ISBN 978-82-326-5806-0 (printed ver.) ISBN 978-82-326-5555-7 (electronic ver.) ISSN 2703-8084 (electronic ver.)

“The impact of curing temperatures on Portland composite cements – hydrate assemblage, porosity, and compressive strength” Pamela Zuschlag 2022:374 ISBN 978-82-326-6521-1 (printed ver.) ISBN 978-82-326-6793-2 (electronic ver.) ISSN 2703-8084 (online ver.)

“Behaviour, modelling and simulation of thin steel plates subjected to combined blast and impact loading” Benjamin Stavnar Elveli 2022:392 ISBN 978-82-326-5179-5

(printed ver.) ISBN 978-82-326-5383-6 (electronic ver.) ISSN 2703-8084 (electronic ver.)

«Load effects of alkali-silica reaction in reinforced concrete beam bridges - Material testing, Constitutive modelling and Numerical simulation» Simen Sørgaard Kongshaug 2023:20 ISBN 978-82-326-6952-3 (printed ver.) ISBN 978-82-326-5497-0 (electronic ver.) ISSN 2703-8084 (online ver.)

«Field investigations of crosswinds and vehicle-driver response on bridges» Sebastian Reymert 2023:41 ISBN 978-82-326-6227-2 (printed ver.) ISBN 978-82-326-6117-6 ISSN 2703-8084 (online ver.)

